HYBRID RENEWABLE ENERGY SYSTEM USING DOUBLY-FED INDUCTION GENERATOR AND MULTILEVEL INVERTER

A Thesis
Submitted to the Graduate Faculty
of the
North Dakota State University
of Agriculture and Applied Science

By

Eshita Ahmed

In Partial Fulfillment
for the Degree of
MASTER OF SCIENCE

Major Department: Electrical and Computer Engineering

May 2012

Fargo, North Dakota

North Dakota State University

Graduate School

Title

Hybrid Renewable Energy System Using

Doubly-Fed Induction Generator and Multilevel Inverter

By

Eshita Ahmed

The Supervisory Committee certifies that this ***disquisition*** complies with North Dakota State University's regulations and meets the accepted standards for the degree of

MASTER OF SCIENCE

SUPERVISORY COMMITTEE:

Subbaraya Yuvarajan

Chair

Rajesh Kavasseri

Cristinel Ababei

Sumathy Krishnan

Approved:

05/22/2012

Date

Rajendra Katti

Department Chair

ABSTRACT

The proposed hybrid system generates AC power by combining solar and wind energy converted by a doubly-fed induction generator (DFIG). The DFIG, driven by a wind turbine, needs rotor excitation so the stator can supply a load or the grid. In a variable-speed wind energy system, the stator voltage and its frequency vary with wind speed, and in order to keep them constant, variable-voltage and variable-frequency rotor excitation is to be provided. A power conversion unit supplies the rotor, drawing power either from AC mains or from a PV panel depending on their availability. It consists of a multilevel inverter which gives lower harmonic distortion in the stator voltage. Maximum power point tracking techniques have been implemented for both wind and solar power. The complete hybrid renewable energy system is implemented in a PSIM-Simulink interface and the wind energy conversion portion is realized in hardware using dSPACE controller board.

ACKNOWLEDGEMENTS

This work would have never been completed without the guidance and support of many individuals. "Thank you" will never express my full gratitude for these people, but I assure each and every one of them that I shall never forget, and forever I will be grateful for all I have learned from each of them.

First and foremost, I would like to start by expressing my gratitude to my advisor, Prof. Subbaraya Yuvarajan for giving me the opportunity to work with him and study at North Dakota State University. His patience, vision and guidance have been indispensable in the pursuit of my goal. I would like to acknowledge my thesis committee members, Dr. Rajesh Kavasseri, Dr. Cristinel Ababei and Dr. Sumathy Krishnan, for their guidance and advice. My deepest thanks and respect go to my husband, my parents and my brother who have always been my faithful and enthusiastic supporters. Without their love, encouragement and belief in me, I would not be where I am today. My gratitude also extends to all my friends and colleagues for all the discussions, cooperation and for the wonderful time we have shared.

Finally, I would like to thank North Dakota State University and the ECE department for providing me with financial support.

TABLE OF CONTENTS

LIST OF TABLES

LIST OF FIGURES

LIST OF ABBREVIATIONS

AC	……	Alternating Current
BJT	……	Bipolar Junction Transistor
BLDC	……	Brushless DC
CB-PWM	……	Carrier-Based PWM
CSI	……	Current Source Inverter
DC	……	Direct Current
DF	……	Distortion Factor
DFIG	……	Doubly-Fed Induction Generator
FFT	……	Fast Fourier Transform
FMAC	……	Flux Magnitude and Angle Control
FSIG	……	Fixed Speed Induction Generator
FSWT	……	Fixed Speed Wind Turbine
GSC	……	Grid Side Converter
GTO	……	Gate Turn-Off Thyristor
HAWT	……	Horizontal-Axis Wind Turbine
HRES	……	Hybrid Renewable Energy System
HVDC	……	High Voltage DC
IG	……	Induction Generator
IGBT	……	Insulated Gate Bipolar Transistor

IGCT	……	Integrated Gate-Commutated Thyristor
IM	……	Induction Machine
LOH	……	Lowest Order Harmonic
MCT	……	MOS-Controlled Thyristor
MOS	……	Metal-Oxide
MOSFET	……	Metal-Oxide Field-Effect Transistor
NPC	……	Neutral-Point-Clamped
PI	……	Proportional Integral
PID	……	Proportional Integral Derivative
PLL	……	Phase Locked Loop
PM	……	Permanent Magnet
PMSG	……	PM Synchronous Generator
PV	……	Photovoltaic
PWM	……	Pulse Width Modulation
RCC	……	Ripple Correlation Control
RMS	……	Root Mean Square
RPM	……	Revolution Per Minute
RSC	……	Rotor Side Controller
SCIG	……	Squirrel Cage Induction Generator
SCIG	……	Synchronous Generator
SCR	……	Silicon-Controlled Rectifier

SIT	……	Static Induction Transistor
THD	……	Total Harmonic Distortion
VAWT	……	Vertical-Axis Wind Turbine
VSI	……	Voltage Source Inverter
VSWT	……	Variable-Speed Wind Turbine
WECS	……	Wind Energy Conversion System
WES	……	Wind Energy System
WRSG	……	Wound Rotor Synchronous Generator
WT	……	Wind Turbine

LIST OF SYMBOLS

A	Sweep area of turbine rotor blades
a	Stator to rotor turns ratio of DFIG
C	Capacitance
C_p	Power coefficient of blade
D, d	Duty cycle of chopper circuit
f_c	Cut-off frequency of filter
f_{cri}	Critical switching frequency of converter
f_m	Frequency of control or modulating signal in SPWM
f_{mech}	Mechanical frequency of the rotor of DFIG
f_s	Stator frequency of DFIG
f_{sl} , f_r	Slip or rotor injection frequency of DFIG
f_{sw}	Switching frequency of solid-state switching device
f_{tri}	Frequency of carrier signal in SPWM
I	Photogenerated current in ideal PV cell
I_{cell}	Current from non-ideal PV cell
I_D	Current through the parallel diode in PV cell
i_d	Current through diode in boost converter
i_L	Current through inductor of boost converter
I_{MPP}	Current from PV panel at MPP
I_o	Reverse saturation current of diode

i_r	Three-phase rotor current of DFIG
i_{rd} , i_{rq}	d- and q-axis component of rotor current of DFIG
i_{rdref} , i_{rqref}	d- and q-axis reference rotor current of DFIG
I_{Rsh}	Current through the shunt resistor of PV cell model
i_s	Three-phase stator current of DFIG
I_{SC}	Short-circuit current of PV panel
i_{sd} , i_{sq}	d- and q-axis component of stator current of DFIG
i_{sw}	Current through switch of boost converter
k	Boltzmann's constant ($1.3806503 \times 10^{-23}$ m^2 kg s^{-2} K^{-1})
k_i	Proportionality current constant in fractional I_{SC} based MPPT
K_i	Integral constant of PI controller
K_p	Proportionality constant of PI controller
K_{Popt}	Optimum power coefficient of wind turbine
K_{Topt}	Optimum torque coefficient of wind turbine
k_v	Proportionality voltage constant in fractional V_{OC} based MPPT
L	Inductance
L_m	Mutual inductance between stator and rotor winding of DFIG
L_s , L_r	Stator and rotor inductance of DFIG
m	Number of levels of a multilevel inverter
m_a	Amplitude modulation index in SPWM
m_f	Frequency modulation index in SPWM
n	Diode ideality factor

N_m	Shaft speed of DFIG
N_p	Number of parallel connected cells in PV panel
N_s	Number of series connected cells in PV panel
P	Number of poles of DFIG
P_{cond}	Conduction loss of converter
P_{fixed}	Fixed loss of converter
P_{loss}	Total loss in a converter
P_m	Mechanical power transferred to wind turbine
P_r	Rotor power of DFIG
P_s	Stator power of DFIG
P_{sw}	Switching loss of solid-state switching device
P_w	Wind power
q	Elementary charge
R_{load}	Load resistance connected to PV panel
R_s	Series resistance of PV panel
R_{sh}	Shunt resistance of PV panel
s	Slip of DFIG
T	Absolute temperature
T_e	Electromagnetic torque of DFIG
T_{eref}	Reference torque
T_{off}	Off-time of solid-state switching device
T_{on}	On-time of solid-state switching device

T_s	Switching period of solid-state switching device
V_{A01m}	Amplitude of fundamental component of phase A voltage
v_{cd} , v_{cq}	d- and q-axis component of control voltage
V_{cell}	Voltage across PV panel
v_{ctrl}	Three-phase control voltage in SPWM
v_d	Voltage across diode in boost converter
V_{dc}	DC link voltage
V_i	Input DC voltage to chopper circuit
V_k	rms value of k^{th} harmonic
v_L	Voltage across inductor in boost converter
V_m	Amplitude of control or modulating signal
V_{MPP}	Voltage across PV panel at MPP
V_o, v_o	Output DC voltage from chopper circuit
V_{oavg}	Average output voltage from chopper circuit
V_{OC}	Open-circuit voltage across PV panel
v_r	Three-phase rotor voltage of DFIG
V_{Rsh}	Voltage across shunt resistor of PV cell
v_s	Three-phase stator voltage of DFIG
v_{sd} , v_{sq}	d- and q-axis component of stator voltage of DFIG
V_{sref}	Reference stator voltage of DFIG
v_{sw}	Voltage across the switch of boost converter
V_{tri}	Amplitude of high frequency carrier signal in SPWM

v_w	Wind speed
W	Energy lost in switching process in converter
α	Triggering angle of SCR in controlled rectifier
ρ	Air density (1.225 kg/m^3)
τ	Time constant of PI controller
ω_m	Rotor angular speed of DFIG
ω_s	Stator angular frequency of DFIG
λ_{sd}, λ_{sq}	d- and q-axis component of stator flux linkage of DFIG

CHAPTER 1. INTRODUCTION

World energy consumption is increasing at the rate of 2.3 % per year which causes the fossil-fuel reserve to diminish much faster than the forming of new [1]. Fossil fuels are costly and their production and use are raising some environmental issues. The USA was ranked seventh globally in energy consumption per-capita. They had an annual energy production of 4151 billion kWh in 2010, the second largest, 69.5 % of which came from fossil-fuel sources. Only 10 % of total energy came from renewable sources with 6 % from hydro [2]. Renewable energy resources should be used in power generation because it is safe, reliable, better for public health, environment-friendly, and addresses global climate change. They find their applications mostly in power generation, especially in rural areas, in heating and as transportation fuels. Among all alternative sources, wind and solar power are the most abundant and attractive.

1.1. Hybrid Renewable Energy System

Hybrid renewable energy system (HRES) is a system having multiple renewable energy sources working independently to supply some isolated DC or AC loads or the utility grid. Thus, not only the system efficiency is increased but also the energy supply is more balanced. The increasing demand for power from renewable sources has made it necessary for the sources to behave, as much as possible, like conventional power plants in terms of supporting the network voltage and frequency with good power quality. Several hybrid energy schemes may be used to solve these problems. This thesis proposes a new type of HRES that uses wind and solar to supply an AC load. Unlike conventional HRESs, the two sources do not work in parallel. The system basically uses a wind turbine (WT) to run a doubly-fed induction generator (DFIG) that delivers power to the load. The rotor of the generator is fed by a multilevel inverter that is

controlled for maximum power point tracking (MPPT) and constant stator output. The DC bus voltage of the inverter is provided by the PV panel that is also after ensuring maximum power extraction from solar energy using a boost regulator. The power can also be drawn from grid in case of unavailability of PV power. The AC power from the grid goes through an AC-DC-AC converter system while the PV power goes through a DC-AC converter system.

Normally a HRES requires separate power converters for all its energy sources which increase system complexity and losses. But the proposed system uses a single inverter for all sources making the control simple and reliable. Using PV power for rotor injection adds flexibility to the system by enabling AC power generation even in the absence of grid power. The proposed scheme is helpful for power supply in rural areas and for unreliable utility networks. The system can operate either using grid or PV power after processed by power converter. Besides, the system can even supply in time of low wind speed when the generator acts as a transformer, the rotor being its primary side taking converted solar power as input and the stator being its secondary side supplying the load.

1.2. Doubly-Fed Induction Generator

For wind energy conversion, fixed speed systems using squirrel cage induction generators were implemented in the past. At present, variable-speed systems mostly using DFIGs are being used for system operation with higher efficiency, absence of speed control, and reduced flickering problem. Permanent magnet machines which do not need gear box can also be used, but not for high capacity installations. A DFIG has windings on both the stator and rotor, both of them capable of transferring energy. The most attractive feature of a DFIG is that the system can use power converters as well as filters with lower ratings because they have to transform only a fraction of the total power (slip power) and inject it to the rotor. It has high energy conversion

efficiency and an improved fault-ride through capability. Also its real and reactive power outputs can be controlled independently.

1.3. Multilevel Inverter

Most energy conversion systems use back-to-back two-level PWM converters which are capable of operating in all four-quadrants. Back-to-back multilevel converters can also be used for the same purpose offering better power quality. Multilevel inverter is a DC to AC converter that synthesizes a desired AC voltage (normally of sinusoidal shape) from several levels of DC voltages as inputs. This study uses a three-level neutral-point-clamped (NPC) inverter for one stage of power conversion. For the other stage, there are two options, namely (a) PV voltage using a boost regulator and (b) the grid voltage using a diode rectifier followed by a boost regulator. Both options result in a constant DC-link voltage supplied to the multilevel inverter. The reason behind using a multilevel inverter, despite its complicated power and control circuitry and modulation scheme, is that it is better for high power applications and most importantly, it provides better power quality in terms of reduced harmonics.

1.4. Outline of Thesis

The thesis is organized in six chapters. Chapter 2 consists of a brief description on the renewable energy sources used in the proposed HRES. In the first half, the wind energy is discussed along with some details of wind turbine's (WT) components, various WT technologies and the generators used in them. This part also covers the MPPT of wind energy. The second half deals with solar photovoltaic energy including the operation and different MPPT techniques.

Chapter 3 describes different power converters used in both wind and PV energy conversion systems. Starting with a brief introduction to power conditioning systems, this chapter briefly describes different converters like a rectifier, a chopper, an inverter and a

cycloconverter. While emphasizing the power quality, it introduces the different types of multilevel inverters and sine pulse width modulation technique.

Chapter 4 introduces the proposed hybrid renewable energy system. A complete discussion of all the components is presented with itemized analysis. Converters used in the complete system are described using their equations and simulation results. A comparison between two- and three-level inverter is made based on their harmonic profiles. Finally simulation results of the complete system including variable wind speed, variable load and three-phase short circuit fault are given to validate the design.

Chapter 5 presents the experimental results which support the simulation and analysis made in the earlier chapters. First it validates the fact that the power converters used for proper rotor injection of the DFIG can be rated as low as 20 ~ 30 % of the generator rating. Then it demonstrates using hardware results that the multilevel inverter is better than the two-level one while feeding a resistive load, followed by the experimental results of the complete WECS using both three- and two-level inverters while comparing them with their respective simulation results. Lastly, chapter 6 summarizes the work carried out with some concluding remarks and includes suggestions for future research.

1.5. Contributions

The thesis presents a multilevel inverter based wind energy conversion system using DFIG. It somewhat resembles the system in [3] which is also a DFIG oriented WECS using back-to-back multilevel PWM converter. However, the proposed system adds a rotor injection path from PV energy and a new inverter controller. It also replaces the back-to-back converter by a simple diode rectifier and multilevel inverter based topology. The MPPT of PV panel is adapted from the scheme proposed in [4].

The contributions of the thesis are as follows:

- Hardware implementation of three-level neutral-point-clamped (NPC) inverter for wind energy applications.
- Simpler implementation of voltage control loop using Simulink-dSPACE.
- Simpler implementation of frequency control loop without a phase-locked-loop circuitry.
- Realization of MPPT for wind energy using current loop in a synchronously rotating d-q reference frame.

CHAPTER 2. RENEWABLE ENERGY SOURCES

2.1.Introduction

Electricity generation from renewable energy sources is not a new concept these days. With the fact of having limited conventional energy resources on the earth which are also costly and environment non-friendly, we have to consider alternative ways for power generation. Thus power industry is getting attracted towards renewable energy sources which in these days provide about 19 % of worldwide electric power. Figure 2-1 illustrates the worldwide power generation capacity using different renewable energy sources from 2004 to 2010 [5]. The hybrid renewable energy system introduced in this thesis includes wind and solar energy. In this chapter some of the characteristics of the two energy sources will be presented.

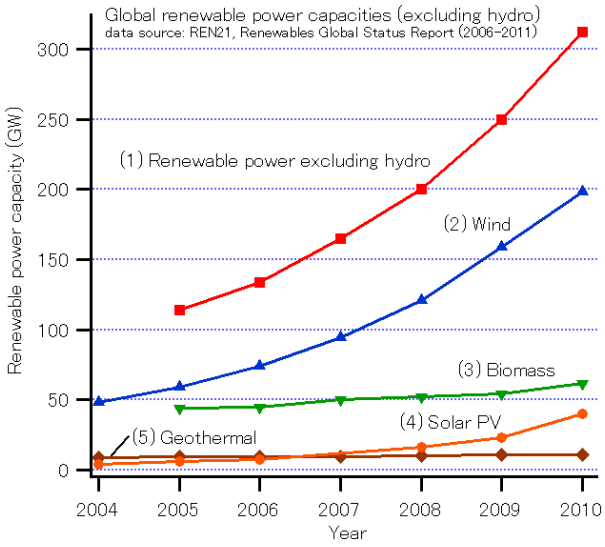

Figure 2-1. Global Renewable Power Capacity [5]

2.2. Wind Energy

After hydro power, wind is the most promising sustainable energy as can be seen by the steadily growing demand [6]. Year by year the demand, as well as the generation capacity of

wind power is increasing (Figure 2-1). With the growing demand for wind-based generation systems, it has become necessary to improve the systems' performance so that it can replace the existing power houses using conventional energy sources. For this improvement, better understanding of the complete system and the overall energy conversion process is very crucial. Ref [7] points out some common problems in integrating wind energy to grid in large scale, like frequency regulation, scheduling, and stabilization. In this section the details of a wind energy system (WES), especially the characteristics of wind turbines and the generators will be given.

2.2.1. Wind turbine (WT)

WESs consist of a WT whose shaft rotates when wind passes over the blades and this rotation is transferred to the generator through a gearbox. The generator then converts the rotational energy into electrical energy. Figure 2-2 shows all the major components of a WT [8]. The anemometer measures the wind speed for the controller to control the generator. The low speed of the turbine shaft is insufficient to generate adequate voltage from conversion process. So the gearbox increases the rotational speed of the generator shaft and thus amplifies the output

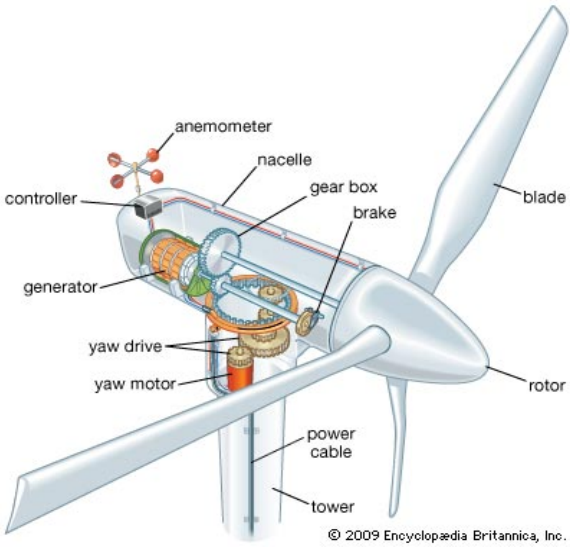

Figure 2-2. Components of Wind Turbine [8]

voltage. The generator, gear box and controlling equipments are housed in the nacelle. The yaw mechanism, comprised of a motor and a drive, is used to turn the whole nacelle in the direction of the wind flow. The tower holds the complete turbine at a certain height.

2.2.1.1. Power relations

A WT extracts the kinetic energy from the swept area of the blades by slowing down the air flow. Theoretically the maximum collectable amount of energy in wind by the rotor of the WT is 59 % of the maximum available energy, known as Betz limit [9]. The power in the air (P_w) flowing at a speed, v_w through an area A is given by

$$P_w = \frac{1}{2}\rho A v_w^3 \tag{2.1}$$

where ρ is the air density (1.225 kg/m^3). The power constant C_p is defined for a particular WT as the ratio of the power transferred to the WT to the power extracted from the air as

$$C_P = \frac{P_m}{P_w}. \tag{2.2}$$

So the mechanical power i.e. the power transferred to the WT can be found from P_w using the following equation

$$P_m = \frac{1}{2}\rho A v_w^3 C_P . \tag{2.3}$$

This states that the output power is proportional to the third power of the wind speed [10]. But this statement is not true for all wind speeds. As can be shown in Figure 2-3, equation (2.3) holds for the speed range from cut-in to nominal speed. After that the power drops, and above cut-out speed, it goes to zero [11]. The cut-in speed is the minimum speed at which the turbine delivers power. The rated wind speed gives the rated output power and the cut-out speed is the maximum speed at which the turbine is allowed to deliver power [10].

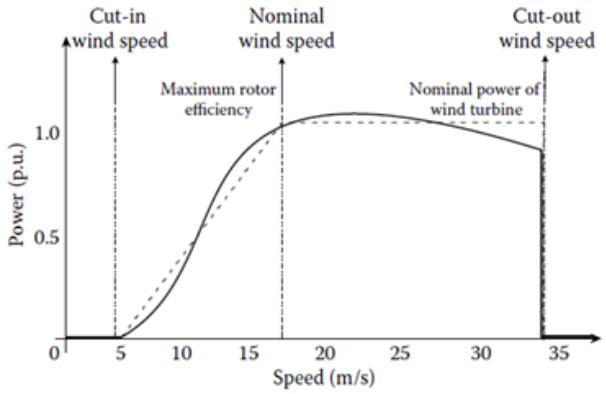

Figure 2-3. Power Curve Characteristics of a WT [11]

2.2.1.2. Wind turbine technology

A WT can be categorized based on the orientation of spin, power capacity and the rotor speed of the turbine. Based on axis of rotation, WT can either be horizontal-axis wind turbine (HAWT) or vertical-axis wind turbine (VAWT), shown in Figure 2-4 [12]. The HAWT, compared to VAWT, has higher energy conversion efficiency and a lower torque fluctuation. So even after being costly and tough maintenance, HAWT is used in wind farms. Based on generation capacity, the WTs can be classified as small (< 20 kW), medium (20 ~ 300 kW) and

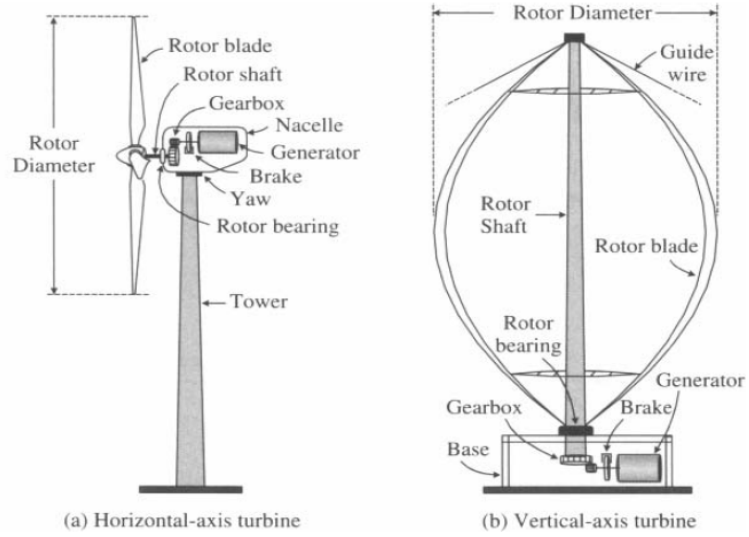

Figure 2-4. Classification of WT Based on Orientation of Spin [12]

large (a few MW) WTs. Finally, based on the rotor speed, the WT can be categorized as fixed-speed and variable-speed turbines. As the name suggests, the fixed-speed turbines rotate at a fixed speed (slip = 1 ~ 2 %) [13], that depends on the gear box ratio, stator frequency (f_s) and number of generator poles. This type of WES is designed to reach maximum energy conversion efficiency only at that fixed speed; at all other speeds, the efficiency drops. Alternatively, the variable-speed systems can be controlled to achieve the maximum efficiency for all wind speeds which makes it more suitable for power generation and other applications. The Variable-speed WT captures about 5 % more energy annually than a fixed-speed system [14]. Generators and power converters used for these systems are different and will be depicted in the next section.

2.2.2. The generator and conversion unit

No particular criterion has been set for a wind energy conversion system (WECS) to decide what generator and energy conversion unit to use. A brushless DC (BLDC) generator, permanent magnet synchronous generator (PMSG), induction generator or synchronous generator is used for this purpose [10], [12].

For fixed speed systems, squirrel cage induction generators (SCIGs) are used exclusively. They have the simplest configuration (Figure 2-5) as no controller is needed. The system only needs a soft starter to limit the high inrush current and a capacitor bank to supply reactive power. The transformer output can be directly connected to the grid or to an isolated load.

Variable speed systems can be classified based on the converters' power rating. Either partially rated converter with doubly-fed induction generator (DFIG) or fully rated converter with SCIG, PMSG or wound rotor synchronous generator (WRSG) can be used. Figure 2-6 shows the DFIG based WECS which in today's power market is the most popular and shared 47% of world energy market in 2002 [13]. A wound rotor induction generator can be controlled

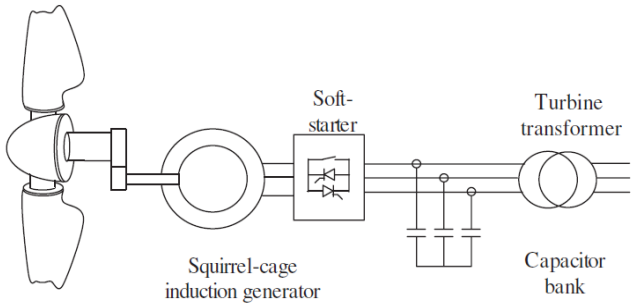

Figure 2-5. A Complete WECS using Fixed Speed WT [10]

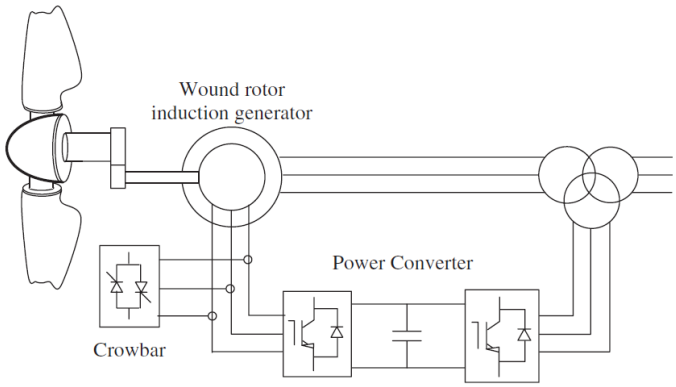

Figure 2-6. A Variable Speed WECS using DFIG and Partially Rated Converter [10]

by accessing its rotor circuitry via slip rings. Since both stator and rotor windings can transfer power between generator shaft and the electrical network, it is termed as “doubly-fed”. At sub-synchronous speeds, the converter takes power from the grid, converts it and feeds controllable voltage into the rotor at slip frequency. At super-synchronous speeds, the converter extracts power from rotor and supplies to the grid. The main advantage of a DFIG based systems is that its power converter has to process only the slip power i.e. about 20 ~ 30 % for a slip range of ± 30 % [3], [15]. The fraction depends on the allowable sub- and super-synchronous speed range [16]. So a converter of lower power rating can be used that not only reduces the cost of the system, but also increases the total efficiency. The ratio of the converter’s size to the WT rating is equal to half of the rotor speed span [14]. It is able to provide power beyond the system rating without causing any overheating [17]. They also allow decoupled active and reactive power

control [18], use of small filters, and provide higher efficiency [19]. Ref [20] recommends DFIG to support network as their presence dampens the power oscillation of other synchronous generators in the network.

Figure 2-7 illustrates a WECS with fully rated power converter. As its in-line with the generator it carries the full stator power to grid or load. So the converter rating is the same as that of the generator. The system can compensate for reactive power and smoothly connect to the grid. But its main disadvantage is the high converter rating that increases the system loss and reduces efficiency and also raises the total cost of the system. The design of the control system for a fully rated converter is much complicated compared to that of a partially rated converter. The system has an advantage that, if implemented with permanent magnet synchronous generators (PMSGs), it does not need any rotor injection, thus can totally get rid of the rotor copper losses. Again, the PM machines can have higher number of poles (lower synchronous speed), so the gearbox is not needed for increasing the rotational speed. It not only increases system's efficiency and reduces cost, but also ensures reliability and low maintenance [14].

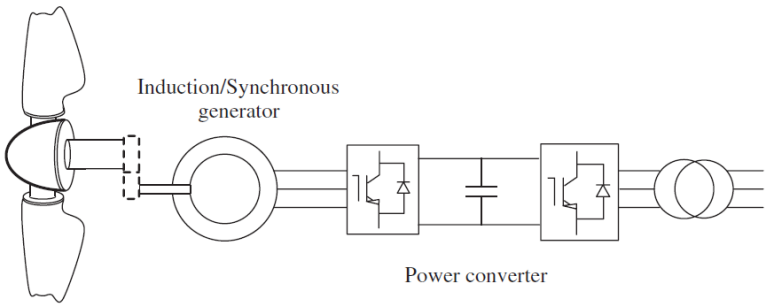

Figure 2-7. A Fully Rated Converter Connected Variable Speed WECS [10]

2.2.3. Maximum power point tracking of WECS

For super-synchronous speeds i.e. above rated wind speed, active or passive stall control or pitch control is applied for obtaining the rated power from the WT. But for sub-synchronous

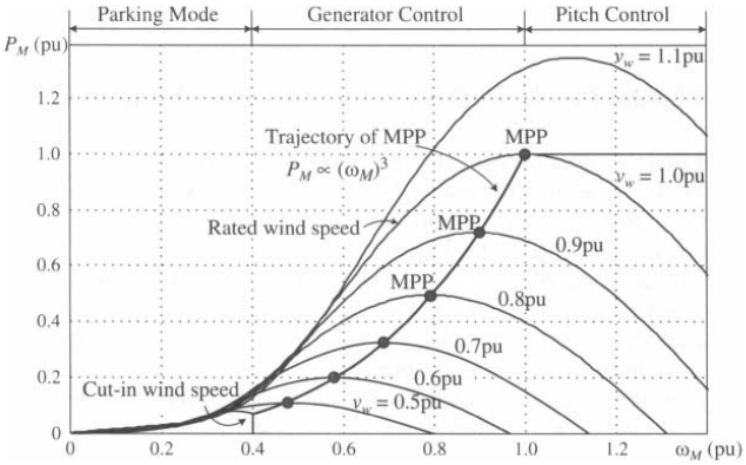

Figure 2-8. P_m versus WT Speed Characteristics for Various Wind Speed with MPP Locus [12]

speeds, the generator is controlled for attaining maximum power point (MPP). Figure 2-8 shows a set of mechanical power output (P_m) versus generator speed curves for different wind speeds. A locus shows the MPPs for different wind speeds, same as that given in equation (2.3). Below cut-in speed (0.4 pu or 5 ms^{-1}), the power drops to zero, named as parking mode and above rated speed (1 pu or 12 ms^{-1}), a desired power level can be attained using pitch control. For the speed range in between, the pitch angle is set to zero and rotor injection is controlled to achieve a certain generator speed that sets the new operating point for the system. Thus with ever changing wind speed, a new generator shaft speed is attained to extract the maximum power from the turbine corresponding to the speed.

The MPP equation can be derived from equation (2.3) as follows:

$$P_m = \frac{1}{2}\rho A v_w^3 C_P \tag{2.3}$$

$$P_m \propto v_w^3 \tag{2.4}$$

$$\omega_m \propto v_w \tag{2.5}$$

$$P_m \propto \omega_m^3 \quad (2.6)$$

$$P_m = K_{Popt} \cdot \omega_m^3 \quad (2.7)$$

$$P_m = T_e \cdot \omega_m \text{ and} \quad (2.8)$$

$$T_e = K_{Topt} \cdot \omega_m^2 \cdot \quad (2.9)$$

In these equations, ω_m is the generator speed which is linearly related to the turbine speed (v_w), and K_{Popt} and K_{Topt} are the optimum power and torque coefficients that can be determined from the machine ratings or given by the turbine manufacturer. Equation (2.7) and (2.9) gives the maximum power and maximum torque equations respectively [12]. They can be used as the reference for the power or torque loop of the controller. The controller minimizes the error between the reference and actual power or torque to generate the required rotor voltage. Thus the maximum power is achieved for all wind speeds.

2.3. Photovoltaic Energy

Figure 2-1 shows the solar (photovoltaic) to be the third most potential renewable energy source. But after 2007, the photovoltaic (PV) generation capacity is rising at a rate higher than biomass and geothermal and the rate is even higher than that of wind. From 2009 to 2010, the growth rate of wind energy is 24.53%, whereas the growth rate for PV energy is about 73.91 % [21]. PV output can be used directly or through a DC-DC converter to feed isolated DC loads or charge batteries. Using a boost regulator followed by DC-AC converter [22], the PV power can also be fed to the grid.

2.3.1. PV cells

A PV panel is an array of several series and parallel connected PV cells. Each PV cell generates electrical energy from the solar radiation absorbed by the cell following photovoltaic

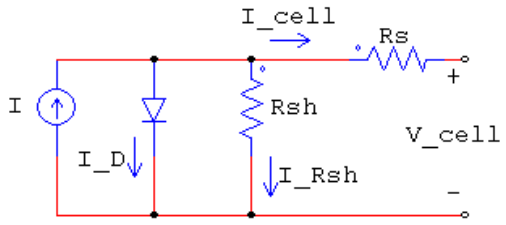

Figure 2-9. Equivalent Circuit of a Solar Cell

(PV) effect. The PV effect somehow relates to photoelectric effect (release of electron upon exposure to solar radiation), but the process is different. In PV effect, the energy of the photons in the absorbed light is transferred to the electrons of the semiconductor device and the electrons move from the valence band to conduction band of the atom. This builds up a voltage (about 0.5 ~ 0.6 V) between the electrodes of the cell and when the external circuitry is completed, a current flows. Connecting the cells in series gives a higher output voltage and when connected in parallel, a higher current can be achieved.

2.3.1.1. Current-voltage and power-voltage relations of a PV panel

The electrical equivalent circuit of an ideal PV cell is basically a current source in parallel with a diode. Figure 2-9 is the practical model of a PV cell with a series resistance (R_s) and a shunt resistance (R_{sh}). The current-voltage relation of a PV panel can be derived as [11], [23], [24],

$$I_{cell} = I - I_D - I_{Rsh} \tag{2.10}$$

where, I_{cell} is the current from the cell, I is the photogenerated current, I_D is the current in the parallel diode, I_{Rsh} is the current in R_{sh}. I_D can be given by Shockley diode equation as

$$I_D = I_o(\exp\left[\frac{q \,.\, V_{Rsh}}{n \,.\, k \,.\, T}\right] - 1) \tag{2.11}$$

where I_o is the reverse saturation current, q is elementary charge in coulomb, V_{Rsh} is the voltage

across R_{sh}, n is the diode ideality factor, k is the Boltzmann's constant, T is absolute temperature in Kelvin. Then from Ohm's law and Kirchhoff's voltage law, the following equations can be written

$$I_{Rsh} = V_{Rsh}/R_{sh} \tag{2.12}$$

$$V_{Rsh} = V_{cell} + I_{cell} . R_s \tag{2.13}$$

where V_{cell} is the voltage across the output terminals of the panel, and R_s is the series resistance. Combining equations (2.10) to (2.13), we can get the current-voltage relation given by

$$I_{cell} = I - I_o \left(\exp\left[\frac{q . (V_{cell} + I_{cell} . R_s)}{n . k . T} \right] - 1 \right) - \frac{V_{cell} + I_{cell} . R_s}{R_{sh}} . \tag{2.14}$$

Neglecting the low current in the R_{sh} branch, equation (2.14) can be written as follows

$$I_{cell} = I - I_o \left(\exp\left[\frac{q . (V_{cell} + I_{cell} . R_s)}{n . k . T} \right] - 1 \right) . \tag{2.15}$$

Equation (2.15) can also be written as a voltage-current relationship [25] as

$$V_{cell} = \frac{n . k . T}{q} \ln\left[\frac{I - I_{cell} + I_o}{I_o} \right] - I_{cell} . R_s . \tag{2.16}$$

A more general form of the voltage-current relationship incorporating the number of cells connected in series (N_s) and that connected in parallel (N_p) can be written as

$$V_{cell} = \frac{N_s . n . k . T}{q} \ln\left[\frac{I - I_{cell} + N_P . I_o}{N_P . I_o} \right] - \frac{N_s}{N_P} I_{cell} . R_s . \tag{2.17}$$

The voltage-current and power-voltage relationship of a PV array is figured out for different irradiance level from Figure 2-10 [24]. The open-circuit voltage (V_{OC}) of the panel, derived from equation (2.14) using $I_{cell} = 0$, is given by

$$V_{OC} = \frac{n . k . T}{q} \ln\left[\frac{I}{I_o} + 1 \right] = V_{Rsh} \tag{2.18}$$

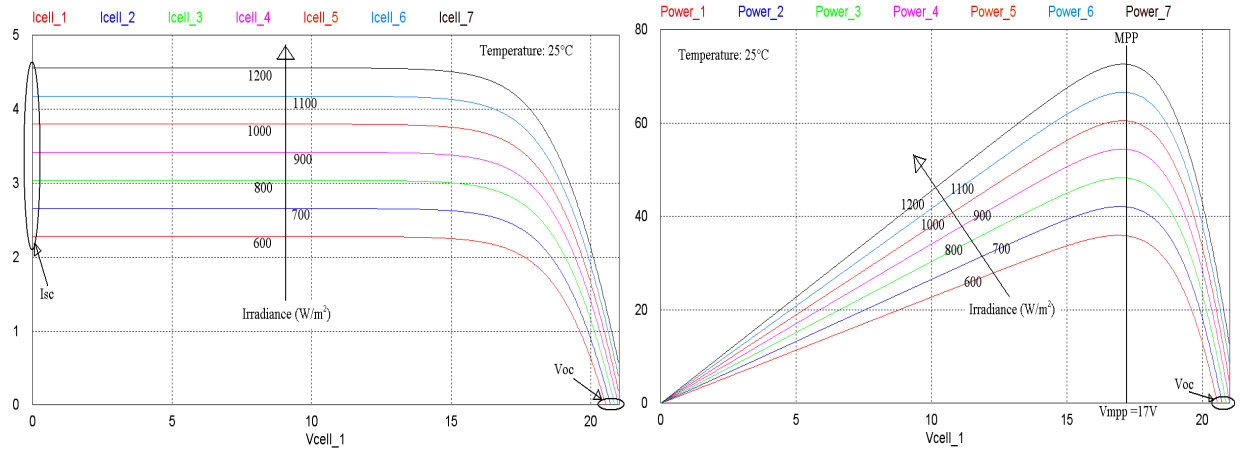

Figure 2-10. Voltage-Current and Power-Voltage Characteristics of a Solar Panel

Similarly with $V_{cell} = 0$, the short circuit current is given by,

$$I_{SC} = I \,. \tag{2.19}$$

2.3.2. Maximum power point tracking of PV panel

The maximum power point (MPP) is the particular point associated with each solar irradiance and ambient temperature at which the power from a solar panel is the highest. The MPP for different irradiance levels can be located on the power-voltage curves in Figure 2-10. Figure 2-11 shows both current versus voltage and power versus voltage curves on the same graph [26]. Basically a maximum power point tracking (MPPT) unit is a controller that automatically adjusts the electrical load i.e. the cell current (I_{cell}) to achieve the MPP. For a variable load connected across panel terminals, the operating point is the intersection of the panel I-V curve and the load I-V curve (a straight line with slope =1/R_{load} for resistive load). So the power output depends on the connected load. Since I_{cell} and V_{cell} are related exponentially, the MPP occurs at the knee of the I-V curve where $dP/dV = 0$. At this point, the load resistance and the characteristic resistance of the panel are equivalent.

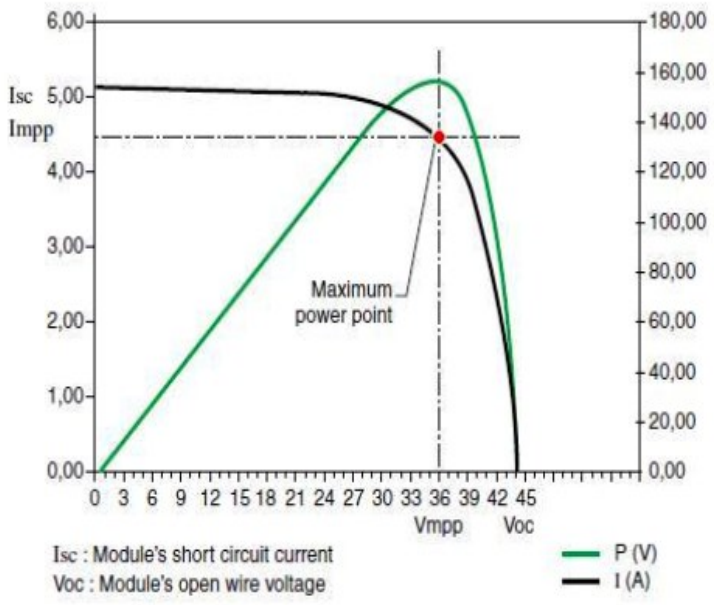

Figure 2-11. Maximum Power Point of a Solar Cell [26]

2.3.2.1. Different MPPT techniques

Several techniques have been used to control the output current and voltage of the panel to ensure operation at MPP [4], [11], [25], [27]-[31]. Some are briefly explained below.

- Incremental conductance based MPPT technique

The basis of this method is that, at the MPP, the instantaneous conductance (I_{cell}/V_{cell}) is equal to negative of incremental conductance ($\Delta I_{cell}/\Delta V_{cell}$) i.e.

$$\frac{I_{cell}}{V_{cell}} = -\frac{\Delta I_{cell}}{\Delta V_{cell}}. \tag{2.20}$$

At a point to the right of the MPP,

$$\frac{I_{cell}}{V_{cell}} < -\frac{\Delta I_{cell}}{\Delta V_{cell}} \tag{2.21}$$

and at a point to the left of the MPP,

$$\frac{I_{cell}}{V_{cell}} > -\frac{\Delta I_{cell}}{\Delta V_{cell}} \tag{2.22}$$

This is the most commonly used method for the MPPT of PV panels. This method offers good performance under varying atmospheric conditions but it needs four sensors [25]. A quite similar method is proposed in [27] where the input resistance of the converter seen by the panel is changed depending on the atmospheric condition.

- Perturb and observe based MPPT technique

This technique observes the power output with changing current [25]. The power is the maximum only for a specific current. While in operation, the current is changed in one direction and the power is measured. If the power is increased, some more change is made in the current in the same direction. Otherwise, if the power is decreased, the current change is made in the opposite direction, which should increase the power. Thus the point of optimum power is achieved. This method is simple and easy to implement.

- Fractional open-circuit voltage based MPPT technique

An approximately linear relationship exists between the open-circuit voltage (V_{OC}) and the voltage at MPP (V_{MPP}) which is the basis of this technique. The relationship is

$$V_{MPP} = k_v \, . V_{OC} \, . \tag{2.23}$$

Here k_v is a constant with a value of 0.71 ~ 0.78 [11], [30] depending on the array characteristics. It is the easiest to implement but since the value of k_v is not the same for all PV panels, it needs to be calibrated every time.

- Fractional short-circuit current based MPPT technique

Similar to equation (2.23), there exists a linear relation between the short-circuit current (I_{SC}) and the current at MPP (I_{MPP}) which is the basis of this technique. The relationship is

$$I_{MPP} = k_i \, . I_{SC} \, . \tag{2.24}$$

Here k_i is a constant with a value varying in the range of 0.78 ~ 0.92 depending on the array characteristics [11], [30]. Similar to fractional open-circuit voltage based MPPT technique, it is also easy to implement but has the same calibration problem. One other problem with this technique is that the short-circuit current (I_{sc}) is not the same for all irradiance levels. This problem can be solved by measuring the I_{sc} at a specific interval by shorting the panel terminals and controlling the actual cell current to maintain the fraction (k_i) [4]. This technique is used in the thesis.

- Ripple correlation control (RCC) based MPPT technique

This technique correlates the time-derivative of the time-varying power with time-derivative of time-varying voltage or current. Below MPP, if $dv/dt > 0$ or $di/dt > 0$, then $dp/dt > 0$ and over MPP, if $dv/dt > 0$ or $di/dt > 0$, then $dp/dt < 0$. Thus at MPP,

$$\frac{dp(t)}{dt} \cdot \frac{dv(t)}{dt} \text{ or } \frac{dp(t)}{dt} \cdot \frac{di(t)}{dt} = 0 . \tag{2.25}$$

At a point to the right of the MPP,

$$\frac{dp(t)}{dt} \cdot \frac{dv(t)}{dt} \text{ or } \frac{dp(t)}{dt} \cdot \frac{di(t)}{dt} < 0 \tag{2.26}$$

and at a point to the left of the MPP,

$$\frac{dp(t)}{dt} \cdot \frac{dv(t)}{dt} \text{ or } \frac{dp(t)}{dt} \cdot \frac{di(t)}{dt} > 0 . \tag{2.27}$$

There are other MPPT techniques like linearized I-V characteristics based technique, fuzzy logic control based technique, neural network based technique, current sweep based technique, DC link capacitor droop control based technique, etc.

2.4. Conclusion

Wind and solar PV energy are the two most promising alternative sources of electricity generation and also the two used in the proposed hybrid system. Different types of WTs and their

comparison, the generators and theoretical analysis of maximum power point tracking of wind are described in the first half of this chapter. As stated, WESs are of two types – the fixed speed and the variable speed, among which the variable speed is of prime interest in today's power market. Variable speed systems also can be of two types based on the rating of the power converter used: one that uses DFIG with low rated converter and the other that uses the fully rated converter.

In the second half of the chapter, details have been given for solar energy and PV panels. Characteristics of PV cells and some commonly used MPPT techniques have been investigated throughout. In this thesis, the DFIG with partially rated converter is used and the PV panel is used to supply the rotor of a DFIG. In the absence of the sunlight, a fraction of the stator power of the DFIG will be taken for rotor injection. The MPPT for both wind and solar (using fractional short-circuit current based technique) is ensured in the system. Details of the system components will be given in the upcoming chapters.

CHAPTER 3. POWER CONVERTERS FOR WIND AND PV ENERGY SYSTEMS

3.1. Introduction

The power generated from renewable energy sources cannot be used directly to feed the grid or isolated loads. It needs to be converted to a proper form which depends on the grid or the load. In WESs, the amplitude and frequency of the output voltage changes with wind speed, so does the maximum power point. Thus a power converter is needed to adjust the rotor injection of the DFIG based on the wind speed to extract the maximum power from the wind turbine while maintaining a consistent stator output. It is important to select a proper converter for the system, based on its rating, cost, losses, reliability, etc. and to design an efficient and fast controller. Similarly in PV systems, the output is a DC voltage and most often a low voltage whose value depends on the number of cells in series. So it needs to be boosted to a higher level while ensuring the maximum power extraction from the panel for all irradiance level as well.

The power converters basically consist of capacitors, inductors, transformers and most importantly switched-mode semiconductor devices [32], [33]. Different semiconductor devices, mainly silicon based, like power diode, power MOSFET, bipolar junction transistor (BJT), insulated gate bipolar transistor (IGBT), thyristor (SCR, GTO, MCT, IGCT), etc. are used in power processing. The criteria, based on which the device is selected for a particular application, are the on-state resistance, breakdown voltage and switching time. According to the type of input and output voltage, a power converter can be classified as, AC-DC converter (rectifier), DC-DC converter (chopper), DC-AC converter (inverter), and AC-AC converter (cycloconverter). These converters along with their operations and input-output waveforms will be discussed in details in this chapter.

3.2. AC-DC Converter: Rectifier

Rectifiers are the type of converters that can transform AC voltage into DC voltage. The power supplied by the utilities is AC whereas most electrical equipments run on DC which requires a rectifier. Rectifiers are used in different electrochemical processes, adjustable speed drives (both AC and DC), HVDC systems, power supplies, etc. Rectifiers are basically of two types based on the switching device used– diode rectifiers and thyristor rectifiers.

Since diode works based on the voltage across it, it can be used to generate a unidirectional voltage from an AC source. Based on this different rectifier configurations have been developed and being widely used. In this study, the concentration will be on three-phase full bridge diode rectifiers (Figure 3-1). It has six diodes, two per phase. In each $1/6^{th}$ of cycle ($\pi/3$), a combination of two diodes – one from the upper converter (one with the highest positive voltage) and one from the lower converter (one with the highest negative voltage) conducts to complete the external circuit. Thus each diode will conduct for $2\pi/3$ [33]. The average output DC voltage of a full bridge rectifier is,

$$V_{oavg} = 1.35 \, . V_{L-Lrms} \tag{3.1}$$

where $V_{L\text{-}Lrms}$ is the rms value of the line to line input voltage. Using thyristor rectifiers, also known as phase-controlled rectifiers, the average output voltage of the rectifier can be varied by varying the triggering angle (α) of the thyristor.

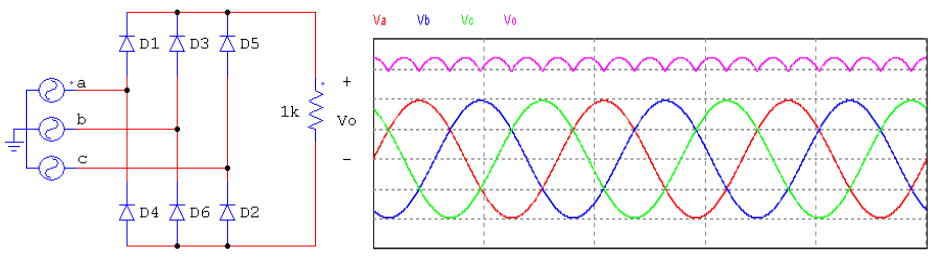

Figure 3-1. Three-Phase Full-Wave Diode Rectifier

3.3. DC-DC Converter

Using a DC-DC converter or chopper, an input DC can be converted into a DC of desired magnitude and polarity. DC-DC converters can be designed with reduced size, high efficiency, and more reliable operation [34]. Each DC-DC converter basically consists of inductors, diodes, high-frequency switches and capacitors. The inductor basically limits the current peak and stores energy. The capacitor does the same for voltage, i.e. it smoothes the voltage output and stores energy [35]. The voltage level can also be regulated in spite of the changes in the input voltage and output current [36]. Some researchers have proposed double-input DC-DC conversion systems [37], [38], [39] which can be very useful in a hybrid renewable energy system proposed in this work. Depending on the level of input and output, DC-DC converters can be classified as buck, boost, buck-boost, etc. that will be described in this section.

3.3.1. Buck converter

A buck or step-down converter provides an output voltage equal to or less than the input voltage. It uses a PWM controller with some energy storage components to hold the output when the switch is off [36]. Figure 3-2 shows a buck converter with the switching pulse, the inductor current and the output voltage. As can be seen from the circuit, when the switch is on (T_{on}), source supplies energy, the diode is reverse biased and the inductor and capacitor are charged. Then during the off-period (T_{off}), the inductor and capacitor discharge through the load. The change in the inductor current is the same for both T_{on} and T_{off}. The following equations give the duty cycle (D) and the average output voltage V_o:

$$D = \frac{T_{on}}{T} = T_{on} \cdot f_{sw} \tag{3.2}$$

$$V_o = D.V_i \tag{3.3}$$

where f_{sw} is the switching frequency of the converter, T_s is the switching period ($T_s = 1/f_{sw}$) and V_i is the input DC voltage. The output level in a buck converter is set by the duty cycle (D) of the switch. Since $D < 1$, for a buck converter, $V_o < V_i$.

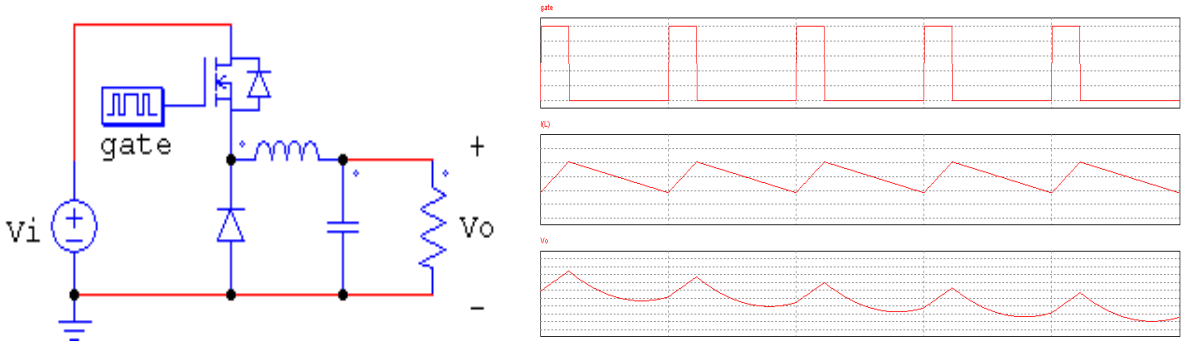

Figure 3-2. Buck Converter (D = 22.22 %)

3.3.2. Boost converter

The output voltage of a boost converter also depends on the duty cycle and it is higher than the input voltage. Figure 3-3 shows a boost converter with the switching pulse, the inductor current and the output voltage. As can be seen from the circuit, when the switch is on (T_{on}), the inductor is charged and the capacitor is discharged through the load. Then during the off period (T_{off}), both the DC input voltage and inductor supply power to the load and charges the capacitor. The change in the inductor current is the same for both T_{on} and T_{off}. The following equation

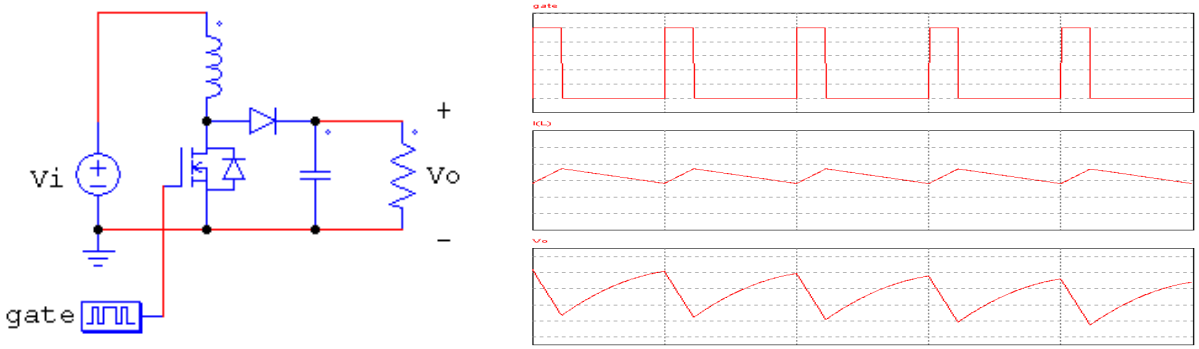

Figure 3-3. Boost Converter (D = 22.22 %)

describes the of the boost converter:

$$V_o = \frac{V_i}{1 - D}. \tag{3.4}$$

Since $0 < D < 1$ in equation (3.4), $V_o > V_i$ giving an output voltage higher than the input voltage. A boost converter, digitally controlled in real time, is implemented in Ref [34].

3.3.3. Buck-boost converter

The features of both buck and boost converters are combined in a buck-boost converter. Depending on the duty cycle, the output voltage can either be lower or higher than the input voltage. An important feature of this converter is that the polarity of the output will be opposite to that of the input voltage. The following equation gives the input-output relation of the buck-boost converter:

$$V_o = -\frac{DV_i}{1-D}. \tag{3.5}$$

The circuit, the switching pulse, the inductor current and the output voltage of a buck-boost converter are shown in Figure 3-4. When the switch is on (T_{on}), the inductor is charged and the capacitor supplies the load. When the switch is off (T_{off}), the inductor supplies the capacitor and load. As can be seen from equation (3.5), for $D < 0.5$, the converter will operate in the buck mode and for $D > 0.5$, it will operate in the boost mode.

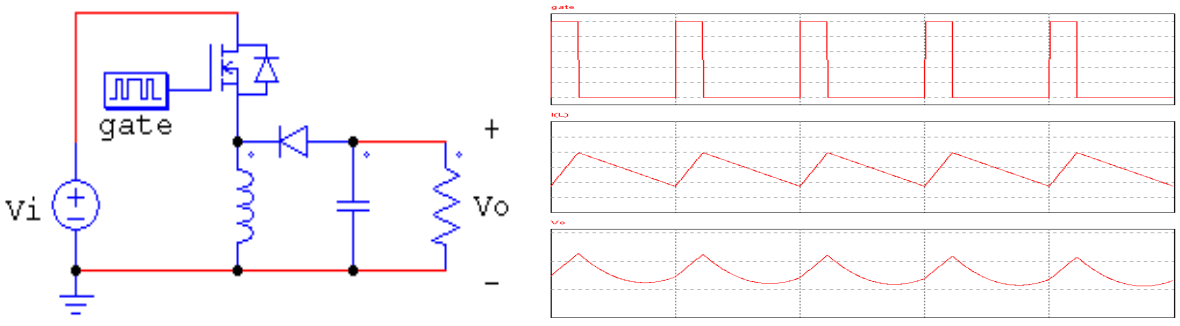

Figure 3-4. Buck-Boost Converter (D = 22.22 %)

3.4. DC-AC Converter: Inverter

Inversion is the process opposite to rectification i.e. it generates an AC voltage from a DC source. The goal here is to generate an AC signal of a desired shape (sinusoidal), voltage amplitude and frequency using switching devices, filters, control circuits and transformers. Inverters are used in switching power supplies, variable-frequency drives and power conversion of PV sources. Inverters are basically of two types – voltage source inverter (VSI) and current source inverter (CSI). In this study, a three-phase VSI will be considered. Most inverters presently used are two-level inverters. They can be also designed to have a multilevel output.

3.4.1. Power quality

There are several restrictions imposed on an AC source so that the system powered by the source functions properly without considerable loss of performance. The parameters related to power quality are – continuity of service, change in voltage magnitude, voltage or current transients and harmonics. To ensure the highest power quality, the harmonics at the output have to be minimized. There are several definitions related to harmonics like the lowest order harmonic (LOH), total harmonic distortion (THD), distortion factor (DF), etc.

The LOH is the order of the lowest harmonic present in a waveform. The THD is defined as the ratio of the sum of all harmonic powers to the fundamental frequency's power. It can also be expressed in terms of rms voltages as the following equation:

$$\text{THD} = \frac{\sqrt{V_2^2 + V_3^2 + V_4^2 + \ldots\ldots\ldots V_\infty^2}}{V_1} = \frac{\sqrt{\sum_{k=2}^{\infty} (V_k^2)}}{V_1} \tag{3.6}$$

Here V_k is the rms value of k^{th} harmonic in the voltage and for the fundamental frequency, $k = 1$. The THD is computed from the amplitudes of all the harmonics without considering their order. The higher order harmonics are not as important as lower order ones since the former can

easily be eliminated using a filter. Thus it is very important to consider the order of the harmonics in expressing the distortion as done by DF. It is defined by the following equation for up to n^{th} harmonic:

$$\text{THD} = \frac{\sqrt{\frac{V_2^2}{2^4} + \frac{V_3^2}{3^4} + \frac{V_4^2}{4^4} + \dots\dots\dots\dots\frac{V_n^2}{n^4}}}{V_1} = \frac{\sqrt{\sum_{k=2}^{\infty}(\frac{V_n^2}{n^4})}}{V_1} \tag{3.7}$$

As can be seen from (3.7), the higher the order of the harmonic, the lower is its effect in distorting the waveform.

3.4.2. Three-phase two-level inverters

These inverters are widely used as AC power supplies and for AC motor drives. Figure 3-5 shows a three-phase quasi-sine inverter. It is made up of three half-bridges in parallel with 120° phase shift, analogous to a three-phase system. Six switches ($Q_1 - Q_6$) with six anti-parallel diodes ($D_1 - D_6$) are connected in a bridge configuration, similar to a bridge rectifier. Based on the six gate pulses, the output can be square wave, quasi-sine wave or pure sine wave. It is

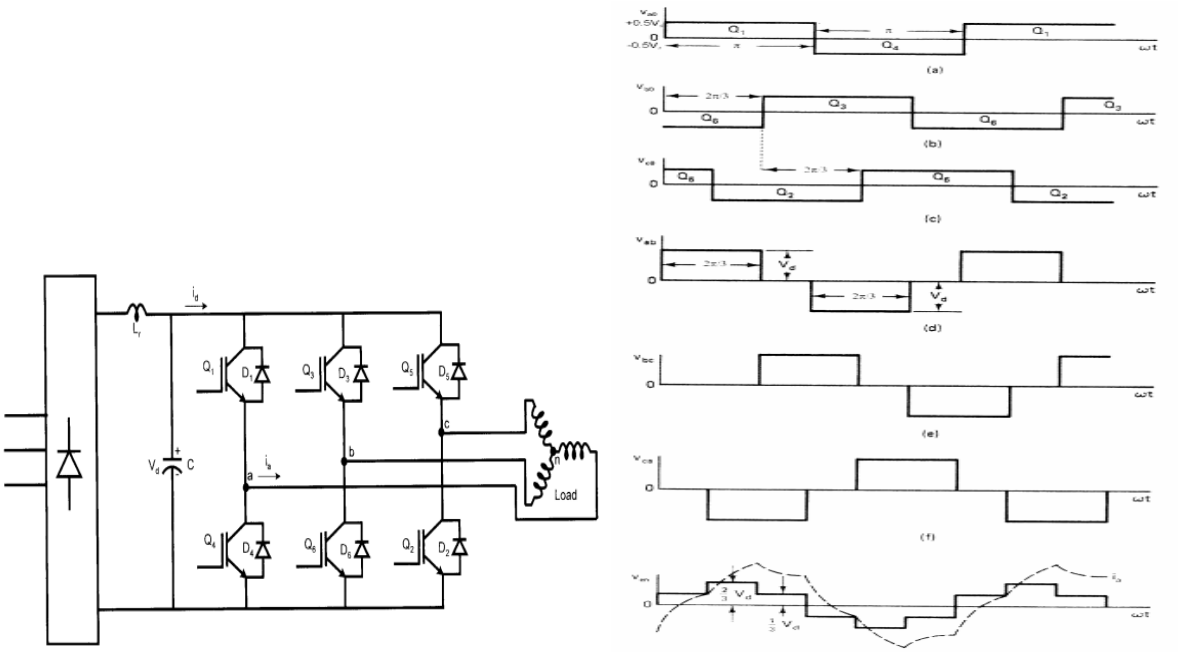

Figure 3-5. Three-Phase Quasi-Sine Inverter: Power Circuit and Waveforms [33], [61]

always easy to generate a square wave from an inverter, but such an inverter cannot be used in most power applications because of their high harmonic content. Most equipment require, for better operation, a pure sine wave (THD < 3 %), which is hard to generate. A more feasible and cheap solution is to use quasi-sine wave inverter whose voltage shape is quite similar to square wave with some dead time between two transition states. It can replace sine wave inverter in many applications including rotor injection of DFIG in wind applications [40]. Figure 3-5 shows the output waveforms of the quasi-sine inverter.

3.4.3. Multilevel inverter

In a two-level inverter, the line voltages have only three levels ($+V_{dc}$, 0, $-V_{dc}$). But in a multilevel inverter, the number of levels in the output voltage can be increased and if it can be increased to infinity, it will be a pure sine wave inverter with zero harmonic distortion. The reduced harmonic distortion allows the use of lower reactive components and has lower losses and torque pulsation [41]. For high voltage operations with two-level inverters, either devices with higher ratings have to be used or they have to be connected in series that increases the cost of the system. With matched series-connected devices, it is easy to share the static voltage, but very difficult to share the dynamic voltage. Multi-level inverters are normally used for high power applications, above 2 ~ 3 MW [6] and high voltage ratings even up to 6 kV [42], since they use more devices per phase. They also reduce ripple in torque output. The disadvantages of the multilevel inverter are the complexity of the power and control circuitry. Its modulation scheme is difficult [6] and offers a higher switching loss lowering the upper limit of switching frequency. Another problem is the voltage unbalance in the DC bus [43]-[45]. They find application in high capacity AC-drives, VAR compensators, HVDC transmission systems, active filtering, etc [44].

3.4.3.1. Types of multilevel inverters

Multilevel inverters are of three types [46], [47]: (a) diode clamped inverter, (b) flying capacitor inverter, and (c) cascaded-inverter with separate DC sources.

a) Diode clamped inverter

This inverter (*m* level) uses (*m*-1) dc-link capacitors across the dc bus to provide the voltage levels and clamping diodes to set the mid-point of each series connected high-speed switches to the proper voltage level (Figure 3-6(a)). So by proper switching of the devices (similar to that explained in [46]), the output voltage can be clamped to that particular voltage. Figure 3-6 shows the output line voltage of an inverter that has ($2m$-1 = 9) voltage levels. Among the multilevel inverters, this topology is the most popular [6], [41]-[46], [48]. A three-phase three-level diode-clamped inverter also known as neutral-point-clamed (NPC) inverter, used for rotor injection of DFIG in this work, will be discussed in detail in later chapters.

b) Flying capacitor inverter

This type of inverter (Figure 3-6(b)) uses the same *m*-1 capacitors (dc-link capacitors) to create the *m* voltage levels, but the diodes are replaced by a network of capacitors (inner-loop balancing or flying capacitors). In this inverter, the flying capacitors set the mid-point to the desired voltage level based on the switching of the transistors. This configuration is more flexible than the diode-clamped one, as the same voltage level can be achieved at the output with more than one switching combination [46]. Since this circuit needs a higher number of storage capacitors, this inverter is expensive and bulky and also its control is very complicated.

c) Cascaded-inverter with separate DC sources (SDCs)

Cascaded-inverter, as the name suggests, is a combination of series connected single-phase full-bridge inverters, each supplied by a separate DC source and thus eliminating the use

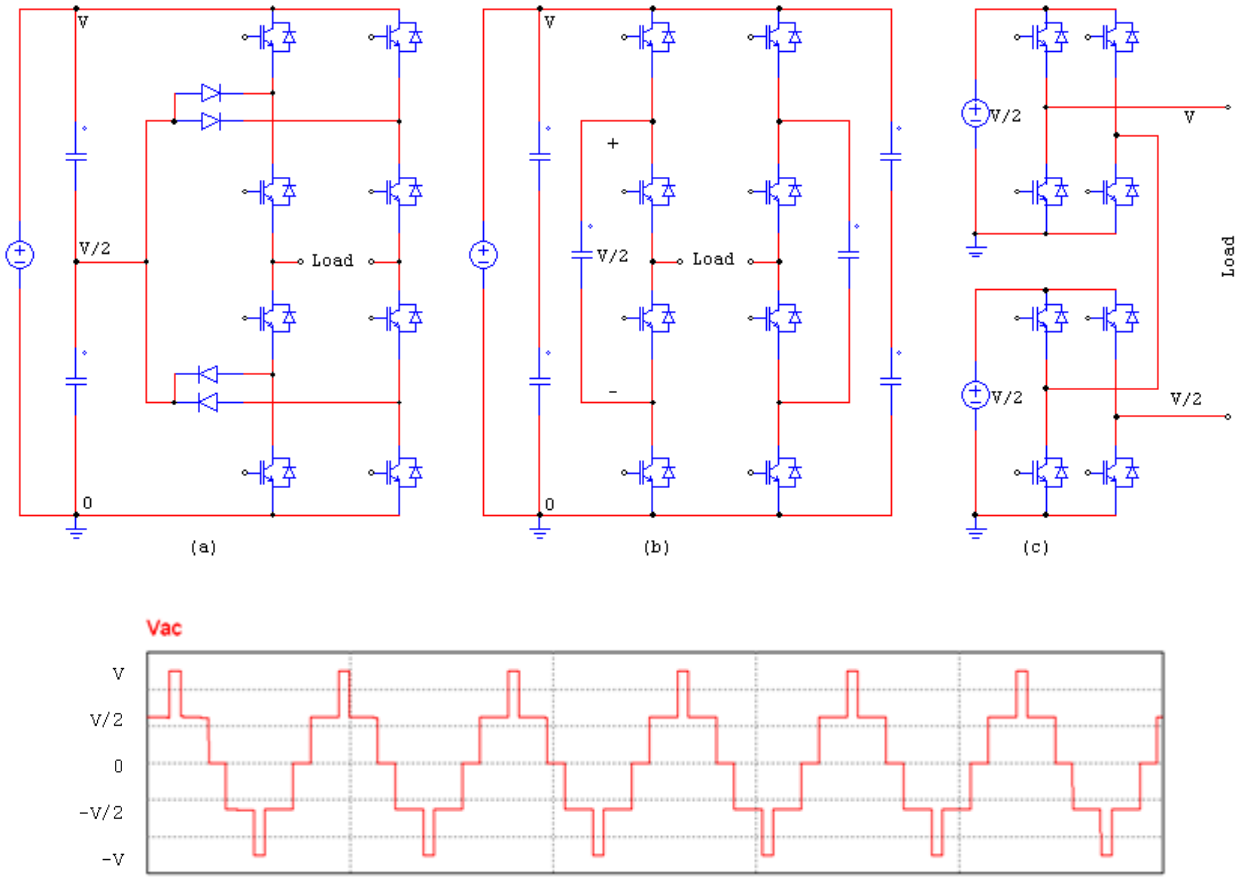

Figure 3-6. Single-Phase Three-Level Diode-Clamped, Flying-Capacitor and Cascaded Inverter with the AC Output Waveform

of extra clamping diodes or storage capacitors (Figure 3-6(c)). The output terminals of each inverter are connected in series to provide a multilevel output by controlling the conduction angle of the switches in each inverter. An *m*-level cascaded-inverter requires (*m*-1)/2 SDCs with (*m*-1)/2 full-bridges. Though this inverter requires the least number of components and do not need any clamping-diode or flying-capacitor, its application is somewhat limited because of the need of SDCs [46]. Also it requires a complicated control circuit.

3.4.4. Pulse width modulation (PWM) techniques in inverter

The six-step inverter is simple to control and also has a lower switching loss due to the use of a switching frequency which is the same the inverter frequency. But the output, being a

square wave, has a high harmonic content with all lower order harmonics present. Filtering them is costly and increases the physical size of the system. PWM techniques provide a solution to these problems. It is assumed that the switching frequency is very high compared to the inverter frequency. PWM-VSIs have replaced converters using thyristor due to their improved dynamic performance, extensive operating region, lower line harmonics and ability to operate at improved power factors [42]. The PWM can be of various types like, uniform PWM, sinusoidal PWM (SPWM), selected harmonic elimination PWM, minimum ripple current PWM, space-vector PWM, random PWM, hysteresis band current control PWM, delta modulation, sigma-delta modulation, etc. SPWM is the one considered in this work and will be explained here.

In SPWM, a sine wave of fundamental frequency (f_m) is compared to a high frequency (f_{sw}) triangular-wave carrier to generate the switching pulses. In a three phase inverter, the same carrier is used for all the three phases. Figure 3-7 shows the SPWM for a three-phase inverter with the control voltage, the carrier signal, the generated gate pulse for Q_1, and the output line and phase voltages. There are two important parameters in SPWM – amplitude modulation index (m_a) and frequency modulation index (m_f), given by,

$$m_a = \frac{V_m}{V_{tri}} = \frac{V_{A01m}}{V_{dc}/2} \tag{3.8}$$

$$m_f = \frac{f_{tri}}{f_m} \tag{3.9}$$

where $V_{m,}$ V_{tri} and V_{A01m} are the amplitudes of the modulated (control) signal, carrier signal and fundamental component of phase A voltage respectively and f_m and f_{tri} are the control signal and carrier frequency. The output voltage level depends on m_a and the harmonic profile of the output depends on m_f. The ratio m_f should be an odd integer and also a multiple of 3 for a three-phase system. If m_f is not odd, DC components and even-order harmonics will be present in the output

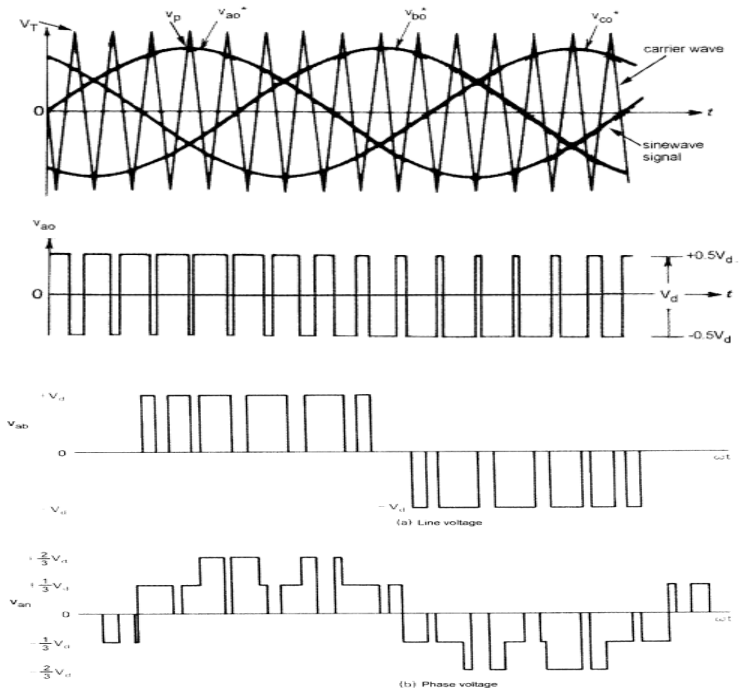

Figure 3-7. Waveforms of Three-Phase Sine PWM Inverter [33]

of inverter, and if m_f is not an integer, sub-harmonics will arise [49].With a higher m_f, the LOH is high and the output practically approaches a sine wave but it also offers a higher switching loss.

3.4.4.1. Types of SPWM techniques

SPWM can be either bipolar or unipolar. In unipolar SPWM, the output voltage in each half cycle is either $+V_{dc}$ or $-V_{dc}$ while in the case of bipolar SPWM, both $+V_{dc}$ and $+V_{dc}$ levels will be present in each half cycle. They generate different harmonic profiles, with bipolar SPWM giving LOH = $m_f - 2$ and unipolar SPWM giving LOH = $2m_f - 3$.

3.4.4.2. Switching frequency

One important parameter associated with all these circuits is the switching frequency of the converter. Since the efficiency of a power converter is very important, all the losses, like fixed losses, conduction losses and switching losses, must be considered in the design. The switching loss in these devices are given by [32],

$$P_{sw} = W \cdot f_{sw} \quad (3.10)$$

where W is the energy lost in the switching process in one switching period and f_{sw} is the switching frequency. The total loss in a converter is given by

$$P_{loss} = P_{fixed} + P_{cond} + W \cdot f_{sw} \quad (3.11)$$

where P_{fixed} is the fixed loss and P_{cond} is the conduction loss. Equation (3.11) shows that the switching loss dominates at higher switching frequencies. So, for a converter, there is an upper limit for f_{sw} above which the efficiency drops rapidly and it is actually the frequency at which the switching loss is equal to the sum of other losses. The critical switching frequency (f_{cri}) is given by,

$$f_{cri} = \frac{P_{fixed} + P_{cond}}{W} \quad . \quad (3.12)$$

3.5. AC-AC Converter: Cycloconverter

The last type of converter is the one used to convert one frequency to another in a single step. It is mostly used in very large variable frequency drives like cement and ball mill drives, rolling mill drives, slip power recovery Scherbius drives and aircraft power supplies (400 Hz) [33]. In addition to the desired frequency, a cycloconverter generates the harmonics and sub-harmonics (frequencies lower than output frequency) and inter-harmonics (frequencies between harmonic frequencies). The elimination of unwanted frequencies requires large filters. A cycloconverter also produces a DC component if output frequency is exactly one half of the input frequency.

3.6. Power Converters in WECS with DFIG

A discussion on the basic improvement of power electronics and the power converters in WES perspective is given in Ref [13], [14], [17]. In a DFIG, the converter is used as an interface

between the grid and the rotor (Figure 2-8). The converters commonly used in DFIG are static Kramer drives, back-to-back PWM converters, Vestas converter systems, matrix converters, etc. A particular converter is selected based on its reliability, efficiency and cost.

A static Kramer drive consists of a diode rectifier as the rotor-side converter and an SCR inverter as the grid-side converter. This drive considers only operation at super-synchronous speeds at which power flows out of the generator from both the stator and the rotor [50]. A more technically improved version is the back-to-back PWM converter [15], [16], [18]-[20], [51]-[60]. They can operate in both sub-and super-synchronous speed region using the bi-directional power flow capability of the converter. Here, both the rotor- side and grid-side converters are bi-directional PWM-VSIs. This system can work in all four quadrants. In the sub-synchronous speed region, the grid-side converter (rectifier) is controlled to give a constant DC-link voltage and reactive power. On the other hand, the rotor-side converter (inverter) ensures the MPPT operation. The sequence of conversion is just the reverse for operation at super-synchronous speeds. The third system, proposed by Vestas, works in the sub-synchronous speed range. It consists of a diode rectifier as the grid-side converter and a PWM inverter as the rotor-side converter. A similar topology is also used in the proposed work. A matrix converter converts the variable-frequency AC from the generator to a fixed-frequency AC in a single step [17]. Its advantage is that no energy storage system is needed and only one controller is required. But the number of semiconductor switches required is very high.

3.7. Conclusion

A DFIG-based WECS requires a converter for proper rotor injection to ensure a constant output voltage at constant frequency. In the proposed system, the rotor of the DFIG is supplied either from the grid or from the PV panel. For drawing injection power from the grid, an AC-

DC-AC conversion unit is needed which in this study uses a three-phase full-bridge diode rectifier, a boost regulator and a multilevel inverter. For drawing injection power from PV panels, a boost regulator and an inverter are used. The outputs of the boost regulators in either case charge a battery that provides the DC-link voltage to the inverter. All the converters to be used in the study are described and comparison is made between similar types.

CHAPTER 4. PROPOSED HYBRID RENEWABLE ENERGY SYSTEM

4.1. Introduction

Hybrid renewable energy system (HRES) is not a new term in renewable energy sector. Rather many researchers have already worked on it [14], [39], [62]-[64]. In all the existing hybrid systems in these references, two or more energy sources work in parallel to supply the grid. Generally they all feed a DC bus being independent of the other sources. The DC power is then inverted and connected directly to the grid. The proposed scheme is different from the existing topologies since it uses both wind power to supply the load or grid and takes solar as a supplementary power for rotor injection of the generator. This chapter describes the overall system and all the components including the machine, the converters and their controllers. It also shows a comparison of the conventional two-level inverter and the three-level inverter that has been used in the system. All the simulation results are also included.

4.2. System Overview

The main component of the proposed system is a DFIG driven by a wind turbine. Its stator either supplies a grid or an isolated load. The rotor is supplied with variable-frequency variable voltage three-phase power. As the wind speed changes with time, the shaft speed of the turbine as well as the generator speed changes. This speed change affects the stator output power, voltage amplitude and frequency. But the output needs to be regulated to give a constant frequency and amplitude. So if we can adjust the rotor power with wind speed i.e. generator speed, we can maintain a constant output from the DFIG.

In the proposed system, a new power converter has been used to adjust the rotor injection with wind speed. The proposed converter uses a diode rectifier followed by a boost regulator and

a multilevel inverter, whereas most DFIG-based WECSs use two back-to-back connected two-level VSIs [3], [15], [16], [18]-[20], [51]-[60], [65], [66], with a very few using multilevel VSIs [3], [67]. The main challenge with a multilevel inverter is their complicated power and control circuitry. But the advantages they provide, like high voltage/power handling capacity and lower harmonic distortion cannot be overlooked. The thesis presents a multilevel inverter based rotor injection system for DFIG. The DC link voltage of the inverter is provided by two rechargeable batteries which are charged either using a small fraction of the stator power through a converter system or using PV power depending on its availability. Ref [64] presents a comparable hybrid scheme which mainly focuses on power factor correction and frequency control.

Figure 4-1 shows the complete block diagram of the proposed system simulated using the software PSIM [68] and MATLAB-Simulink [69]. PSIM has a wind turbine model with variable wind speed and blade pitch angle input and a wound rotor induction machine model that can be used as a DFIG. PV power is used as the main source to supply the rotor. Using a boost converter, MPPT has been ensured for the PV output at all irradiance levels. This system can provide a constant DC voltage for the inverter. In the absence of sunlight, a portion of the stator output is used for the same purpose. The three-phase AC voltage from the stator is first rectified using a simple diode rectifier instead of a PWM rectifier. This not only reduces the complexity of the system but eliminates the need for additional control. The rectified output thus have higher ripple in it but the use of the boost regulators provide a constant dc-link voltage (100V) for the inverter. The presented scheme uses a three-level neutral-point-clamped (NPC) inverter whose output voltage is controlled by controlling the amplitude modulation index. The control voltage needed for the inverter switches is generated by the inverter controller based on vector control scheme that uses the d-q axis current control [51]. Using maximum power point tracking

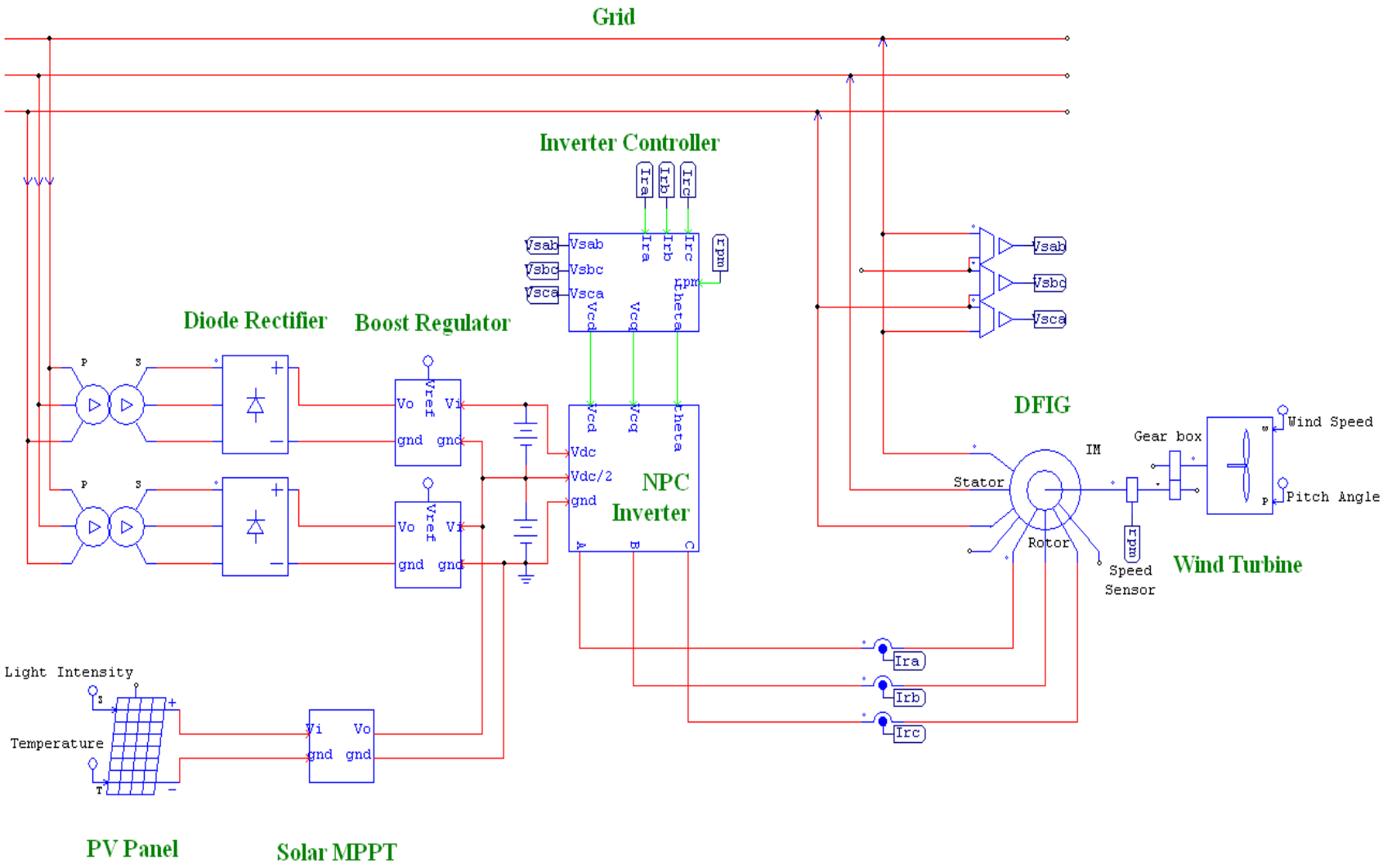

Figure 4-1. Block Diagram of Proposed System

(MPPT) technique, the torque reference (T_{eref}) is calculated for a given generator speed. The q-axis current reference (i_{rqef}) is then computed from the reference torque. On the other hand, the d-axis current reference (i_{rdref}) is generated by controlling the stator voltage. The d-q axis reference rotor currents provide the control voltage (v_{ctrl}) which is used to generate the gate pulses for the 12 switches of the inverter. The inverter voltage is then fed to the rotor of the DFIG.

4.3. Boost Regulator

The system uses a boost regulator for maintaining a constant DC link voltage. Reference [70] uses a buck-boost regulator for a WECS using a PMSG. In a boost regulator, the voltage stress on the chopper switch is lower and the leakage inductance of the generator and cable can be used as an equivalent DC inductor [71]. Figure 4-2 shows the schematic and the input and output waveforms of a boost regulator. Its output is constant irrespective of the fluctuations in the input voltage and load. It is done by varying the duty cycle (D) for the switch so that the output voltage given by the equation,

$$V_o = \frac{V_i}{1 - D} \tag{4.1}$$

is always constant. The output voltage is compared to a preset reference voltage. The error is

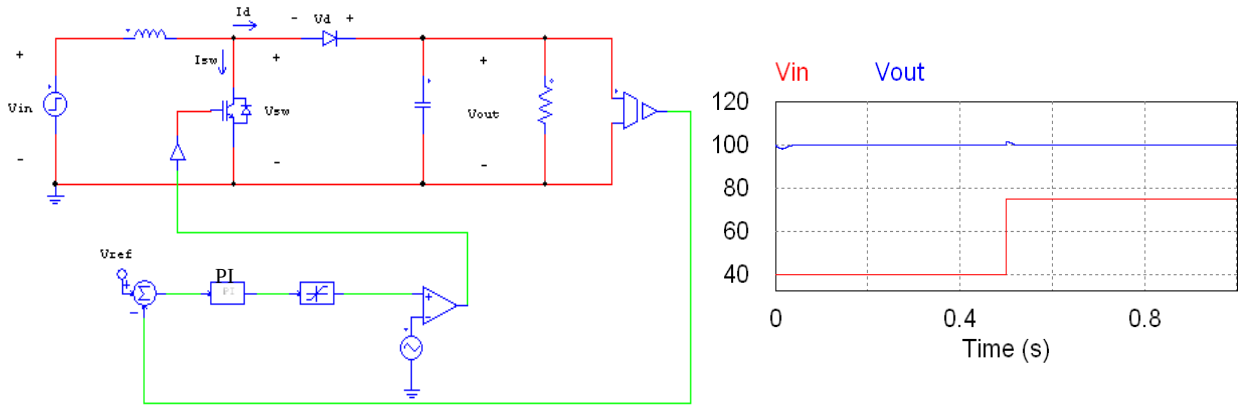

Figure 4-2. Boost Regulator and Output Waveform

send to the PI controller which gives a control voltage. The control voltage is then compared to a high-frequency carrier (f_{sw}) to generate the switching pulses. So when the output is higher than the reference voltage, D is reduced by the PI controller and the output automatically comes down and vice versa. The output voltage in Figure 4-2(b) shows a constant level of 100 V regardless of the change in input voltage and there is also a very low settling time and overshoot, much lower compared to Ref [34] and [72]. For fast simulation, the average model of the boost regulator has been used. Most average models of DC-DC converters use a transformer whose turns-ratio are controllable and is equal to (1-D):1 [73]. Average modeling has also been used for discontinuous current mode of operation [73]. In the present study, an average model is used for continuous mode of operation, since the inductor is large enough to avoid any discontinuity in current. Figure 4-3 gives the regulator output voltage ($v_o(t)$), voltage across ($v_{sw}(t)$) and current through the switch ($i_{sw}(t)$), voltage across ($v_d(t)$) and current through the diode ($i_d(t)$) and current through the inductor ($i_L(t)$). It's actually used to derive the relations between $v_{sw}(t)$ - $v_d(t)$ and $i_{sw}(t)$ - $i_d(t)$ based on their relation to $v_o(t)$ and $i_L(t)$ respectively in terms of $d(t)$ which can be written as:

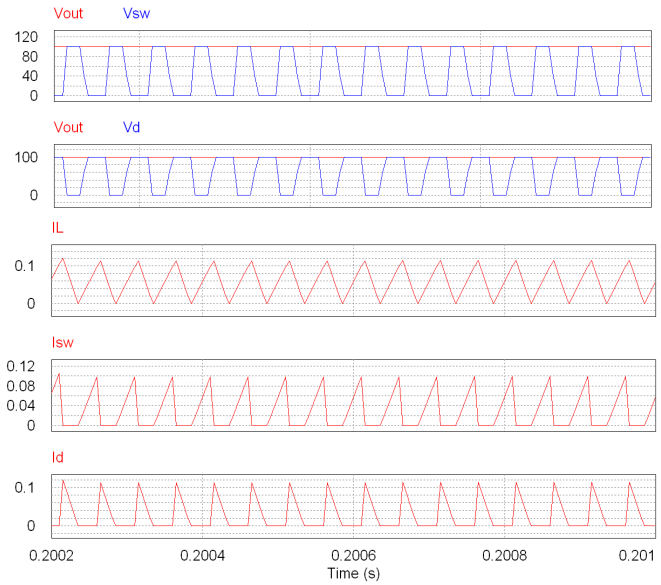

Figure 4-3. Waveforms of a Boost Converter used for Average Modeling

$$v_{sw}(t)|_{T_s} = \big(1 - d(t)\big).\, v_o(t)|_{T_s} \tag{4.2}$$

$$i_{sw}(t)|_{T_s} = d(t).\, i_L(t)|_{T_s} \tag{4.3}$$

$$v_d(t)|_{T_s} = d(t).\, v_o(t)|_{T_s} \tag{4.4}$$

$$i_d(t)|_{T_s} = \big(1 - d(t)\big).\, i_L(t)|_{T_s} \tag{4.5}$$

where $d(t)$ is the duty cycle and T_s is the switching period. Equation (4.2) and (4.4) can be combined to give

$$v_{sw}(t)|_{T_s} = \left.\frac{1 - d(t)}{d(t)} \,.\, v_d(t)\right|_{T_s}. \tag{4.6}$$

Similarly equation (4.3) and (4.5) can be combined to give

$$i_d(t)|_{T_s} = \left.\frac{1 - d(t)}{d(t)} \,.\, i_{sw}(t)\right|_{T_s}. \tag{4.7}$$

The switch-diode combination in the boost converter can be replaced by two dependent sources as shown in Figure 4-4. Both the dependent sources have a gain factor of (1 - *x*)/*x* in equation (4.6) and (4.7) where $x = d(t)$. Table 4.1 gives the values of different parameters used in the boost regulator.

4.4. MPPT for PV Panel

As stated earlier, a PV panel is used to provide rotor injection power to the DFIG. It can operate in parallel to the supply path from the stator to charge the batteries. Figure 4-5 shows the MPPT scheme based on fractional short-circuit current method [4]. The short-circuit current is measured by applying a long pulse to the switch. Using a sample and hold circuit, the value of the short-circuit current is held up until the next pulse is applied. This value is used to calculate the current at the MPP using the following equation

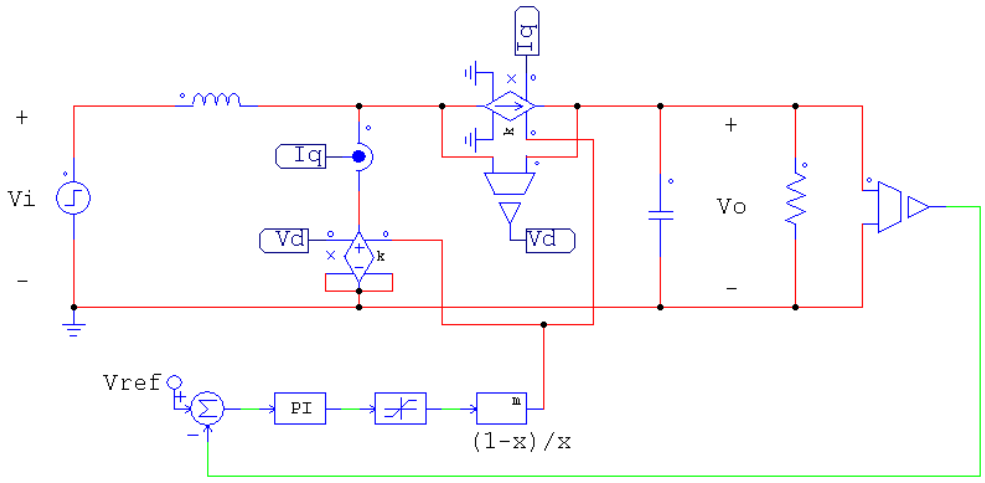

Figure 4-4. Average Model of Boost Regulator

TABLE 4.1 BOOST REGULATOR PARAMETERS

Parameter	**Value**	**Unit**
Inductance	570	µH
Capacitance	660	µF
Proportional Constant, K_p	0.1	-
Integral Constant, K_i	10	-
Time Constant, τ	10	ms
Switching Frequency, f_{sw}	20	kHz

$$I_{MPP} = 0.921 \, . \, I_{SC} \tag{4.8}$$

where the constant 0.921 is specific for this PV panel. Then I_{MPP} is compared to the actual current from the cell (I_{cell}) and the error is minimized using a PI controller. The output of the controller is compared to a high frequency (10 kHz) carrier wave to generate the gate pulse for the switch. The extended pulse has a frequency of 10 Hz and duty cycle of 0.075 %. Figure 4-5

also contains the power, voltage and current waveforms for the panel. The simulation results show that the output power from the panel closely follows the maximum power curve. A step in the maximum power is obtained by applying a step change in the light intesity (500 to 1000 W/m^2). For both levels of light irradiance, the average voltage is about 16.9V, where V_{MPP} is 17.1 V. Again the average cell currents for the two light levels are 1.75 A and 3.5 A where the

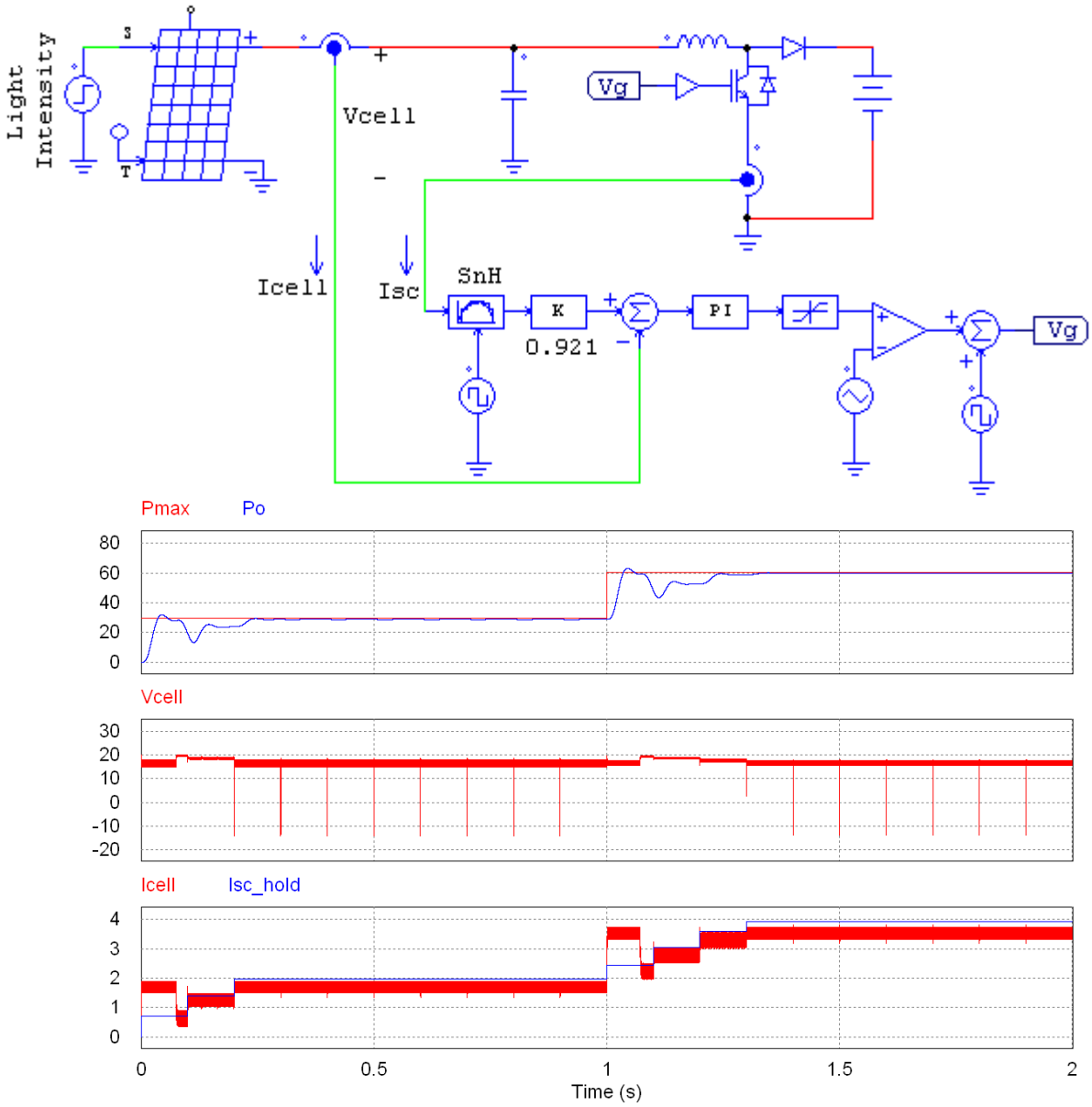

Figure 4-5. MPPT for PV panel and Tracking Response

values of I_{SC} are 1.9 A and 3.8 A respectively giving a ratio close to 0.921. The PV panel parameters and those of the MPPT circuit are given in Table 4.2 and Table 4.3. The L and C values are chosen as a compromise betwee settling time and ripple in output voltage and current.

4.5. Multilevel Inverter

The most important component of the WECS is the inverter. Unlike most of the existing systems which use a two-level (0, V_{dc}) inverter, this scheme uses a three-level (0, $V_{dc}/2$, V_{dc}) neutral-point-clamped (NPC) inverter. The line-to-line voltage thus has five levels in it (0, $+V_{dc}/2$, $+V_{dc}$, $-V_{dc}/2$, $-V_{dc}$). Figure 4-6 shows two three-phase inverters, a three-level NPC inverter and a conventional two-level inverter. Figure 4-7 gives the four gate pulses for phase A of the NPC inverter. The pulses for the Qa1 and Qa3 are complementary and similarly pulses for Qa2 and Qa4 are also complementary. Gate signal for Qa4 is 180° out of phase to that for Qa1. The operation of the main switches Qa1 and Qa4 is similar to the two switches of one phase in the conventional inverter. The auxiliary switches Qa2 and Qa3 along with diodes Da1 and Da2 help to provide an extra level (midpoint) in the output. In the first half of the cycle, Qa4 is off and Qa2 is on, as can be seen from the gate pulses. During this period, when Qa1 is on, the phase A voltage is V_{dc} and when Qa3 is closed, the phase A voltage is $V_{dc}/2$. Figure 4-8 shows the line-to-line voltages of a NPC inverter and a two-level inverter and also their filtered version clearly shows that NPC inverter's output is less distorted. Even though both inverters have the same LOH (m_f -4), the NPC inverter provides a lower THD, less than half to that of a two-level inverter. The performance of the two inverters when feeding the rotor of a DFIG is compared by calculating their THD. It is found that the THD of the system with three-level inverter is 12.33 % while the system with the two-level inverter have a THD of 24.8 % (f_{tri} = 600 Hz). For simple resistive loads without any filter, the THD becomes 42 % and 91 % respectively.

TABLE 4.2 PV PANEL PARAMETERS

Parameter	**Value**	**Unit**
No. of Cells	36	-
Standard Light Intensity	1000	W/m^2
Reference Temperature	25	°C
Series Resistance	0.008	Ω
Shunt Resistance	1000	Ω
Short Circuit Current	3.87	A
Saturation Current	21.6	nA
Band Energy	1.12	eV

TABLE 4.3 SOLAR MPPT PARAMETERS

Parameter	**Value**	**Unit**
Inductance, L	2	mH
Capacitance, C	0.2	μF
Proportional Constant, K_p	0.01	-
Integral Constant, K_i	10	-
Time Constant, τ	1	ms
Switching Frequency, f_{sw}	10	kHz
Frequency of Extended Pulse	10	Hz
Duty Cycle of Extended Pulse	0.075 %	-

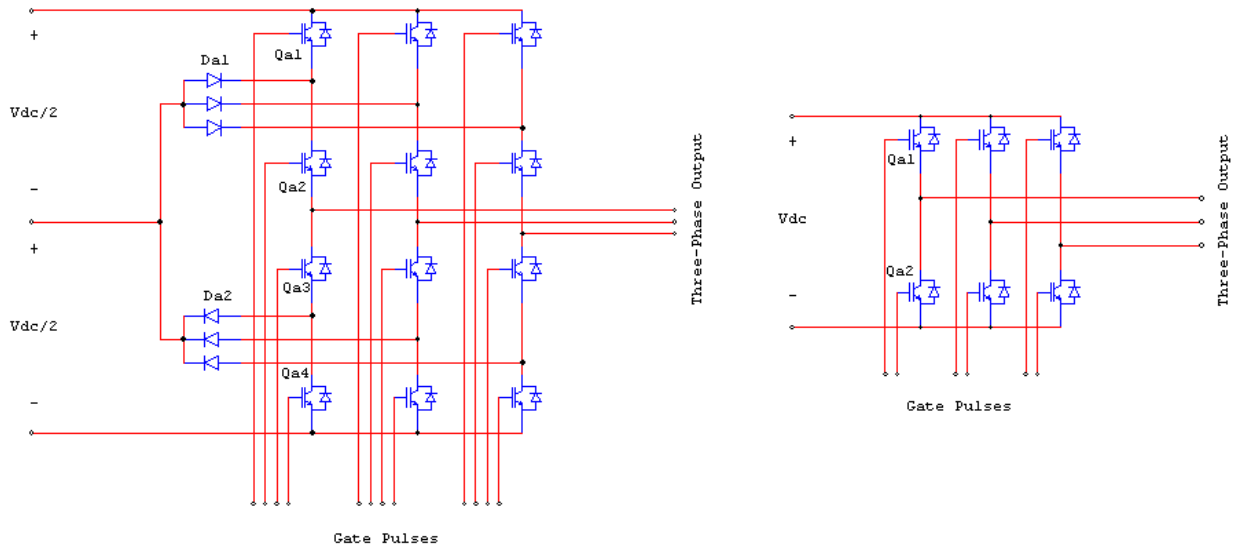

Figure 4-6. Three- and Two-Level Inverters

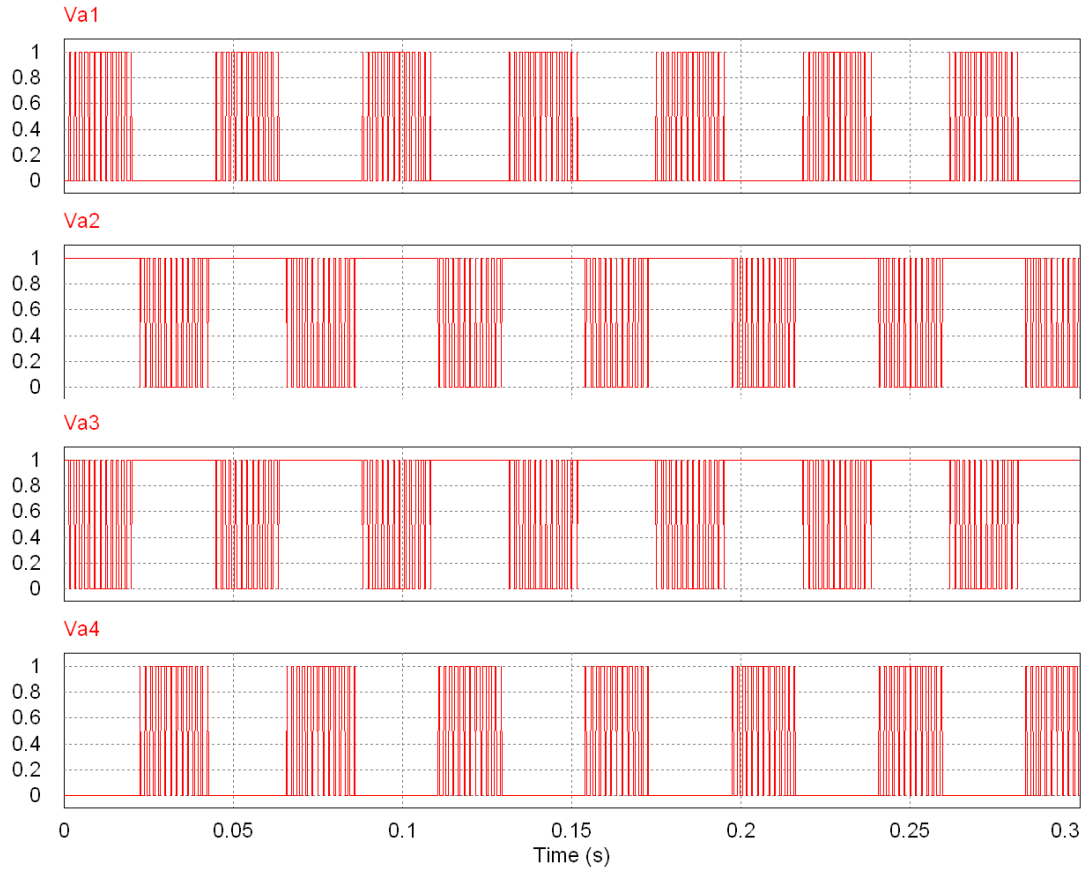

Figure 4-7. Gate Pulses for Phase A of the Three-Level NPC Inverter

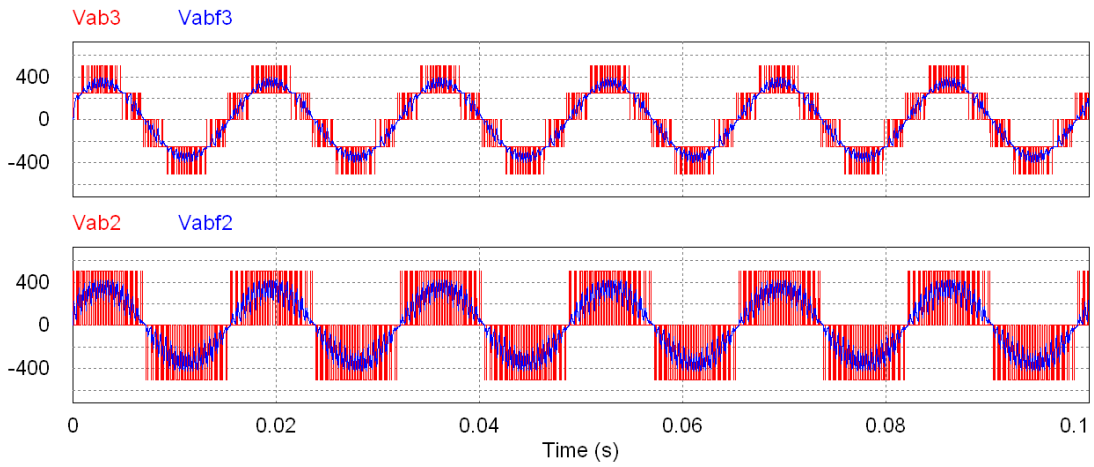

Figure 4-8. Output Waveforms for 3- and 2- Level Inverters w/o and with Filter (f_c = 1000 Hz)

4.6. Inverter Controller

To adjust the rotor injection with changing wind speed, a controller is needed to control the injection voltage level and the injection frequency. Ref [51] compares three different control schemes, i.e. slip control, flux magnitude and angle control (FMAC) and vector control, for a DFIG based WECS. Based on that analysis, it is found that slip and vector control is better in terms of robustness. The basis of vector control is to convert the three-phase currents into two phase currents in the direct and quadrature axes. It is easy to control these two currents since they are decoupled and can be controlled independently. While supplying the wind power to a load or grid, three things must be ensured: (a) maximum power extraction from wind turbine, (b) constant stator voltage amplitude, and (c) constant stator frequency. Figure 4-9 gives the inverter controller used in the proposed system. It has two loops. The inner loops which are faster control the rotor current and generate the control voltages for the inverter. In the inverter, these voltages are used to modulate the carrier signal in order to generate the gate pulses. One of the outer loop controls the shaft torque and the other one controls the stator voltage. For flux-based rotating frames, real power is controlled by controlling the q-axis components and reactive power is

controlled by controlling the d-axis components [53]. The output of the controller depends on the converter size, stator to rotor voltage ratio and modulation factor of converter (m_a). Different parts of the controller are explained in the following sub-sections.

4.6.1. Torque control for maximum energy extraction from wind turbine

The torque or power controller is designed for tracking the maximum power point of the turbine. It is done using the torque equation of a DFIG given in equation (2.9) which is

$$T_e = K_{Topt} \cdot \omega_m^2 \cdot \tag{4.9}$$

The value of K_{Topt} for this particular generator, calculated using the rated values, is 3.8195μ Nm/(rad/s)^2. Using the shaft speed of the generator, the reference torque is calculated using (4.9). This torque reference is then compared to the actual machine torque. In PSIM, a torque sensor is used to measure the actual torque and a PI controller, minimizing the torque error, generates the q-axis component of the rotor current reference. In hardware implementation, the reference torque is used to calculate the q-axis component of the rotor current reference. The electromagnetic torque of a generator is given by [7]

$$T_e = \frac{3 \cdot P}{2} (i_{sq} \cdot \lambda_{sd} - i_{sd} \cdot \lambda_{sq}) \tag{4.10}$$

where P is the number of machine poles, i_{sd} and i_{sq} are the d- and q-axis stator current components and $\boldsymbol{\lambda}_{sd}$ and $\boldsymbol{\lambda}_{sd}$ are d- and q-axis components of stator flux linkage.

The stator currents i_{sd} and i_{sq} can be expressed in terms d- and q- axis components of rotor currents (i_{dr} and i_{qr}) as

$$i_{sd} = (\lambda_{sd} - L_m \cdot i_{rd})/L_s \tag{4.11}$$

$$i_{sq} = (\lambda_{sq} - L_m \cdot i_{rq})/L_s \tag{4.12}$$

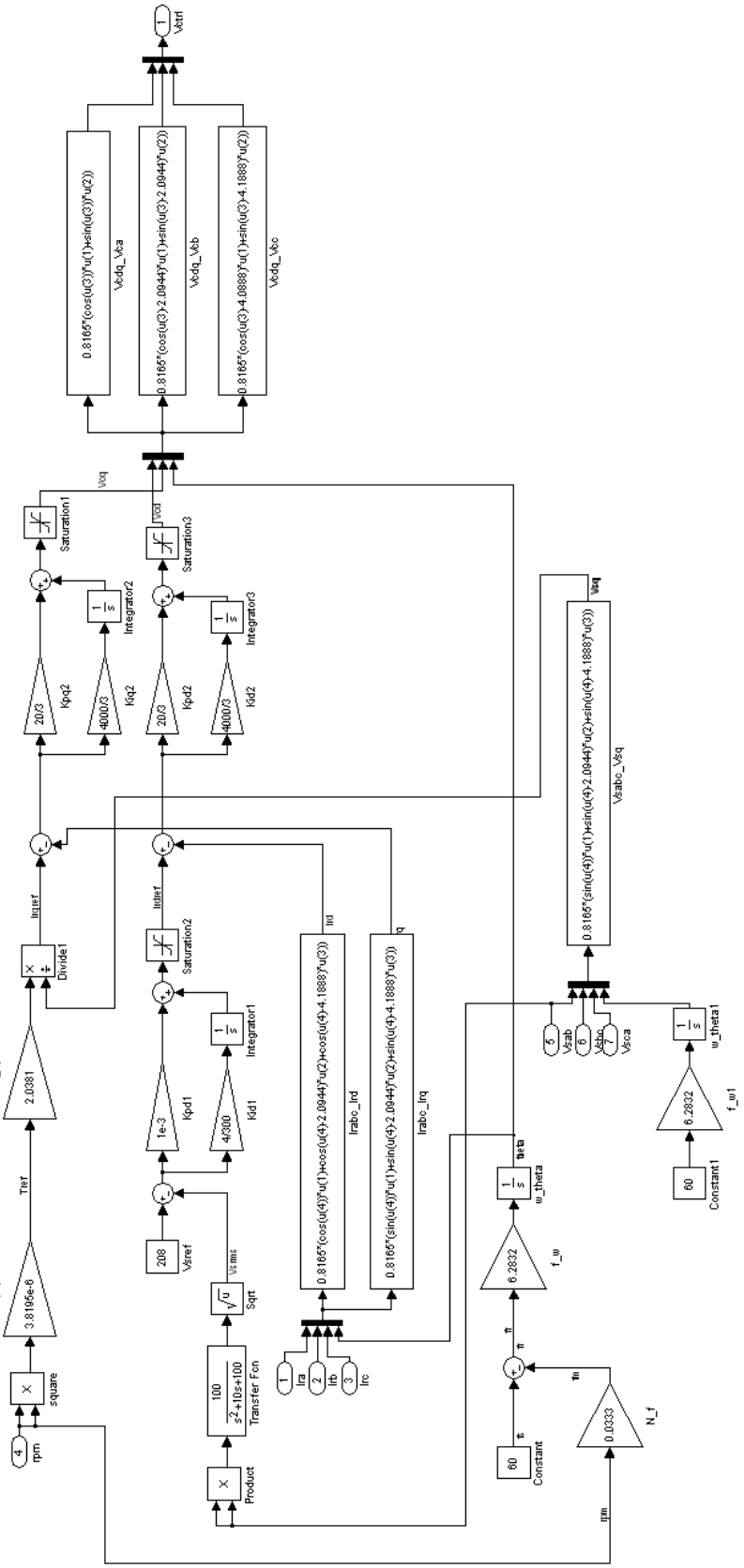

Figure 4-9. Inverter Controller

where L_s, L_r and L_m are stator, rotor and mutual inductances of the generator respectively. So equation (4.10) can be written as

$$T_e = \frac{3 \,.\, P \,.\, L_m}{2 \,.\, L_s} \left(- i_{rq} \,.\, \lambda_{sd} + i_{rd} \,.\, \lambda_{sq} \right). \tag{4.13}$$

Now the flux linkages can be written in terms of stator currents and voltages as

$$\lambda_{sd} = (v_{sq} - R_s \,.\, i_{sq}) / \omega_s \tag{4.14}$$

$$\lambda_{sq} = (v_{sd} - R_s \,.\, i_{sd}) / \omega_s \tag{4.15}$$

where R_s and R_r are the stator and rotor resistances, ω_s is the stator frequency in rad/s and v_{sd} and v_{sq} are the d- and q-axis stator voltage components. Substituting the values of flux linkages in equation (4.13) and neglecting R_s, which is very small for DFIG, we have

$$T_e = - \frac{3 \,.\, P \,.\, L_m}{2 \,.\, L_s} \left(i_{rd} \,.\, v_{sd} + i_{rq} \,.\, v_{sq} \right). \tag{4.16}$$

The use of stator flux oriented reference frame sets $v_{sd} = 0$. So equation (4.16) becomes

$$T_e = - \frac{3 \,.\, P \,.\, L_m}{2 \,.\, L_s} \, i_{rq} \,.\, v_{sq}. \tag{4.17}$$

from which the q-axis current reference can be obtained as

$$i_{rqref} = - \frac{2 \,.\, L_s \,.\, T_e}{3 \,.\, P \,.\, L_m \,.\, v_{sq}} = - \frac{2.0381 \,.\, T_e}{v_{sq}} \tag{4.18}$$

The reference for q-axis rotor current (i_{rqref}) can be computed from (4.18) and compared to the actual i_{rq} [10]. The error signal is applied to the PI controller to generate the q-axis component of control voltage (v_{cq}).

4.6.2. Constant stator voltage control

The d-axis part of the controller controls the stator voltage amplitude which can be done by adjusting the rotor injection voltage. The required rotor injection voltage (v_r) can be computed using the slip (s) and stator voltage reference (V_{sref}) from the following equation [19], [59]:

$$v_r = s\frac{v_{sref}}{a} \tag{4.19}$$

where *a* is the stator to rotor turns ratio. A PI controller is used to control the stator voltage and make it constant regardless of any change in the operating condition. The reference rms value of line-to-line stator voltage (208 V) is compared to the rms value of actual line-to-line stator voltage to generate the d-axis rotor current reference (i_{rdref}) which is then used to control i_{rd}. The error signal ($i_{rdref} - i_{rd}$) sets the d-axis component of control voltage (v_{cd}). An estimate of the initial stator-voltage PI controller constants is made using the following equations [56]:

$$K_{pd1} = \frac{L_m + L_r}{L_m \,.\, \omega_s \,.\, \tau} \tag{4.20}$$

$$\tau_{d1} = \frac{L_m + L_r}{R_r} \tag{4.21}$$

Using an arbitrary closed-loop time-constant (τ) of 10 ms and other machine parameters, the constants K_{pdl} and τ_{dl} are found to be 0.27 and 0.33 respectively.

4.6.3. Frequency control

The last component of the controller is the frequency controller which sets the frequency of the injected rotor voltage equal to the slip frequency. For a DFIG, the stator frequency (f_s) is equals the sum of the frequency at which the shaft rotates (f_{mech}) and the frequency of the injected voltage as (f_{sl}) [65]:

$$f_s = f_{mech} + f_{sl}. \tag{4.22}$$

For both abc - dq0 or dq0 - abc transformations, the slip frequency is used to calculate the angle. Thus the frequency of the injection voltages and currents generated by the controller are equal to f_{sl}. So the system does not require any phase-locked-loop for measuring the stator or rotor angle needed for Park's transformation.

All the parameters of the controller are specified in Table 4.4 and Table 4.5. The generated signals from the controller will be obtained in the next section.

TABLE 4.4 INVERTER CONTROLLER PARAMETERS (D-AXIS)

Parameter	**Value**	**Unit**
Reference Stator Voltage Level	294	V
Capacitance	0.01	μF
Proportional Constant, K_{pd1}	1m	-
Integral Constant, K_{id1}	0.01333	-
Time Constant, τ_{d1}	75	ms
Proportional Constant, K_{pd2}	50	-
Integral Constant, K_{id2}	10k	-
Time Constant, τ_{d2}	5	ms

TABLE 4.5 INVERTER CONTROLLER PARAMETERS (Q-AXIS)

Parameter	**Value**	**Unit**
Optimum Torque Coeff., K_{Topt}	3.8195μ	Nm/ $(rad/s)^2$
Proportional Constant, K_{pq}	50	-
Integral Constant, K_{iq}	10k	-
Time Constant, τ_q	5	ms
Cut-off Frequency of Filter	500	Hz

4.7. Simulation Results

Figure 4-10 shows the schematic diagram of the system including all the components. The controller is as it is in Figure 4-9. The simulation is actually done in Simulink with the where the controller is implemented and the power circuit is implemented in PSIM. Both of them are integrated using SimCoupler block. The parameters of the wind turbine and the generator used for the simulation are given in Table 4.6 and Table 4.7. All other parameters used in the system are also given in Table 4.8. This section includes the simulation results of the complete system.

4.7.1. System under normal operating condition

Figure 4-11 gives the line-to-line stator voltage of phase A for a wind speed of 11 m/s. it takes some time to build up the desired voltage level at starting, but once achieved its stable for the rest of the time. The three-phase voltages and currents of the generator are also given that is fed to the three-phase load. Another simulation is run for the same system and under the same operating conditions, but with a two-level inverter. The three-phase stator voltages, given in Figure 4-12, clearly show that the output in Figure 4-11(b) is less distorted.

The zoomed in harmonic profiles of the stator voltage for both systems are shown in Figure 4-13. For the system with NPC inverter, the THD calculated using PSIM for both the voltage and current waveform is 2.14 % respectively, without any filter used in the system, as in [57]. The THD can be lowered using higher switching frequency, higher load and higher number of levels in the inverter. The LOH appears at 540 Hz (m_f - 1) with amplitude of 0.98 V only. The harmonic with the highest amplitude is at 1260 Hz ($2m_f$ + 1) with amplitude of 2.3 V, i.e. only 0.9 % of the fundamental voltage. The system with conventional inverter resulted in a THD = 3.6 %, both being lower than the allowable limit of 5 %. The harmonic profile also confirms the

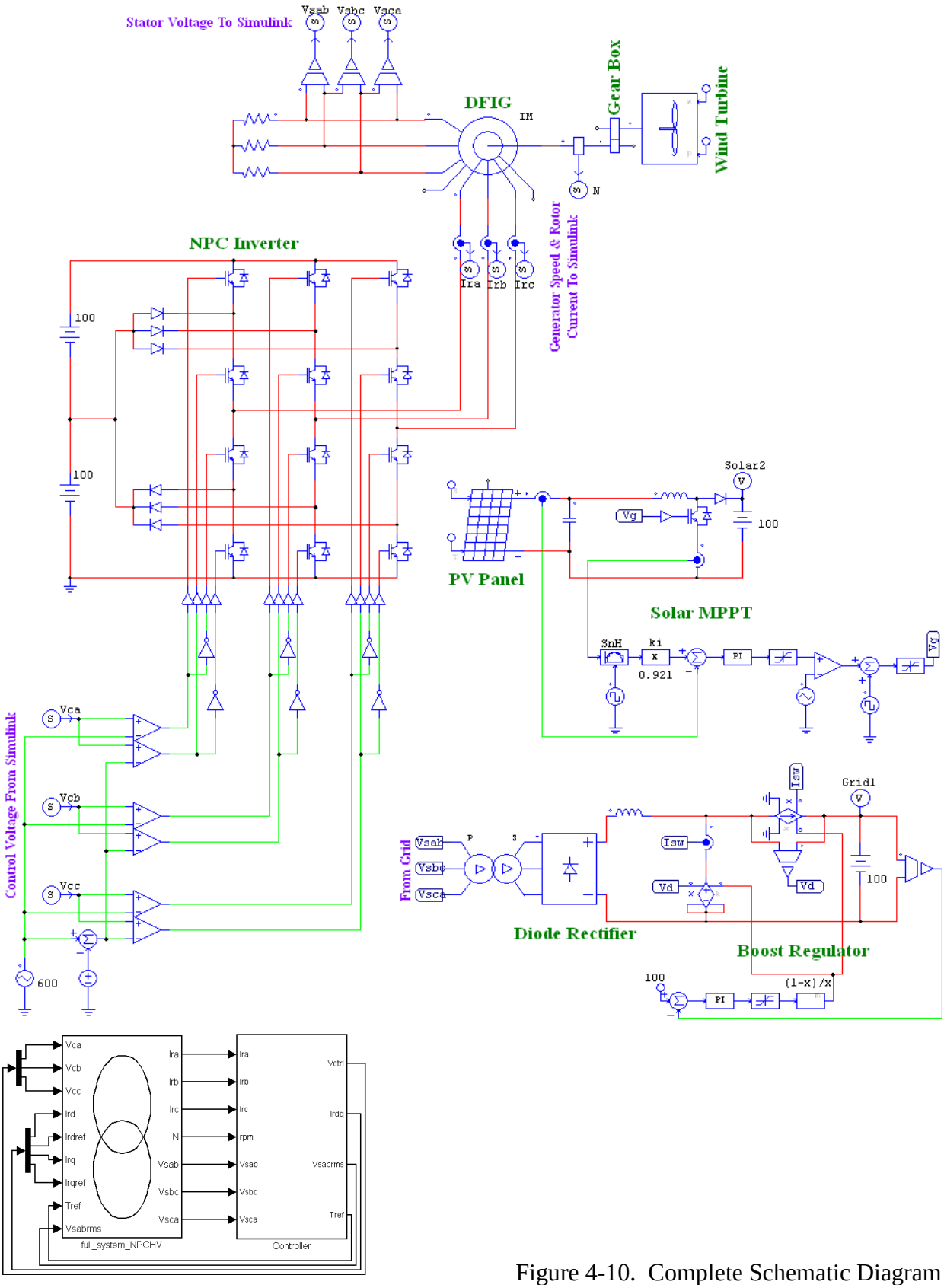

Figure 4-10. Complete Schematic Diagram

TABLE 4.6 WIND TURBINE PARAMETERS

Parameter	**Value**	**Unit**
Nominal Output Power	20	kW
Base Wind Speed	12	m/s
Base Rotational Speed	100	rpm
Initial Rotational Speed	30	rpm
Moment of Inertia	2	$kg.m^2$

TABLE 4.7 DFIG PARAMETERS

Parameter	**Value**	**Unit**
Stator Resistance	0.59	Ω
Stator Inductance	35.81	mH
Rotor Resistance	3.39	Ω
Rotor Inductance	19.894	mH
Mutual Inductance	1.104	H
Stator to Rotor Turns Ratio	1	-
No. of Poles	4	-
Moment of Inertia	0.05	$kg.m^2$

presence of sub-harmonics at 5 Hz of 1 V. The LOH is at 120 Hz with amplitude of 0.8 V and the harmonic with the highest amplitude is at 1260 Hz with amplitude of 5.7 V (2.1 % of the fundamental voltage). A similar system in [55], with 2-level inverter, gives a THD of 8.31 % and also has harmonics higher than 3 % of fundamental voltage even after using a carrier frequency

of 10 kHz. Ref [67] presents a synchronous generator based WECS with 25-level cascaded inverter that can achieve a THD of 1.5 % for an 11 kV output voltage but with LOH = 3 (0.2 % of fundamental amplitude).

TABLE 4.8 SYSTEM PARAMETERS

Parameter	**Value**	**Unit**
Three-Phase Load	100	Ω
Gear Box Ratio	10	-
DC-Bus Voltage	2*100	V
Switching Frequency	600	Hz

4.7.2. System operation with variable wind speed

Figure 4-14 shows the system response with a step change in wind speed (9 m/s to 11 m/s). The total simulation time is 8 seconds and the step in wind speed was applied at 4 seconds. The change in wind speed results in a change in generator speed from 1245 rpm to 1527 rpm. The figure shows the waveforms at different points in the controller. Figure 4-14(b) confirms that the rms value of the stator voltage is strictly constant at 208 V for all wind speeds. Figure 4-14(d) shows the change in torque reference with wind speed, which sets a new operating point for the system. Figure 4-14(c) and Figure 4-14(e) demonstrate that how closely the rotor current components follow their respective references. Figure 4-14(f) and Figure 4-14(g) show the waveforms of the injected rotor current and voltage. It can be seen that the injection frequency changes with wind speed from 9 Hz to 18.5 Hz to maintain a constant stator frequency of 60 Hz.

Figure 4-15(a) gives the phase A stator voltage which is constant even with a step change in wind speed (also verified in Figure 4-14(b) in terms of rms value). In Figure 4-15(b), the stator

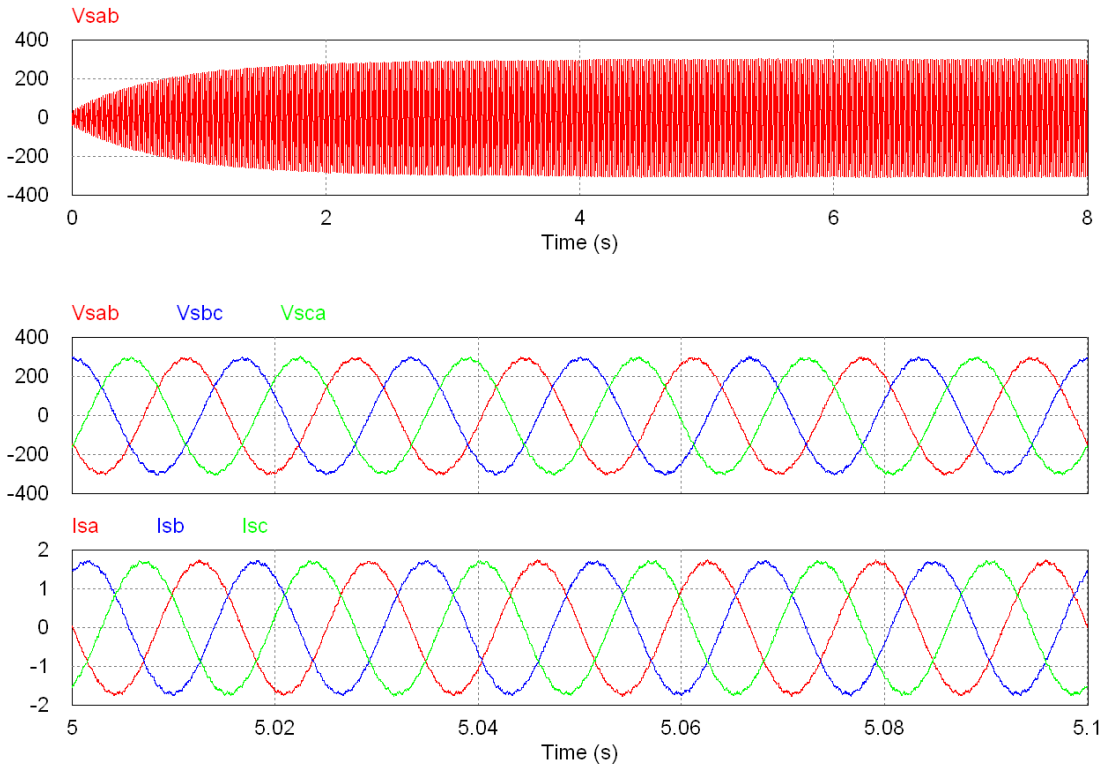

Figure 4-11. System Response under Normal Operating Condition
a) Phase A stator voltage, b) three-phase stator voltage, and c) three-phase stator current

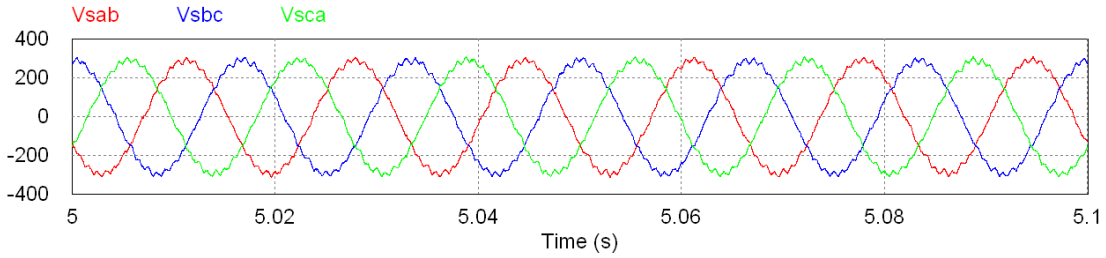

Figure 4-12. System Response under Normal Operating Condition: Three-Phase Stator Voltage with Two-Level Inverter

output power and the required injection power are sketched out. The stator power is constant (433 W) throughout the time span since a fixed load is connected to the stator. For the wind speed at 9 m/s, the power drawn from the rotor is about 129 W (≈ 29 %) and for 11 m/s it is about 82 W (≈ 18.94 %). It shows that at high wind speeds, the generator takes less power from rotor. This also verifies the statement that if the speed is in the range of ± 30 % of the rated

value, the converter rating can be as low as 20 ~ 30 % of the generator rating.

The system is also tested for voltage and frequency regulation when the wind turbine was supplied with a set real wind data for North Dakota state [74]. The waveforms, showing constant stator voltage across a 22 Ω/phase load, are given in Figure 4-16.

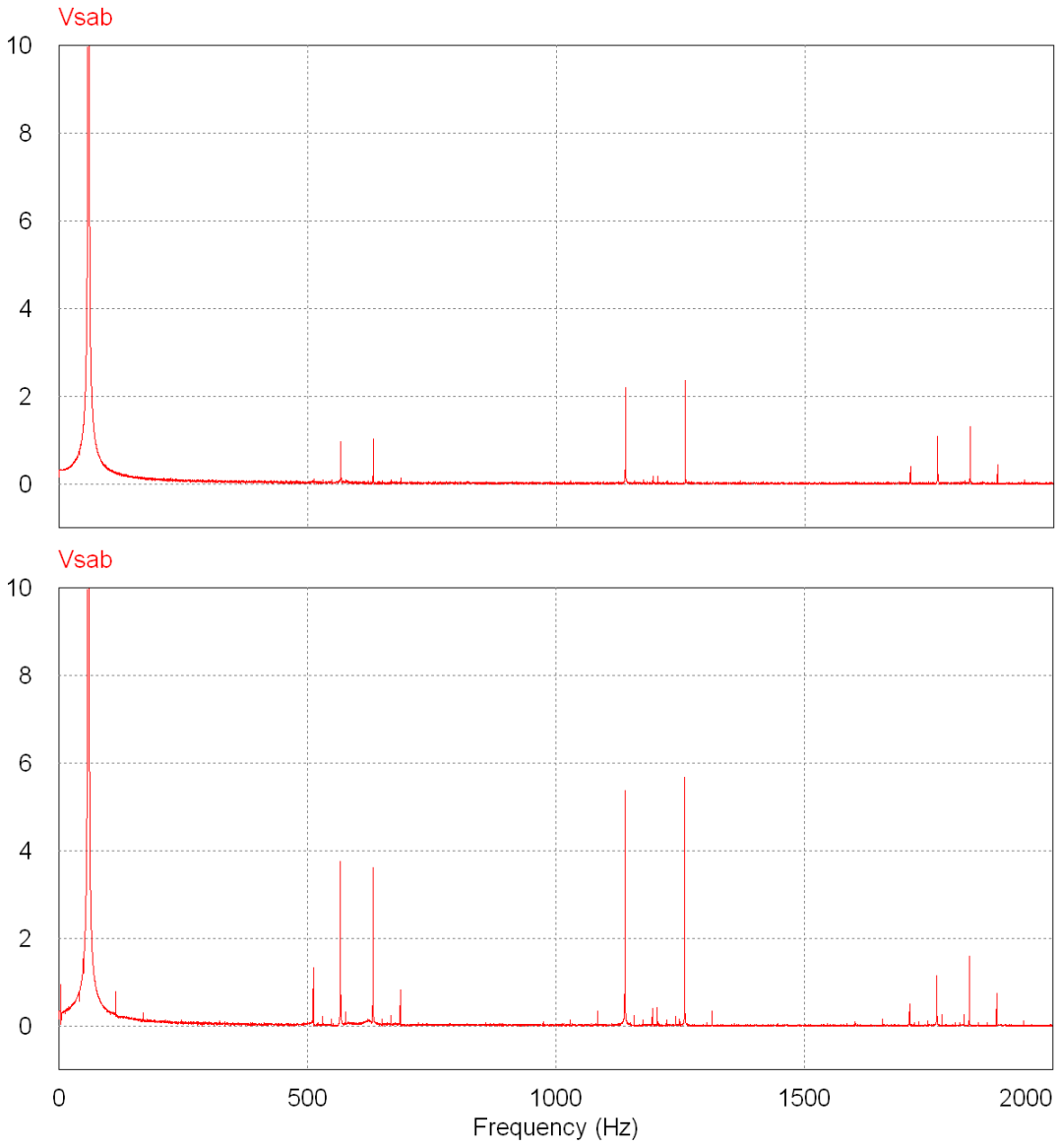

Figure 4-13. System Response under Normal Operating Condition: Harmonic Profile of Stator Voltage using a) Three-level NPC inverter, and b) two-level conventional inverter

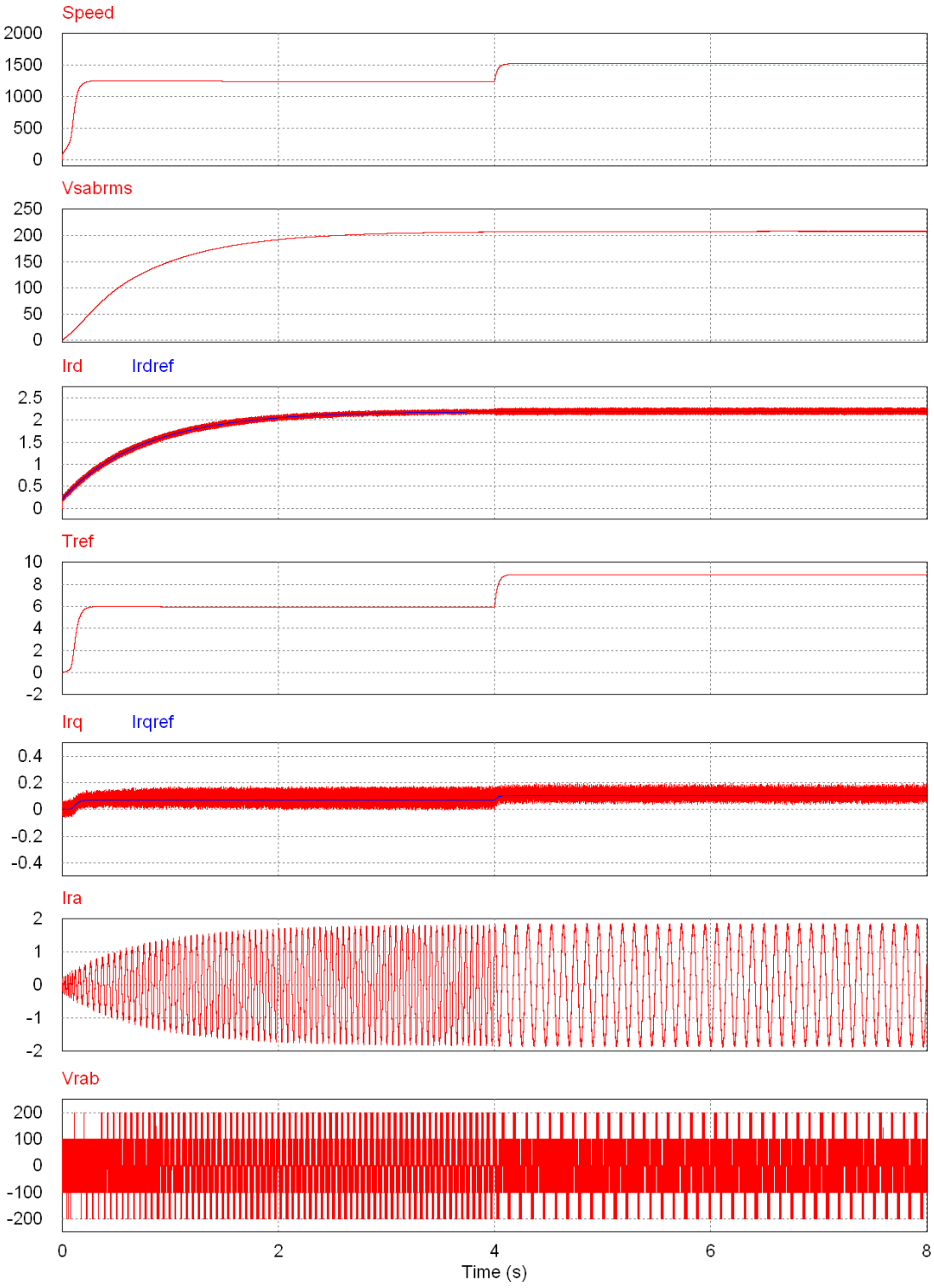

Figure 4-14. System Response to Variable Wind Speed
a) Generator shaft speed, b) amplitude of stator voltage, c) d-axis component of reference and actual rotor current, d) reference torque from MPP equation, e) q-axis component of reference and actual rotor current, f) injected phase-A rotor current, and g) injected phase-A rotor voltage

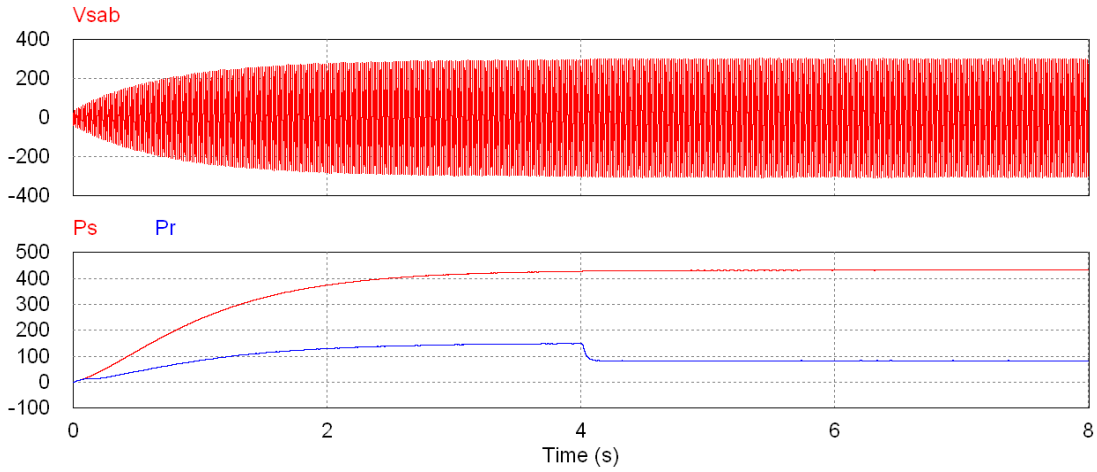

Figure 4-15. System Response to Variable Wind Speed
a) Phase A stator voltage, and b) stator and injected rotor power

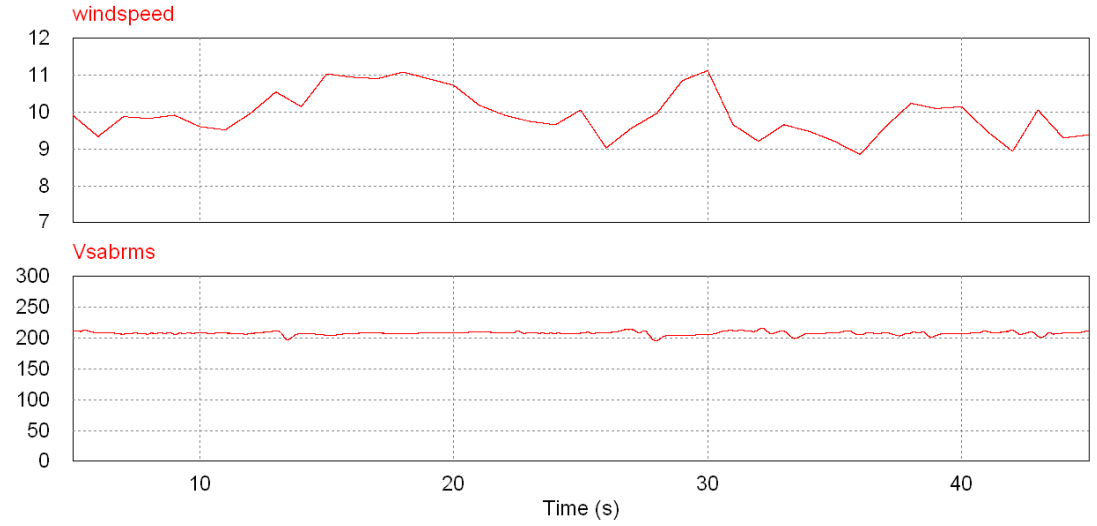

Figure 4-16. System Response to Real-Time Wind Speed
a) Wind Speed [74], and b) rms value of line-to-line stator voltage

4.7.3. System under variable load

Figure 4-16 shows the system response to variable load. The initial load is three-phase Y-connected resistive load of 1000 Ω per-phase. Another 1000 Ω per-phase resistive load was placed in parallel (total resistance = 500Ω/phase) at *t* = 2 seconds. At t = 4 seconds, an R-L load of 1000 Ω and 100 mH per-phase was added in parallel. As expected, the stator voltage is almost

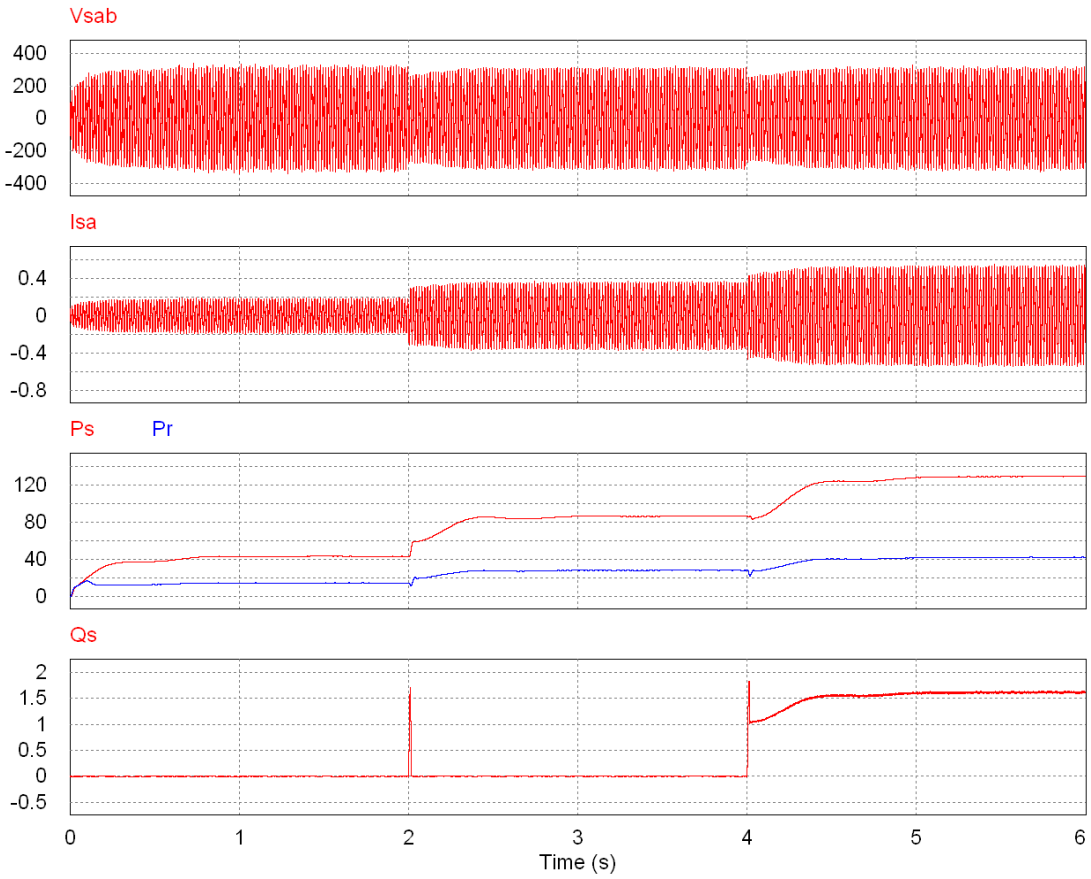

Figure 4-17. System Response to Variable Load
a) Phase A stator voltage, b) phase A stator current, c) stator and rotor real power, and d) stator reactive power

constant, with a small dip of 0.14 pu at the time of switching, and the load current and power goes up as the load is increased. Figure 4-16(d) shows the reactive power output of the system.

4.7.4. System under grid fault condition

Finally the system was tasted for a three-phase short circuit fault. The load was shorted for about 110 ms. After the short was removed, it came to a steady state condition in about 35 ms (Figure 4-17), much faster compared to 280 ms in Ref [56] and 100 ms in Ref [3]. The voltage, speed and power waveforms in Ref [3] are given in Figure 4-18 for comparison. They created a short circuit of 100 ms and during that time the stator voltage and power dropped to zero. It took

about 1.2 seconds for the power to reach its original value, whereas for the proposed system in this study, this time was only 0.88 seconds. The system in Ref [3] also has a change in speed about 0.07 pu, very high compared to the almost constant speed of the proposed scheme. The voltage overshoot for the system in Ref [3] is about 1.5 pu, much higher compared to that of the proposed system (1.1 pu).

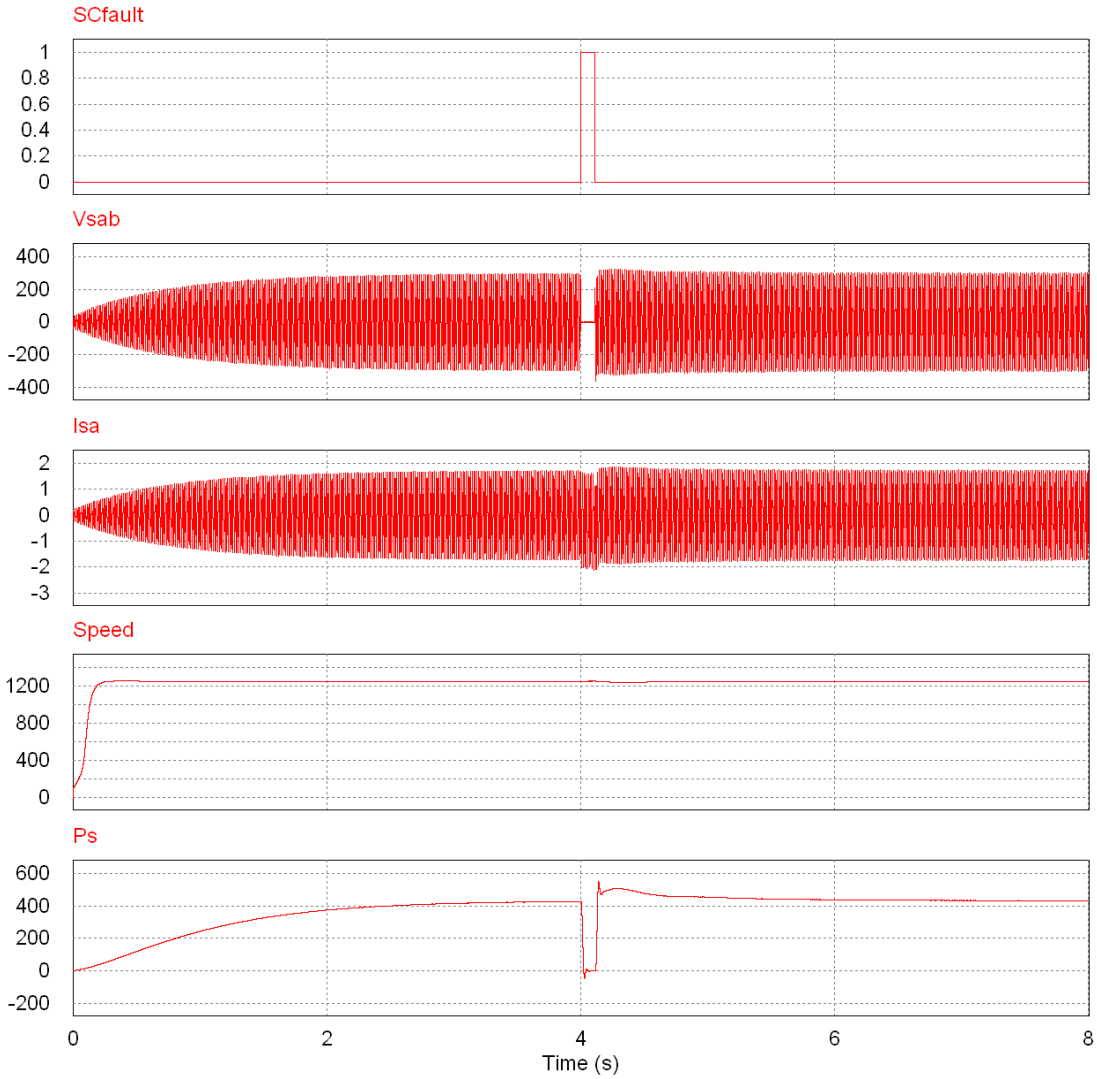

Figure 4-18. System Response to Three-Phase Short Circuit Fault
a) Short circuit signal, b) phase A stator voltage, c) phase A stator current, d) generator speed, and e) stator power

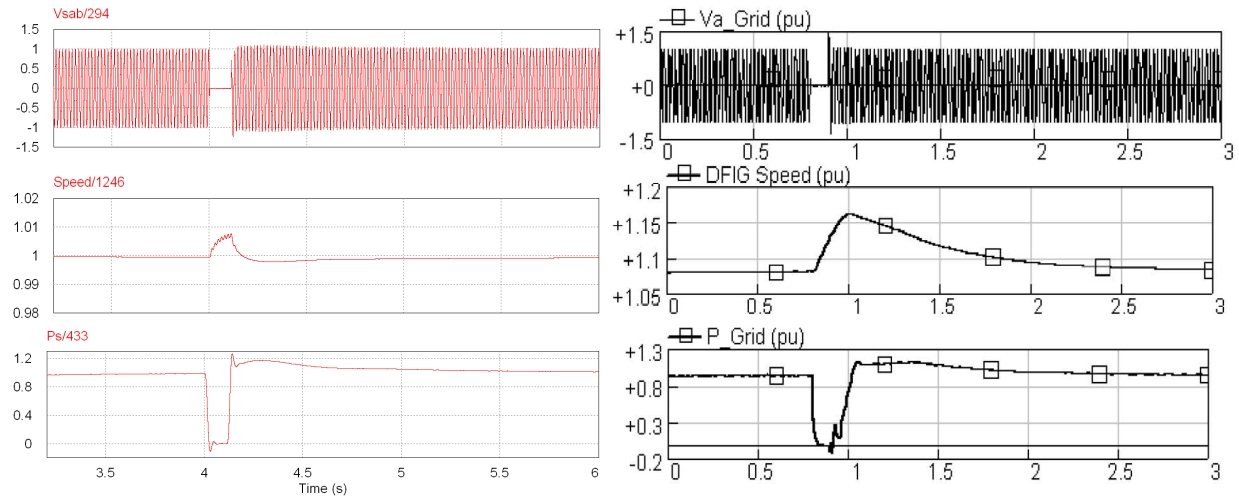

(a) (b)

Figure 4-19. Comparison of System Response under Short Circuit Fault Condition
(a) Proposed System and (b) System in Ref [3]

4.8. Conclusion

A simple and economical power converter system has been designed to extract the power from wind turbine and feed either to the grid or to an isolated load. To reduce the power drawn by the rotor from the grid, an auxiliary source i.e. a PV panel has been included in the system. MPPT technique used for the wind turbine ensures high efficiency at all wind speeds reducing the power rating of the converter. The surplus power output from the PV panel, if available, can The source for the converter can be selected manually or based on the availability of PV power. MPPT technique used for the wind turbine ensures high efficiency at all wind speeds reducing the power rating of the converter. The surplus power output from the PV panel, if available, can be stored in the battery for future use. The use of NPC inverter reduces the THD in the stator voltage. Both the boost regulator and the inverter controller have good dynamic response with a very low overshoot and a low settling time. This chapter presents a complete system overview proposed in this thesis with some supporting results obtained from simulation.

CHAPTER 5. EXPERIMENTAL RESULTS

5.1. Introduction

This chapter presents the results of all experiments conducted to verify the proposed wind energy conversion system described in earlier chapters. The experiments are carried out with the power circuits including the inverter in hardware and the generator. Instead of a wind turbine, a DC motor is used here to run the DFIG. The control circuit is implemented in Simulink and the interfacing is done using dSPACE controller board RT1104. First it is verified that the converter in DFIG based WECS processes only the slip power and thus components with lower rating can be used in the rotor circuitry. Then two- and three-level inverters supplying a three-phase resistive load have been compared. Similar comparisons are made with these converters feeding the rotor of the DFIG. Finally the system is tested under variable-speed conditions to ensure its frequency and voltage regulation.

5.2. Rotor Injection Power

The injected rotor power to the DFIG is equal to the product of the required stator power and the slip (s) of the generator. So if the slip can be maintained to be less than 30 %, the rotor power will also be low. So all the components used on the rotor side, like the converter, filter, etc., can have lower ratings compared to the ratings of the converters used in systems with synchronous generators. Table 5.1 and Table 5.2 validate the relation between stator and rotor power from simulation and experimental respectively. For the experimental data, a 5 hp DFIG is used to supply a three-phase resistive load and a variable-frequency power supply (360-ASX) is used for rotor injection. The injection voltage and frequency are controlled manually at different speeds to get a constant frequency (60 Hz), constant voltage (80 V) stator output.

TABLE 5.1 STATOR AND INJETED ROTOR POWER AT DIFFERENT WIND SPEEDS

(SIMULATION RESULT) – V_{sanrms} = 120 V, R_{Load} = 100 Ω

Wind Speed v_w **(m/s)**	**Slip** s **(%)**	**Stator Power** P_s **(W)**	**Rotor Power** P_r **(W)**	**Power Ratio** P_r/P_s **(%)**
9	25	433	129	29
11	8.33	433	82	19

TABLE 5.2 STATOR AND INJETED ROTOR POWER AT DIFFERENT WIND SPEEDS

(EXPERMENTAL RESULT) – V_{sanrms} = 80 V, R_{Load} = 22 Ω

Shaft Speed N_m **(rpm)**	**Slip** s **(%)**	**Stator Power** P_s **(W)**	**Rotor Power** P_r **(W)**	**Power Ratio** P_r/P_s **(%)**
1038	42.3	873	563	64.5
1176	34.6	873	387	44.3
1340	25.6	873	321	36.8

5.3. Three- versus Two-Level Inverter

Different types of inverters are explained in Chapter 3. In Chapter 4, some simulation results are shown to verify that a multilevel inverter generates fewer harmonics by introducing intermediate levels in output voltage. In this section the above statement is verified using hardware experiments. The two-level inverter is implemented using IRAM136-3063B which integrates the three-phase full bridge inverter and its gate drivers. This IC is rated at 600 V and 30 A, suitable for motor applications. For a three-level inverter, similar IC can be found only for a maximum current of 2 A. So separate ICs, APTGF30TL601G and IRS 26310DJPbF, are used

as the power module and the driver respectively. APTGF30TL601G is a three-level single-phase IGBT bridge with high voltage and current ratings (600 V and 42 A at 25°C respectively). Three of them are connected in parallel to the DC bus for three-phase output. No dedicated drivers are available for supplying gate pulses to the twelve switches of the three-level bridge supporting such high voltage. So three IRS 26310DJPbF drivers, which are actually drivers for two-level bridges, are used for supplying the three-level bridge. Figure 5-1 shows the connection diagram of the NPC inverter circuitry using three APTGF30TL601G, three IRS 26310DJPbF and one SN74LS04N, a hex logic inverter. Six of the triggering pulses, for the top two switches in each phase, are generated using Simulink and the rest are obtained by inversion. Since each driver can supply one signal per phase with isolated ground and its inverted one with respect to the system ground, one driver is used to supply the second and the fourth switch (the one with the common ground) of all phases. The other drivers supply the first and the third switches with the inverted outputs left unused since their grounds are not isolated. Each driver supplies identically positioned switches in all three-phases. Figure 5-2 and Figure 5-3 show the inverter modules.

Both inverters are tested under same input conditions. The DC bus voltage is set to 6 V. The frequency modulation index, $m_f = 33$ ($f_{tri} = 1980$ Hz) and amplitude modulation index, $m_a = 0.8$. The output waveforms of both inverters with their FFT are shown in Figure 5-4 and Figure 5-5. The NPC inverter has its LOH at $m_f - 4$, i.e. at 1740 Hz whereas the two-level inverter's output contains some sub-harmonics and other lower order harmonics resulting in a high THD and a high DF. Both inverters have the harmonic with highest amplitude at $2m_f - 1$, i.e. 3900 Hz, but the amplitude being 23 % and 36 % of fundamental amplitude for NPC and two-level inverters respectively. Table 5.3 shows the results of THD and DF calculation (disregarding the sub- harmonics for both) showing a close agreement between the simulation and experimental

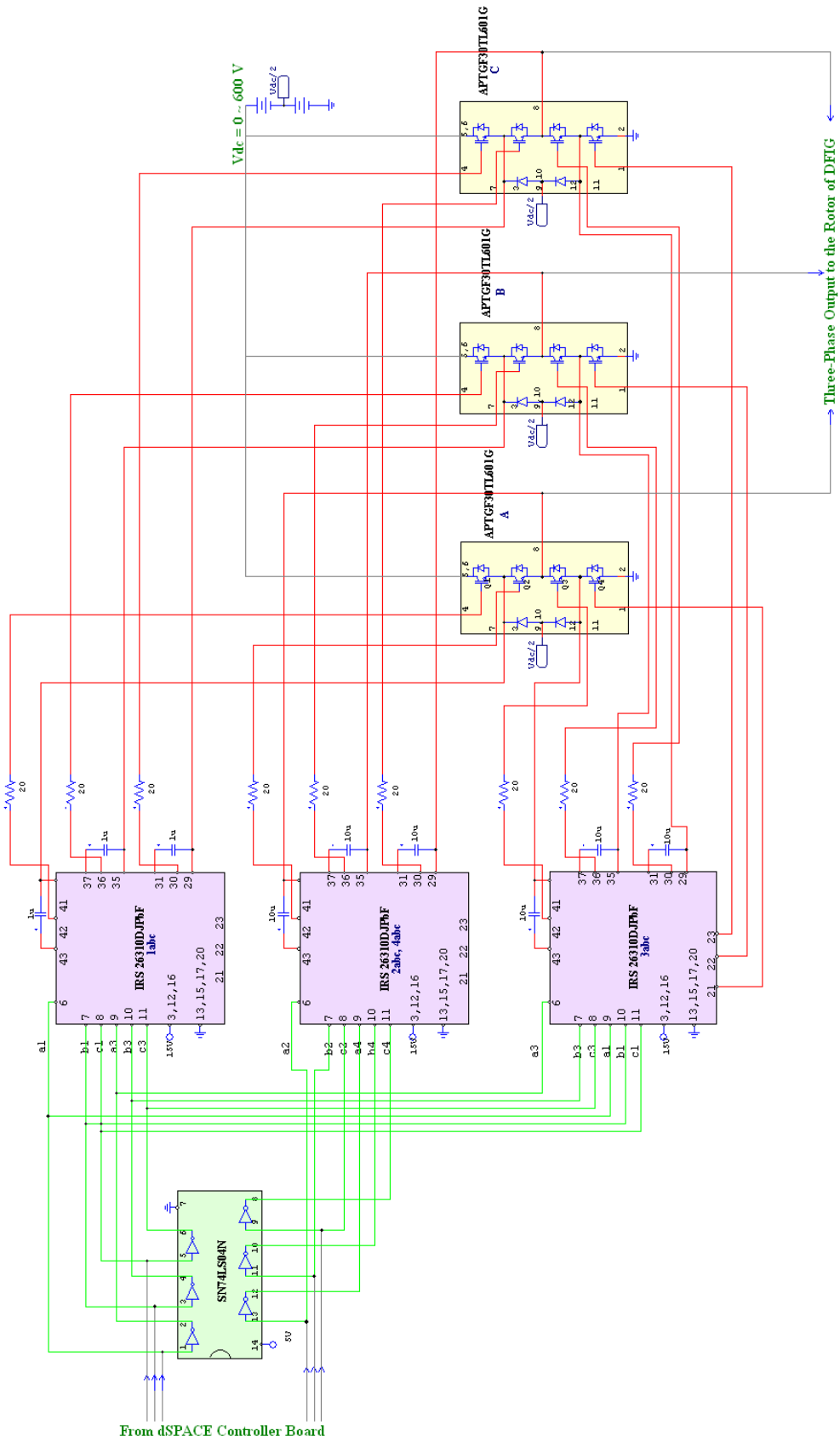

Figure 5-1. Connection Diagram of Multilevel Inverter

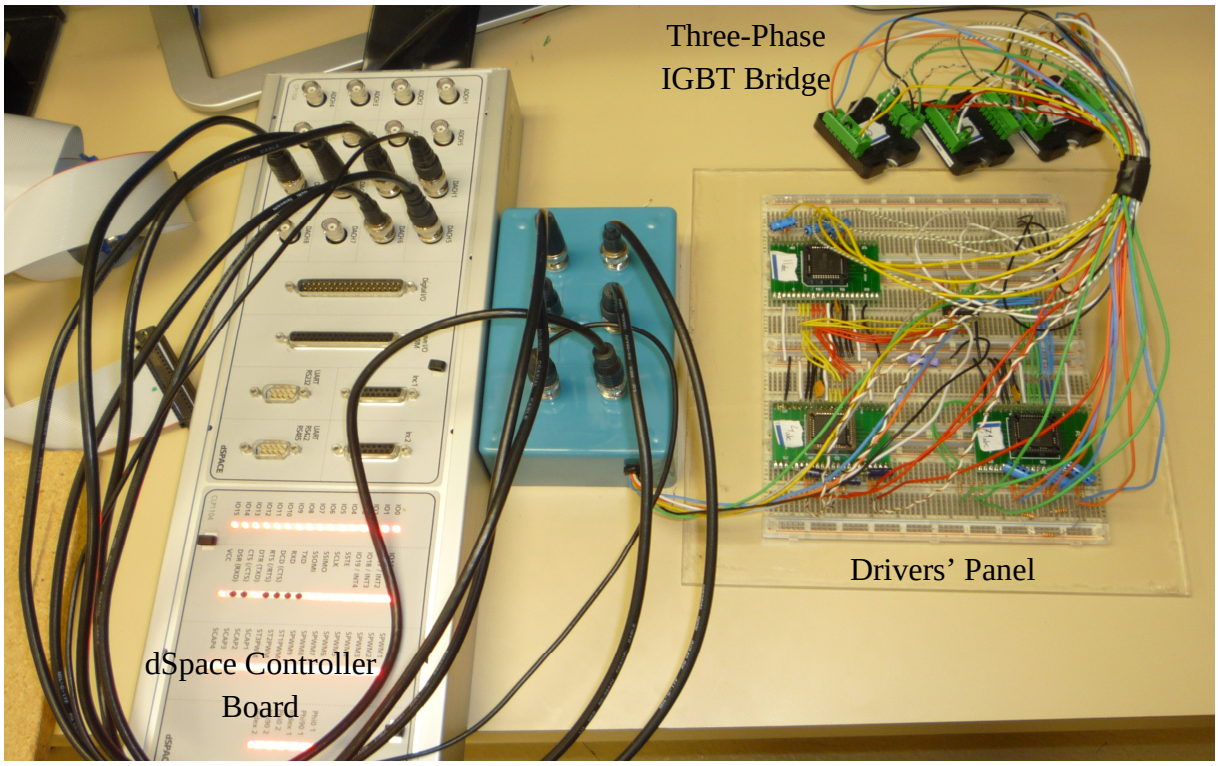

Figure 5-2. Hardware Implementation of Three-Level Inverter

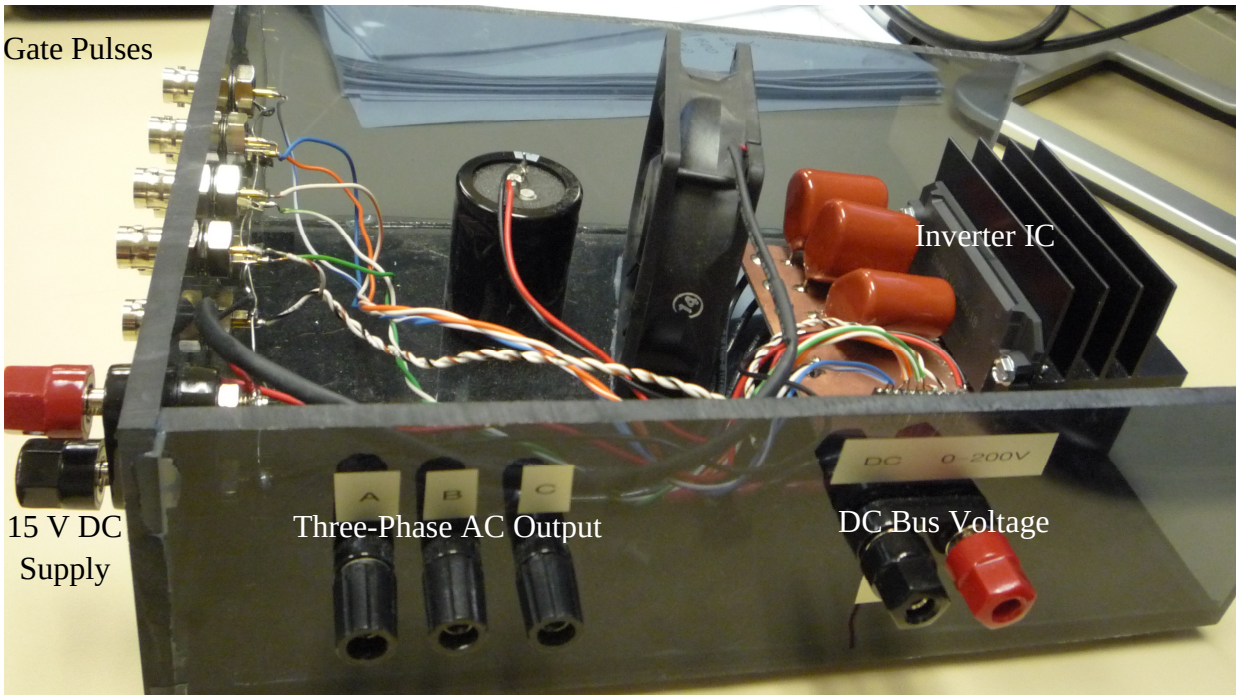

Figure 5-3. Power Module for Two-Level Inverter

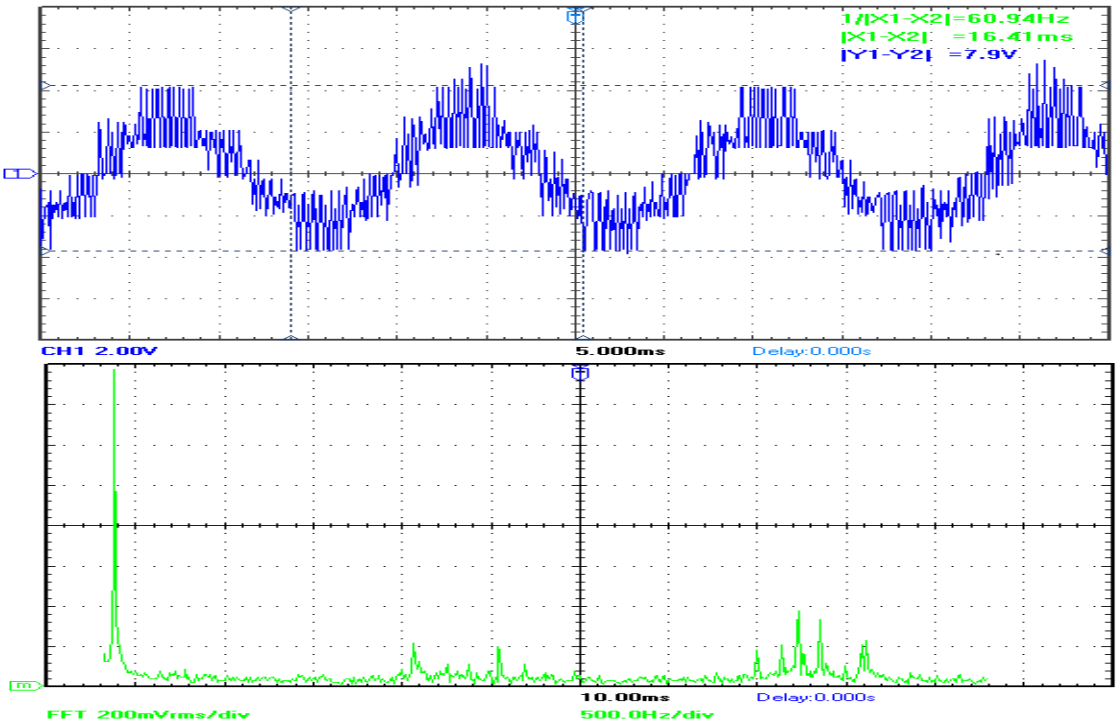

Figure 5-4. Waveforms of Three-Level NPC Inverter
a) Line-to-line output voltage (V_{ab}), and b) fast Fourier transform (FFT) of V_{ab}

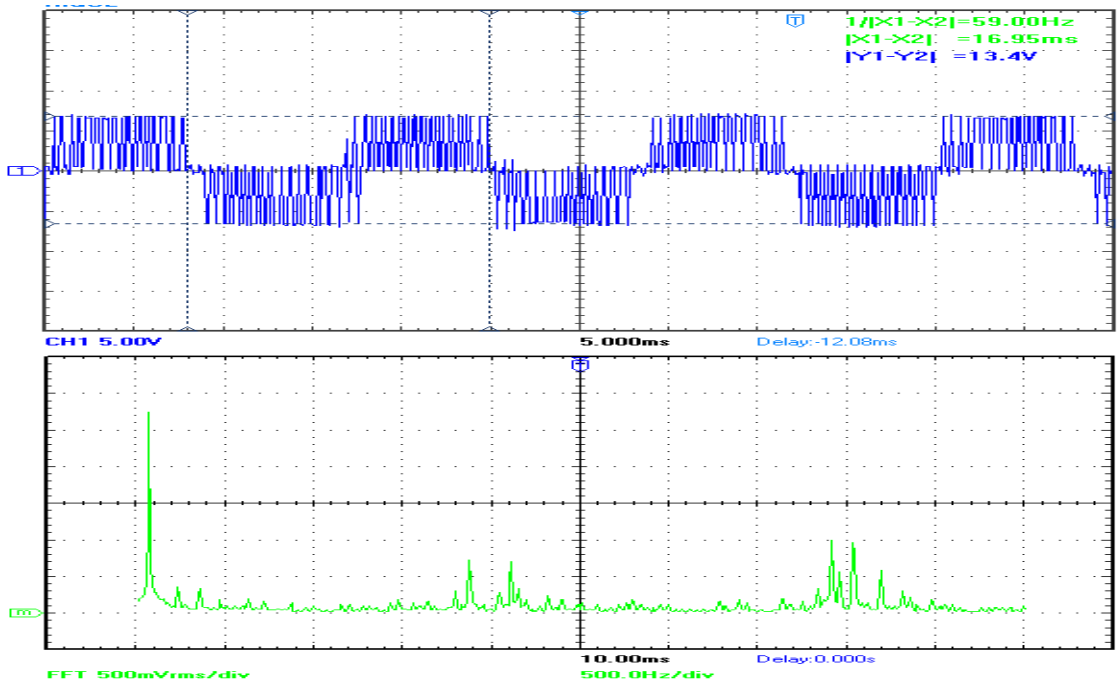

Figure 5-5. Waveforms of Two-Level Sine PWM Inverter
a) Line-to-line output voltage (V_{ab}) and b) fast Fourier transform (FFT) of V_{ab}

TABLE 5.3 THREE- VERSUS TWO-LEVEL INVERTER WITH RESISTIVE LOAD (f_{tri} = 1980 Hz)

		3-Level Inverter	**2-Level Inverter**
Simulation	LOH	$m_f - 4$	$m_f - 4$
	THD	42.2 %	91.9 %
	DF	0.018 %	0.038 %
	THD with filter (f_c = 1000 Hz)	10.7 %	23.7 %
Hardware	LOH	$m_f - 4$	4
	THD	43.43 %	78.93 %
	DF	0.022 %	1 %

results and also proves that for NPC inverter, not only the THD is 50% of the value for a two-level inverter but also the DF is much lower. Figure 5-6 shows the inverter output after passing through a digital low-pass filter with a cut-off frequency (f_c) of 1000 Hz which also proves superior performance of the NPC inverter.

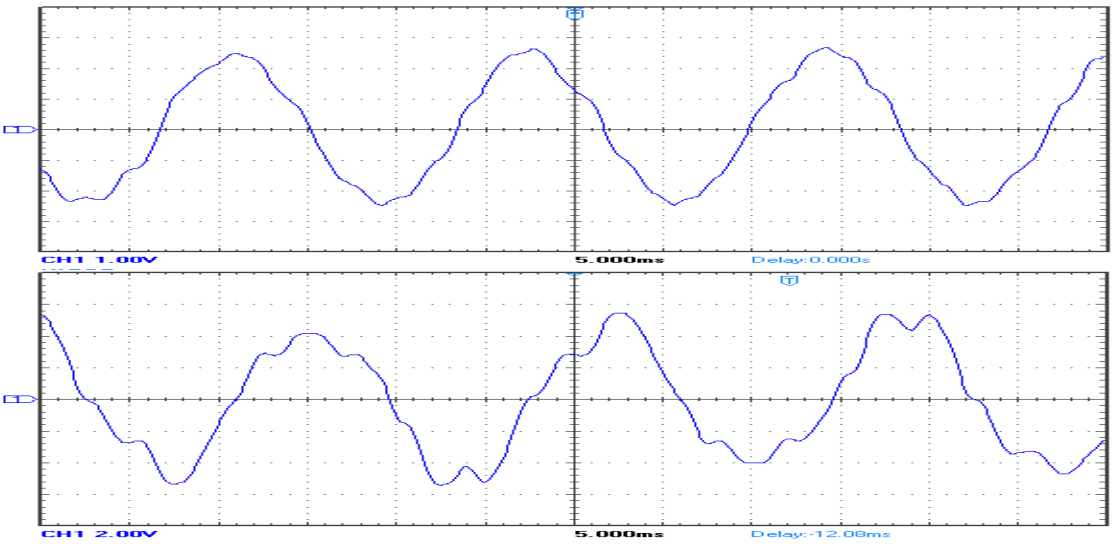

Figure 5-6. Filtered Voltage V_{ab} (f_c = 1000 Hz) for Three-and Two-Level Inverters

5.4. Performance of the WECS under Variable Wind Speed Condition

Figure 5-7 and Figure 5-8 show the complete experimental setup including both the hardware and the dSPACE unit. The DFIG supplies a 3-phase resistive load having 22 Ω/phase with the rotor injection coming from a Semikron three-phase inverter module. In this case, the rechargeable batteries are replaced by a MASTECH DC power supply (50 V, 20 A). Only the stator voltage and frequency regulation are tested in the experimental setup. The system does not use any filter in the rotor injection side, i.e. the rotor is being supplied directly from the inverter output. Only digital filters are being used at the output of the ADCs of the dSPACE board such that the filtered signals are used by the controller. The speed data is fed to the controller manually using dSPACE ControlDesk. The ControlDesk is also used to set the stator reference voltage and to view the stator, rotor and controller waveforms.

Figure 5-9 shows the performance characteristics of the WECS at various speeds. It gives the stator voltages for three different speeds, 1020, 1210, and 1475 rpm. For all speeds, the stator voltage is constant with a line-to-neutral rms voltage of 15 V (26 V line-to-line rms). Figure 5-10 gives the harmonic profile of the stator output voltage showing that the harmonics are suppressed more at higher speeds and also sub-harmonics appear at lower speeds. Table 5.4 shows the calculated THD and DF from both simulation and experiment using the two different inverters and also some results of earlier research works for comparison. The results not only prove that the system provides about 50 % less distortion by adding just one more level in the inverter but also gives better performance when compare to some existing systems. Figure 5-11 gives the stator voltage and rotor current of the WECS using the three-level inverter at 1050 rpm. The reason for its low voltage is that the maximum DC bus voltage and current has been set to 15 V and 1 A, for the protection of the inverter module. Figure 5-12 shows the change in the stator

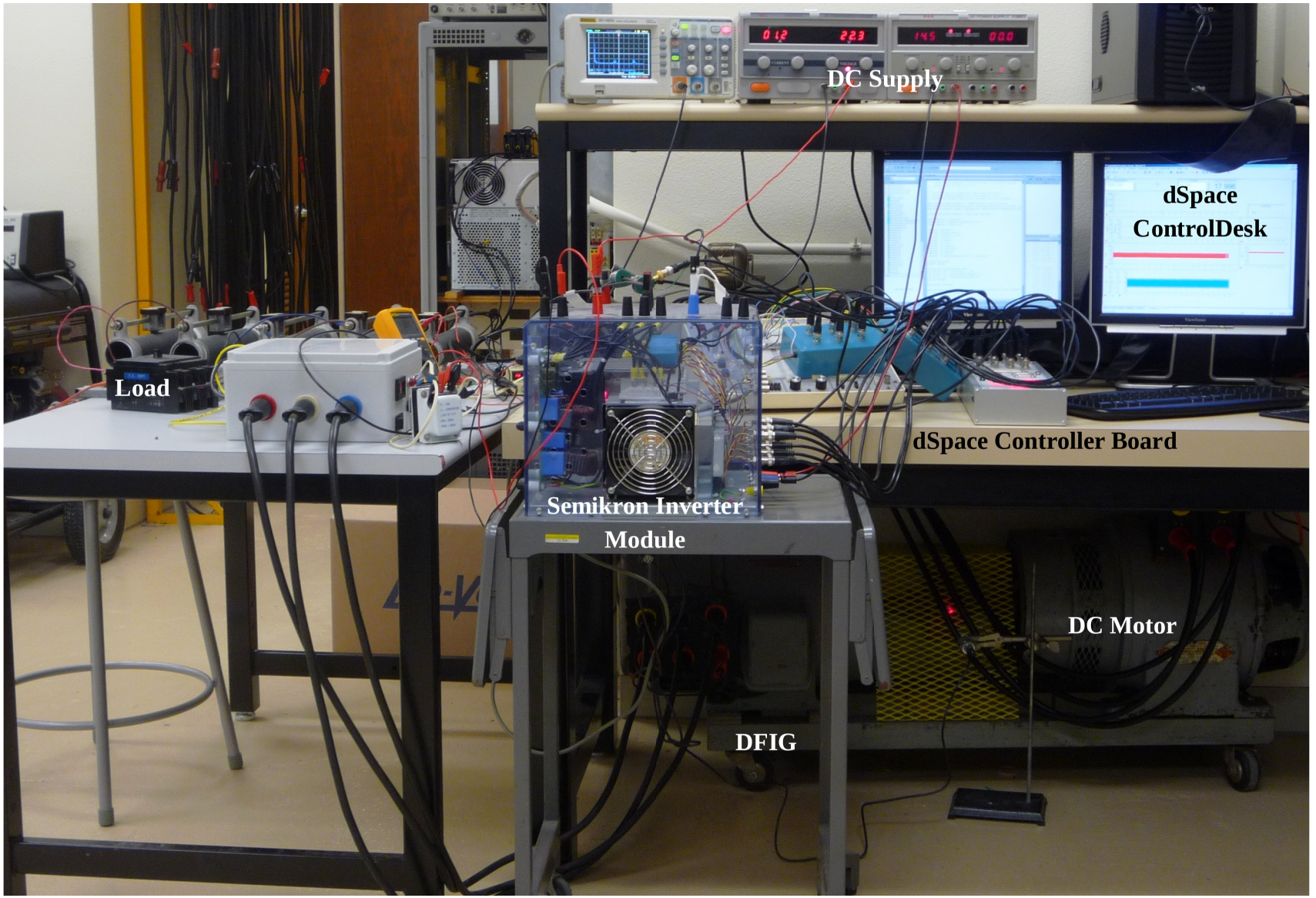

Figure 5-7. The Complete Hardware Setup of the WECS

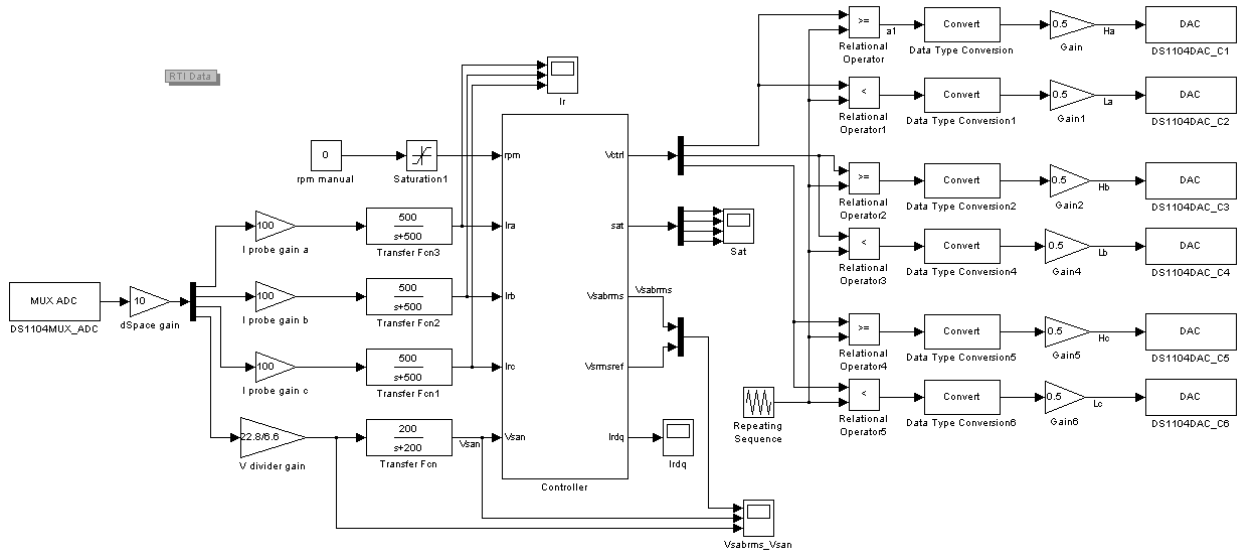

(a)

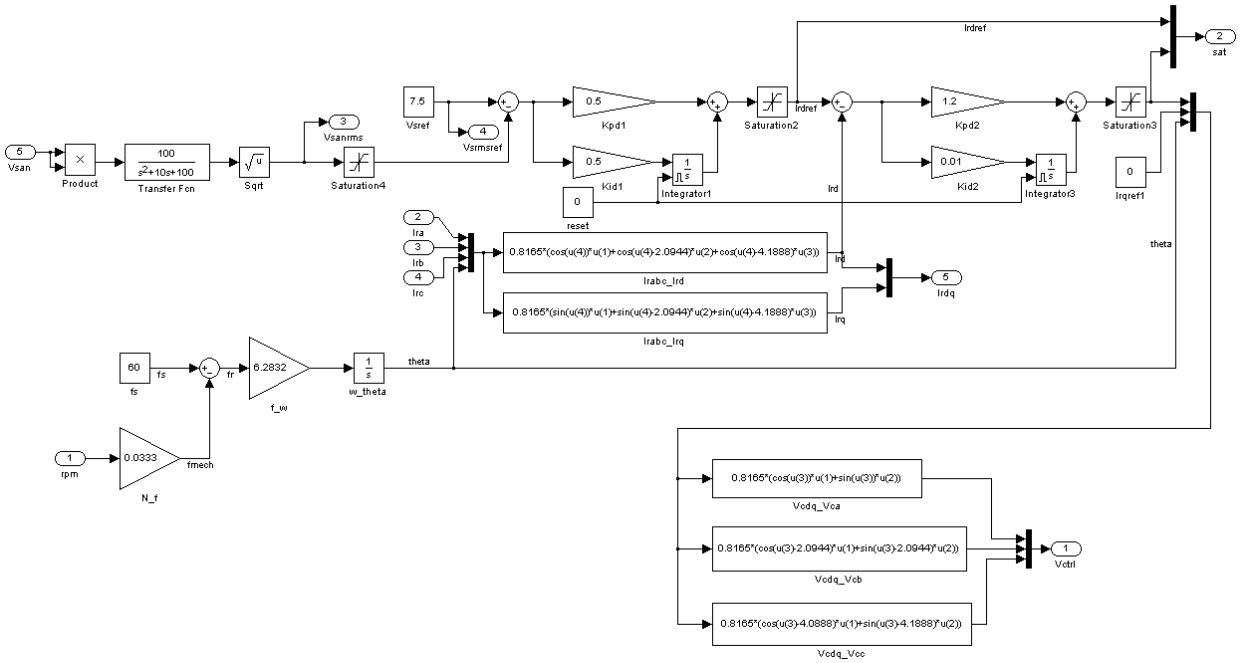

(b)

Figure 5-8. Simulation Diagram of a) WECS and b) controller subsystem

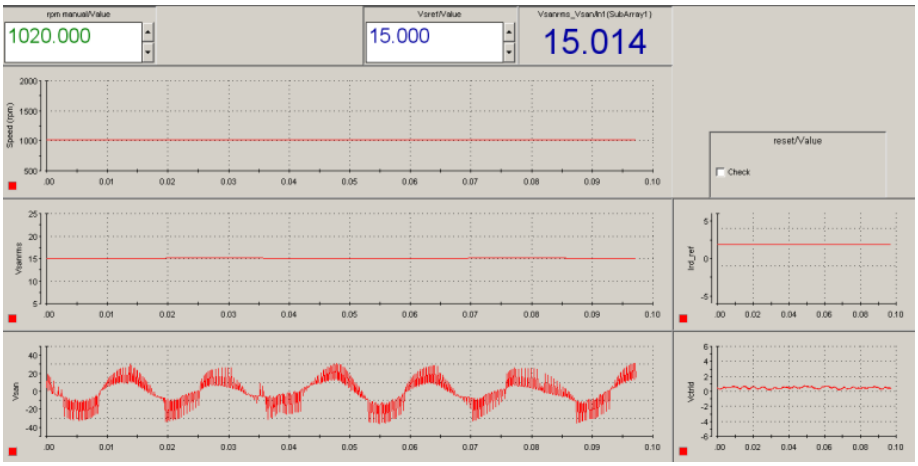

(a)

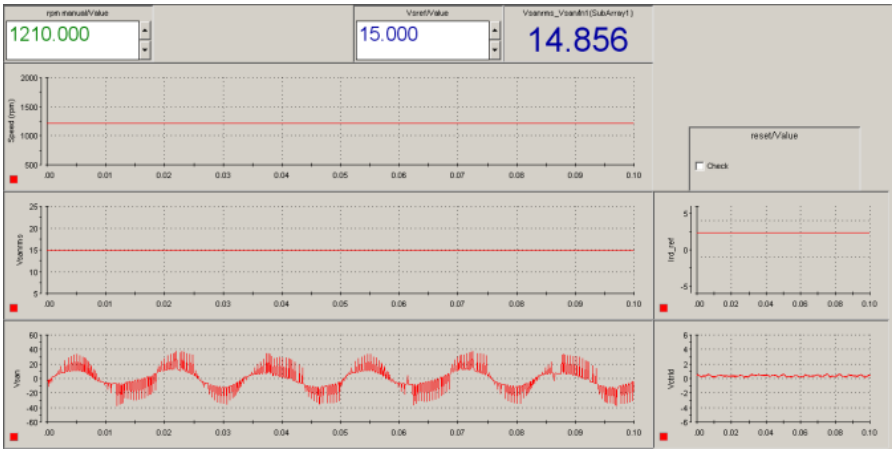

(b)

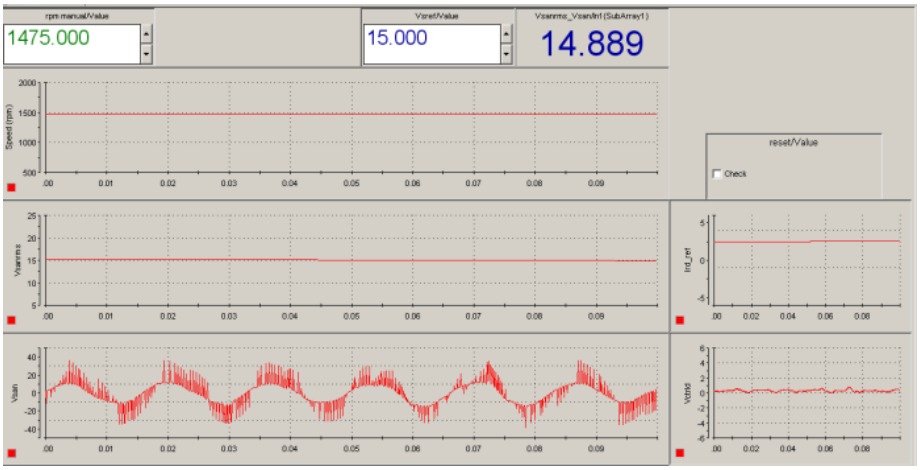

(c)

Figure 5-9. Stator Line-to-Neutral Voltage and its rms Value at a) 1020 rpm, b) 1210 rpm, and c) 1475 rpm

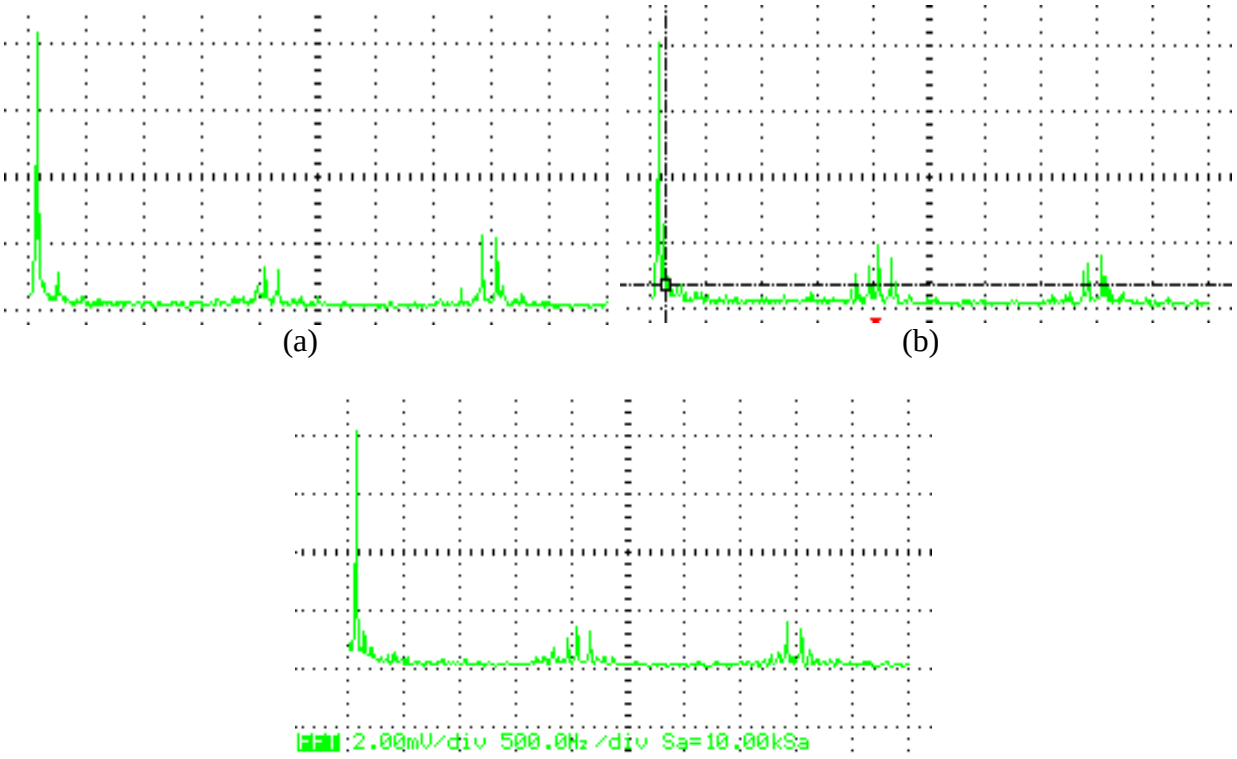

Figure 5-10. Fast Fourier Transform (FFT) of Stator Voltage at a) 1020 rpm, b) 1210 rpm, and c) 1475 rpm

TABLE 5.4 WECS USING THREE- VERSUS TWO-LEVEL INVERTER

		Proposed System (f_{tri} =1980Hz)		**System of Ref [55]**	**System of Ref [67]**
		3-Level Inverter	2-Level Inverter	(f_{tri} = 10 kHz)	(25-Level)
Simulation	LOH	$m_f - 1$	2	3	-
	THD	1.44%	3.58 %	8.31 %	-
	DF	0.0062 %	0.0753 %	-	-
Hardware	LOH	$m_f - 2$	6.7	-	3
	THD	9.08 %	16.13 %	-	1.55 %
	DF	0.0083 %	0.1015 %	-	-

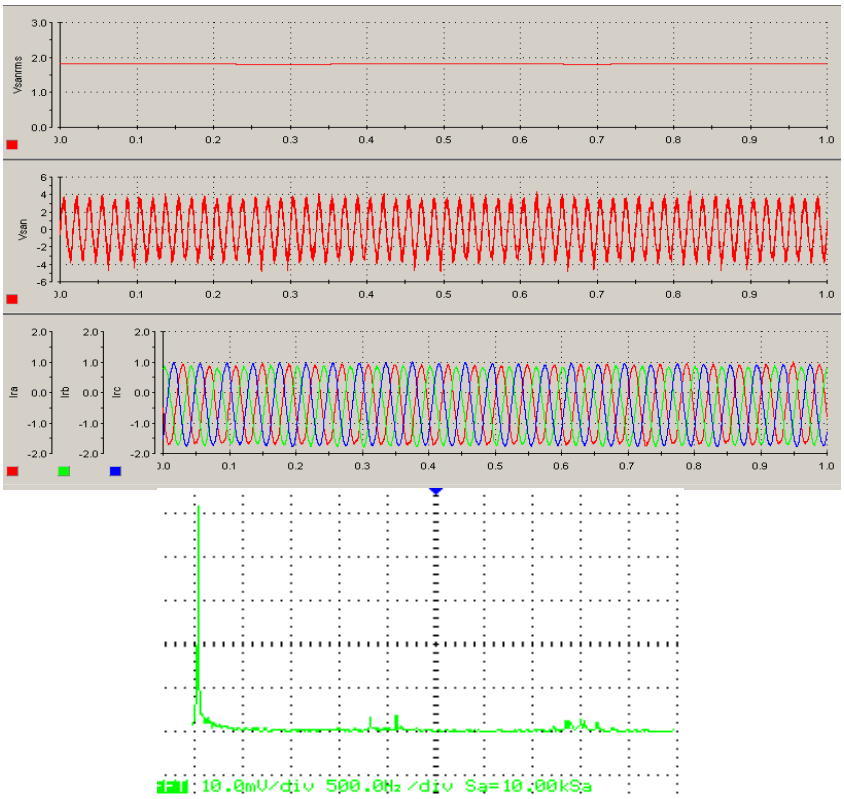

Figure 5-11. Systems Performance using Three-Level Inverter at 1050 rpm
a) rms value of V_{sanrms}, b) V_{san}, c) three-phase injected rotor current, and d) FFT of V_{san}

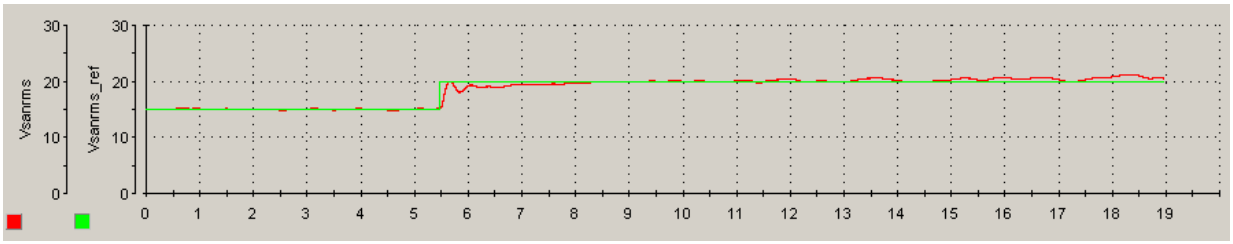

Figure 5-12. V_{sanrms} at 1210 rpm with a Step-Input of 15 V to 20 V at Reference Voltage

output voltage for a change in the reference voltage from 15 to 20 V at 1210 rpm. Table 5.5 and Figure 5-13 illustrate how the frequency regulation works at different speeds. As the speed goes up, the injection frequency is expected to decrease maintaining a constant stator frequency of 60 Hz. The waveforms in the figure and the data in the table also verify this statement. Finally, in figure 5-14, the stator voltage is shown to maintain steadiness for various speeds ensuring that

the system output will be consistent under variable wind speed condition. The speed is dropped from 1475 rpm to 1180 rpm resulting in a higher injection frequency and thus a lower injection current. With a small disturbance, the rms value of the stator voltage again settles down to the reference point of 15 V. The machine parameters are listed in Table 5.6.

TABLE 5.5 FREQUENCY REGULATION AT VARIOUS WIND SPEED

Generator Speed N_m (rpm)	**Mechanical Frequency f_{mech} (Hz)**	**Theoretical Slip Frequency f_{sl} (Hz)**	**Injected Rotor Frequency f_r (Hz)**	**Stator Frequency f_s (Hz)**
1020	34.00	26	26.1	60
1210	40.33	19.67	19.5	60
1475	49.17	10.83	10.8	60

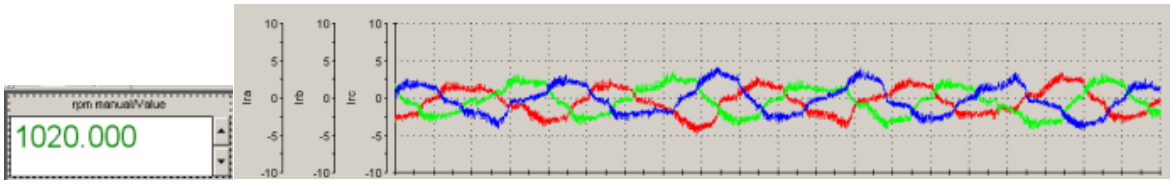

(a)

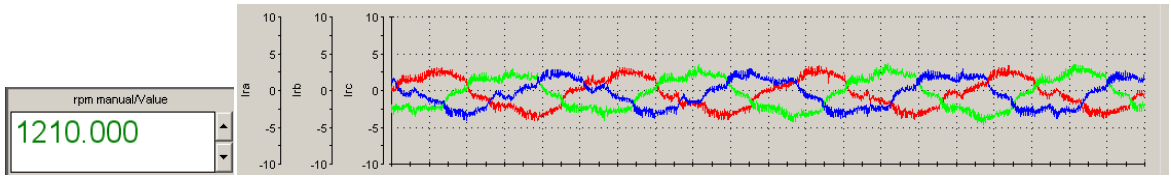

(b)

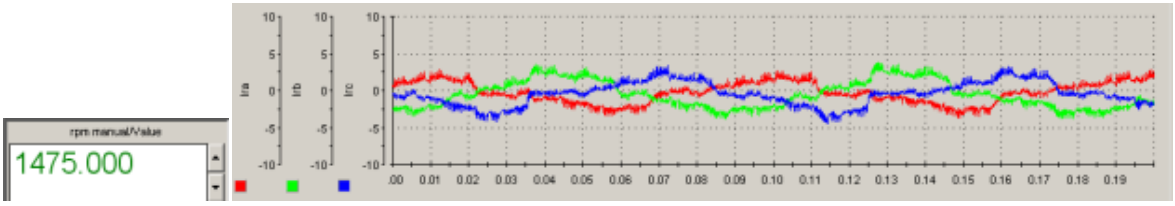

(c)

Figure 5-13. Frequency Variation of Injected Rotor Current with Speed Variation a) 1020 rpm, b) 1210 rpm, and c) 1475 rpm

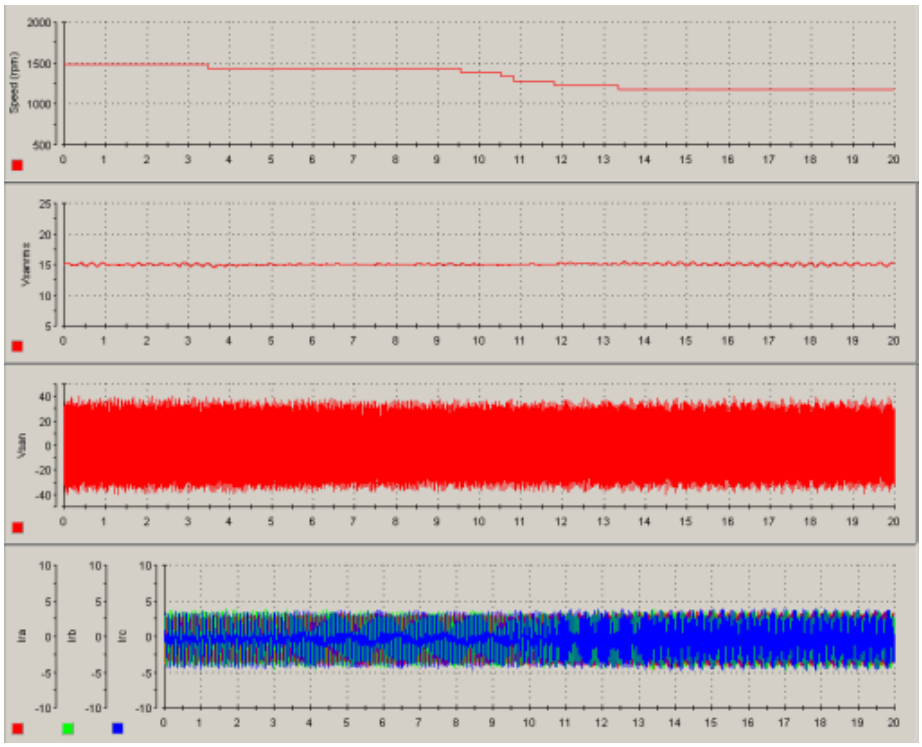

Figure 5-14. Constant V_{sanrms} (15 V) with a Change in Speed (1475 rpm to 1180 rpm)

TABLE 5.6 MACHINE PARAMETERS OF THE DFIG

Rated Power	5	hp
Rated Speed	1725	rpm
Rated Voltage	220/440	V
Stator Resistance	0.32	Ω
Stator Inductance	1.19	mH
Rotor Resistance	0.36	Ω
Rotor Inductance	1.34	mH
Mutual Inductance	39.46	mH
Stator to Rotor Turns Ratio	1.38	-

5.5. Performance of the WECS under Variable Load Condition

Figure 5-15 gives the systems response under variable load condition at 1210 rpm. Initially the load is a three phase resistive load with (22||11) = 7.33 Ω/phase. After some time the 11 Ω load is removed from each phase resulting in a drop in the rotor current. But after some transient, the stator voltage settled down to its reference value of 15 V.

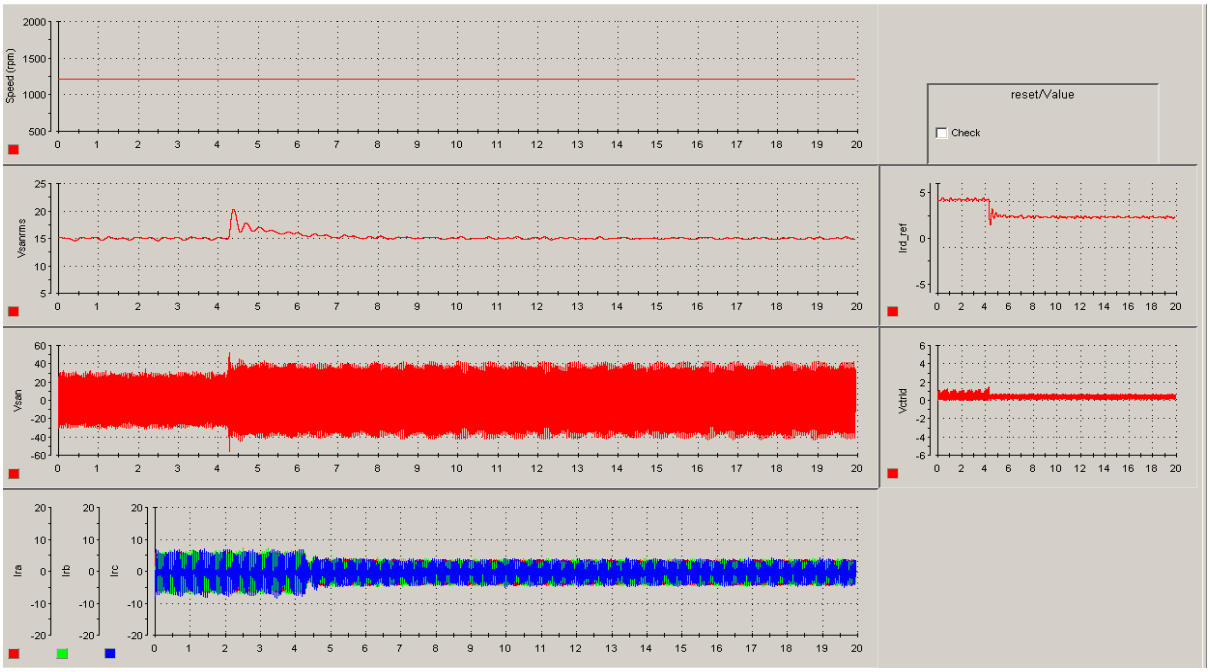

Figure 5-15. Constant V_{sanrms} (15 V) with a Step Change in Load (7.33 Ω/phase to 22 Ω/phase)

5.6. Conclusion

This chapter gives the experimental results obtained on the proposed WECS. The hardware does not include all the aspects of the actual HRES especially the MPPT scheme of both wind and solar. It also uses the DC supplies and not rechargeable batteries using the stator or solar power. But the controller provides a well regulated stator voltage and frequency under variable-speed conditions. Also a harmonic analysis was carried out on the output and a comparison between the two inverters and also with some previous works has been shown.

CHAPTER 6. CONCLUSIONS

6.1. Summary of Presented Work

A new concept of HRES is presented in this thesis that includes wind and PV energy, but the two sources do not just operate in parallel to feed the grid, like most existing HRESs. The WECS uses a DFIG whose rotor injection power is derived from two alternate sources depending on their availability. The rotor of the DFIG can be supplied either by a PV panel or by the stator. This multi-input concept makes the system more flexible and reduces its dependency on any single renewable source, whose availability is highly unpredictable. When possible, PV power is used for feeding the rotor and thus drawing no power from the stator, which increases the system efficiency. Then in the absence of the sunlight, a small fraction of the stator power is used by the rotor. The system can supply the load even in case of low wind speeds using only the PV power, since under that condition the generator acts as a regular transformer.

For drawing power from stator, a simple diode rectifier is used to convert the AC power to DC avoiding the complications of using a PWM rectifier and its controller. The DC voltages from both the sources are maintained constant using boost regulators at a level that matches the voltage of the battery which actually provides a constant bus voltage to the inverter. The boost regulator fed by the PV panel also extracts the peak power available from the panel. The core component of this work is the inverter and its controller. For lowering the harmonic distortion, a three-level neutral-point-clamped inverter has been used. Although it increases the complexity and cost of the converter, it makes the system suitable for high power and high voltage systems where a reduced distortion is worth implementing the scheme. Compared to the existing power converters used for a DFIG based WECS, i.e. a back-to-back PWM converter with two separate

controllers, this concept uses a diode rectifier and an inverter with only one controller for the inverter. The rectifier controller is completely replaced by a boost regulator that is much easy to implement and also cost effective. All other parameters like, the real and reactive powers and the stator voltage and frequency are controlled using the inverter controller. The controller also ensures the MPPT of wind power providing high conversion efficiency over a wide range of wind speeds. The system is tested in a PSIM-Simulink based environment for variable wind speeds and load and three-phase short circuit fault where it demonstrates a very good and fast performance. The controller developed using PSIM is also used for running the experiments.

Compared to similar systems presented earlier, the proposed system offers better power quality without using costly and bulky power filters. The system does not use any lookup table for wind MPPT and also no phase-locked loop is implemented for angle measurement. The digital environment makes it easy to control, adjust controller parameters and set references for stator output.

6.2. Scope for Future Research

The aspects not included in the presented system that can be taken care of under future research are:

- Operation at super-synchronous speeds (speeds higher than synchronous speed), where rotor power can be used to feed grid along with stator power and higher system efficiency can be achieved. This concept needs a back-to-back converter connected to the rotor of the generator to allow bidirectional power flow. Again a multilevel back-to-back converter can be used for better power quality.
- Blade pitch angle control can be tried for extracting rated power from the WT running at super-synchronous speed.

- The system fails to maintain a constant stator voltage for an unbalanced load or any uneven faults since the controller works only on one line-to-line voltage. All the three phase are to be considered in developing the voltage feedback.
- Use of PID controller can further improve the transient response of the system.
- The system is currently designed to supply an isolated load. Grid integration can be considered that needs synchronization of the machine voltages and the grid voltages. In the case of grid connected systems, the power factor or the reactive power can be controlled.

REFERENCES

[1] Wikipedia. (2012, May 10). *Fossil fuel* [Online]. Available: http://en.wikipedia.org/wiki/Fossil_fuel

[2] Wikipedia. (2012, May 10). *Energy in the United States* [Online]. Available: http://en.wikipedia.org/wiki/Energy_in_the_United_States

[3] Lie Xu *et al.*, "Grid integration of large DFIG-based wind farms using VSC transmission," *IEEE Trans. on Power Syst.*, vol. 22, no. 3, pp. 976-984, Aug. 2007.

[4] Subbaraya Yuvarajan *et al.*, "A novel power converter for photovoltaic application," *J. of Power Sources*, vol. 135, pp. 327-331, Mar. 2004.

[5] Wikipedia. (2012, Apr. 23). *Renewable energy* [Online]. Available: http://en.wikipedia.org/wiki/Renewable_energy

[6] Alejandro Calle *et al.*, "Three-level there-phase neutral-point-clamped back-to-back converter applied to a wind emulator," in *13th European Conf. on Power Electron. and Applicat.*, Barcelona, Spain, 2009, pp. 1-10.

[7] Le Xie *et al.*, "Wind integration in power systems: operational challenges and possible solutions," *Proc. of the IEEE*, vol. 99, no. 1, pp. 214-232, Jan. 2011.

[8] Encyclopedia Britannica. (2012, May 02). *Wind power* [Online]. Available: http://www.britannica.com/EBchecked/topic/645063/wind-power

[9] Energy Bible. (2010). *Wind speed and wind energy* [Online]. Available: http://energybible.com/wind_energy/wind_speed.html

[10] Olimpo Anaya-Lara *et al.*, *Wind Energy Generation Modeling and Control*. West Sussex, United Kingdom: John Wiley & Sons Ltd., 2009.

[11] Alireza Khaligh and Omer C. Onar, *Energy Harvesting – Solar, Wind, and Ocean Energy Conversion Systems*. Boca Raton, FL: CRC Press, 2010.

[12] Bin Wu *et al.*, *Power Conversion and Control of Wind Energy Systems*. Hoboken, NJ: John Wiley & Sons Ltd., 2011.

[13] F. Blaabjerg *et al.*, "Power electron. in wind turbine systems," in *CES/IEEE 5th Int. Power Electron. and Motion Control Conf.*, Shanghai, China, 2006, pp. 1-11.

[14] Juan Manuel Carrasco *et al.*, "Power-electron. systems for the grid integration of renewable energy sources," *IEEE Trans. on Ind. Electron.*, vol. 53, no. 4, pp. 1002-1016, Aug. 2006.

[15] Andreas Peterson *et al.*, "Evaluation of current control methods for wind turbines using doubly-fed induction machines," *IEEE Trans. on Power Electron.*, vol. 20, no. 1, pp. 227-235, Jan. 2005.

[16] R. Pena *et al.*, "A doubly fed induction generator using back-to back PWM converters supplying an isolated load from a variable speed wind turbine," *IEE Proc. Electric Power Applicat.*, vol. 143, no. 5, pp. 380-387, Sep. 1996.

[17] J. A. Baroudi *et al.*, "A review of power converter topologies for wind generators," in *IEEE Int. Conf. on Electric Machines and Drives*, San Antonio, TX, 2005, pp. 458-465.

[18] Van-Tung Phan *et al.*, "An effective rotor current controller for unbalanced stand-alone DFIG systems in the rotor reference frame," *J. of Power Electron.*, vol. 10, no. 6, pp. 724-732, Nov. 2010.

[19] S. Muller *et al.*, "Doubly fed induction generator systems for wind turbines," *IEEE Ind. Applicat. Mag.*, vol. 8, no. 3, pp. 26-33, May/Jun. 2002.

[20] F. Michael Hughes *et al.*, "Control of DFIG-based wind generation for power network support," *IEEE Trans. on Power Syst.*, vol. 20, no. 4, pp. 1958-1966, Nov. 2004.

[21] Janet L. Sawin. (2011). *Renewables 2011: global status report* [Online]. Available: http://www.ren21.net/Portals/97/documents/GSR/GSR2011_Master18.pdf

[22] Jih-Sheng (Jason) Lai, "Power conditioning circuit topologies," *IEEE Ind. Electron. Mag.*, vol. 3, no. 2, pp. 24-34, Jun. 2009.

[23] Wikipedia. (2012, Apr.21). *Theory of solar cells* [Online]. Available: http://en.wikipedia.org/wiki/Theory_of_solar_cells

[24] Ewald F. Fuchs and Mohammad A. S. Masoum, *Power Conversion of Renewable Energy Systems*. New York, NY: Springer, 2011.

[25] Chihchiang Hua and Chihming Shen, "Control of DC/DC converters for solar energy system with maximum power tracking," in *23rd Int. Conf. on Ind. Electron., Control and Instrumentation*, New Orleans LA, 1997, vol. 2, pp. 827-832.

[26] Solar Energy Explorer.com. (2010). *Maximum power point tracking* [Online]. Available: http://www.solarenergyexplorer.com/maximum-power-point-tracking.html#axzz1ok8f6EVH

[27] Tamer T. N. Khatib *et al.*, "A new controller for photovoltaic power generation systems," *European J. of Scientific Research*, vol. 33, no. 3, pp. 515-524, 2009.

[28] Kimiyoshi Kobayashi *et al.*, "Novel solar-cell power supply using a multiple-input DC-DC converter," *IEEE Trans. on Ind. Electron.*, vol. 53, no. 1, pp. 281-286, Feb. 2006.

[29] Abrez Mondal and S. Yuvarajan, “MPPT scheme for small scale photovoltaic systems using dSPACE,” in *IEEE Green Technology Conf.*, Tulsa, OK, 2012, pp. 74-76.

[30] Trishan Esram and Patrick L. Chapman, “Comparison of photovoltaic array maximum power point tracking techniques,” *IEEE Trans. on Energy Convers.*, vol. 22, no. 2, pp. 439-449, Jun. 2007.

[31] M. Elshaer *et al.*, “Smart optimal control of DC- DC boost converter in PV Systems,” in *IEEE/PES Transmission and Distribution Conf. and Expo.: Latin America*, São Paulo, SP, 2010, pp. 403-410.

[32] Robert W. Erickson and Dragan Maksimović, *Fundamentals of Power Electron.*, 2nd ed. Norwell, MA: Kluwer Academic Publications, 2004.

[33] Bimal K. Bose, *Modern Power Electron. and AC Drives*. New Jersey, NJ: Prentice Hall PTR, 2001.

[34] Yazici *et al.*, “Real time implementation of a digital controlled boost converter,” in *IEEE Int. Conf. on Elect. and Electron. Engineering*, Bursa, Turkey, 2009, pp. 437-441.

[35] MAXIM. (2001, Nov 29). *DC-DC converter tutorial* [Online]. Available: http://www.maxim-ic.com/app-notes/index.mvp/id/2031

[36] Randal Shaffer, *Fundamentals of Power Electron. with MATLAB.* Boston. MA: Charles River Media, 2007.

[37] Yaow-Ming *et al.*, “Double-input PWM DC/DC converter for High-/Low-voltage sources,” *IEEE Trans. on Ind. Electron.*, vol. 53, no. 5, pp. 1538-1544, Oct. 2006.

[38] Yuvaraj V. *et al.*, “Implementation and control of multi-input power converter for grid connected hybrid renewable energy generation system,” *Student Pulse Academic J.*, vol. 3, no. 6, pp. 1-7, Jun. 2011.

[39] Joanne Hui *et al.*, “A hybrid wind-solar energy system: a new rectifier stage topology,” in *25th Annu. IEEE Applied Power Electron. Conf. and Expo.*, Palm Springs, CA, 2010, pp. 155-161.

[40] Subbaraya Yuvarajan and Lingling Fan, “A doubly-fed induction generator-based wind generation system with quasi-sine rotor injection,” *J. of Power Sources*, vol. 184, no. 1, pp. 325-330, Sep. 2008.

[41] Akira Nabae *et al.*, “A new neutral-point-clamped PWM inverter,” *IEEE Trans. on Ind. Appl.*, vol. IA-I7, no. 5, pp. 518-523, Sep./Oct. 1981.

[42] José Rodríguez *et al.*, “A survey on neutral-point-clamped inverters,” *IEEE Trans. on Ind. Electron.*, vol. 57, no. 7, pp. 2219-2228, Jul. 2010.

[43] Satoshi Ogasawara and Hirofumi Akagi, "Analysis of variation of neutral point potential in neutral-point-clamped voltage source PWM inverters," *Conf. Record of the 1993 IEEE Ind. Appl. Society Annu. Meeting*, vol. 2, pp. 965-970, Oct. 1993.

[44] Nikola Celanovic and Dushan Boroyevich, "A comprehensive study of neutral-point voltage balancing problem in three-level neutral-point-clamped voltage source PWM inverters," *IEEE Trans. on Power Electron.*, vol. 15, no. 2, pp. 242-249, Mar. 2000.

[45] R. Chibani *et al.*, "Input DC voltage of three level neutral point clamped voltage source inverter balancing using a new kind of clamping bridge," *Int. J. of Computer and Elect. Engineering*, vol. 2, no. 5, pp. 879-886, Oct. 2010.

[46] Jih-Sheng Lai and Fang Zheng Peng, "Multilevel Converters – a new breed of power converters," *IEEE Trans. on Ind. Appl.*, vol. 32, no. 3, pp. 509-517, May/Jun. 1996.

[47] José Rodríguez *et al.*, "Multilevel inverters: a survey of topologies, controls and applicat.," *IEEE Trans. on Ind. Electron.*, vol. 49, no. 4, pp. 724-738, Aug. 2002.

[48] René Vargas *et al.*, "Predictive control of a three-phase neutral-point-clamped inverter," *IEEE Trans. on Ind. Electron.*, vol. 54, no. 5, pp. 2697-2705, Oct. 2007.

[49] Ali Keyhani. *Pulse-width modulation (PWM) techniques* [Online]. Available: academic.udayton.edu/markpatterson/ECT459/lect25.ppt

[50] L. Refoufi *et al.*, "Analysis and modeling of the steady state behavior of the static Kramer induction generator," *IEEE Trans. on Energy Convers.*, vol. 14, no. 3, pp. 333-339, 1999.

[51] L. Fan *et al.*, "A comparison of slip control, FMA control and vector control in DFIG converter," in *34th Annu. Conf. of IEEE Ind. Electron.*, Orlando, FL, 2008, pp. 2075-2081.

[52] Viorica Spoială *et al.*, "Control of doubly-fed induction generator system for wind turbines," *J. of Computer Science and Control Systems*, vol. 1, no. 1, pp. 213-218, 2008.

[53] Anca D. Hansen *et al.*, "Co-ordinated voltage control of DFIG wind turbines in uninterrupted operation during grid faults," *Wind Energy*, vol. 10, no. 1, pp. 51-68, 2007.

[54] Z. Miao *et al.*, "Control of DFIG-based wind generation to improve interarea oscillation damping," *IEEE Trans. on Energy Convers.*, vol. 24, no. 2, pp. 415-422, Jun. 2009.

[55] B. Chitti Babu and K. B. Mohanty, "Doubly-fed induction generator for variable speed wind energy conversion systems-modeling & simulation," *Int. J. of Computer and Elect. Engineering*, vol. 2, no. 1, pp. 141-147, Feb. 2010.

[56] K. C. Wong *et al.*, "Direct voltage control for grid synchronization of doubly-fed induction generators," *J. on Electric Power Components and Systems*, vol. 36, vo. 9, pp. 960-976, 2008.

[57] Wei Qiao and Ronald G. Harley, "Grid connection requirements and solutions for DFIG wind turbines," in *IEEE Energy 2030 Conf.*, Atlanta, GA, Nov. 2008.

[58] Yazhou Lei *et al.*, "Modeling of the wind turbine with a doubly fed induction generator for grid integrated studies," *IEEE Trans. on Energy Convers.*, vol. 21, no. 1, pp. 257-264, Mar. 2006.

[59] L. Fan and S. Yuvarajan, "Modeling and slip control of a doubly fed induction wind turbine generator," in *40th North American Power Symp.*, Atlanta, Canada, 2008, pp. 1-6.

[60] Alvaro Luna *et al.*, "Simplified modeling of a DFIG for transient studies in wind power applicat.," *IEEE Trans. on Ind. Electron.*, vol. 58, no. 1, pp. 9-20, Jan. 2011.

[61] Muhammad H. Rashid, *Power Electron. Handbook*. Waltham, MA: Academic Press, 2001.

[62] Lotfi Krichen, "Modeling and control of a hybrid renewable energy production unit," *Int. J. on Automatic Control and Systems Engineering*, vol. 7, no. 1, pp. 1-9, May 2007.

[63] K. Sopian *et al.*, "Optimal operational strategy for hybrid renewable energy system using genetic algorithms," *WSEAS Trans. on Math.*, vol. 7, no. 4, pp. 130-140, Apr. 2008.

[64] S. Yuvarajan and M. Kaderbhai, "Hybrid renewable energy system with wind turbine and PV panels," in *IEEE Green Technologies Conf.*, Grapevine, TX, pp. 1-4, Apr. 2010.

[65] Lngling Fan *et al.*, "A unified model of DFIG for simulating acceleration with rotor injection and harmonics in wind energy conversion systems," in *IEEE Power and Engineering Society General Meeting*, Calgary, AB, Canada, 2009, pp. 1-6.

[66] Lingling Fan *et al.*, "Harmonic analysis of a DFIG for a wind energy conversion system," *IEEE Trans. on Energy Convers.*, vol. 25, no. 1, pp. 181-190, Mar. 2010.

[67] Chong H. Ng *et al.*, "A multilevel modular converter for a large light weight wind turbine generator," *IEEE Trans. on Power Electron.*, vol. 23, no. 3, pp. 1062-1074, May 2008.

[68] PSIM, A Software by Powersim Technologies. Professional Version 9.0.

[69] MATLAB-Simulink, A Software by MathWorks Inc. Version 2010 and 2011a.

[70] Xin Wang *et al.*, "MPPT control for a PMSG-based grid-tied wind generation system," *North American Power Symp.*, Arlington, TX, Sept. 2010.

[71] Katsumi Nishida *et al.*, "A cost-effective high-efficiency power conditioner with simple maximum power point tracking control algorithm for wind-power grid integration", *IEEE Trans. on Ind. Appl.*, vol. 47, no. 2, Mar./Apr. 2011.

[72] S. Arulselvi *et al.*, "Design of PID controller for boost converter with rhs zero," in *Int. Power Electron. and Motion Control Conf.*, Riga, Latvia, 2004, vol. 2, pp. 532-537.

[73] Robert Warren Erickson and Dragan Maksimović, *Fundamental of Power Electron.* Norwell, MA: Kluwer Academic Publisher, 2004, ch. 3, appendix B.

[74] U.S. Department. of Energy. *Wind powering America – data from anemometer loan programs* [Online]. Available: http://www.windpoweringamerica.gov/anemometerloans/projects.asp

APPENDIX. PUBLICATION(S)

1. Eshita Ahmed and Subbaraya Yuvarajan, “Hybrid renewable energy system using DFIG and multilevel inverter, ” in *IEEE Green Technologies Conf.*, Tulsa, OK, pp. 1-6, Apr. 2012.

2. Eshita Ahmed *et al.*, “Variable speed wind energy conversion system using interior permanent magnet synchronous generator and multilevel inverter”, accepted by *IAS Annu. Meeting*, 2012.